Towards accurate greenhouse gas accounting in Canada: The impact of peat extraction management practices on land use emissions

Steffy Velosa

Department of Geography
McGill University
Montreal, Canada

December 2024

A thesis submitted to McGill University in partial fulfillment of the requirements of the degree of Master of Science

In Loving Memory of Richard Taylor (Ricky-D)

In your vast knowledge, I found inspiration and curiosity.

In your endless wisdom and generosity, I found qualities I aspire to embody.

In your unwavering belief in me, I found ambition to pursue my greatest potential.

And in your fearless voice, I found the courage to speak my own.

Abstract

Peatlands are a type of wetland ecosystem characterized by water-saturated soil conditions that enable the accumulation of peat—a carbon-rich, soil-like substance consisting of partially decomposed biomass, providing long-term carbon storage. However, some peatlands undergo land-use change for peat extraction, which can transform them from net carbon sinks into carbon sources.

My study examines the impacts of different management practices associated with peat extraction on greenhouse gas (GHG) emissions. Fieldwork was conducted at two actively harvested peatland sites in Rivière-du-Loup, Quebec, from May to November 2022, each employing distinct management strategies. I assessed the effects of heavy machinery on the uppermost peat layer when preparing the fields for extraction and quantified emissions from stockpiles of harvested peat stored on-site, comparing those covered with an impermeable reflective tarp to those left uncovered.

Using a closed chamber and trace gas analyzer, we measured carbon dioxide (CO_2) and methane (CH_4) fluxes across four extraction phases: harrowed, drying, conditioned, and vacuum-harvested. My results show that CO_2 emission rates did not differ significantly between phases. CH_4 emissions, while lower overall than those from undisturbed peatlands, were notably increased during the harrowed, conditioned, and vacuum-harvested phases compared to the drying phase. The increase in CH_4 was attributed to a disturbance effect caused by heavy machinery, regardless of varying surface peat conditions, with CH_4 peaking immediately post-disturbance before stabilizing over time.

For both covered and uncovered stockpiles, surface flux measurements were taken at various positions, while gas samples from within the piles were analyzed using gas chromatography. Uncovered stockpiles exhibited low CH_4 emissions but had above average CO_2 emissions compared to extracted peat fields, with a mean emission rate of approximately 5 g CO_2-C m^{-2} day^{-1}. Uncovered stockpile fluxes varied seasonally, and were significantly higher at the top of stockpiles than at the bottom. Conversely, CO_2 emissions through the tarp of covered stockpiles were ten times lower than those from uncovered

piles. However, more CH_4 (0.6 g CH_4-C m^{-3}) and CO_2 (61.1 g CO_2-C m^{-3}) were stored within covered stockpiles, compared to uncovered ones (CH_4 < 0.005 g CH_4-C m^{-3}; CO_2: 6.7 g CO_2-C m^{-3}). Since fluxes measured over holes in the tarp indicated the release of stored CO_2, I assumed—though I could not measure it—that the stored gases would be released as the cover was removed and the peat was taken away for processing. Although stockpiles represented less than 1% of the total study area, they accounted for 1-2% of overall site emissions when including surface fluxes and emissions released during stockpile removal.

My findings contribute to a more comprehensive understanding of land-use-related GHG emissions in Canada, offering insights for improved GHG accounting and guiding the peat industry toward best management practices.

Résumé

Les tourbières sont un type d'écosystème humide caractérisé par des conditions de sol saturé d'eau qui permettent l'accumulation de tourbe—une substance riche en carbone, semblable au sol, composée de biomasse partiellement décomposée—fournissant un stockage du carbone à long terme. Cependant, certaines tourbières subissent des changements d'affectation des terres pour l'extraction de la tourbe, ce qui peut engendrer la transformation de puits de carbone nets en sources de carbone.

Mon étude examine les impacts des différentes pratiques de gestion associées à l'extraction de la tourbe sur les émissions de gaz à effet de serre (GES). Les enquêtes sur les terrains ont été effectuées sur deux sites de tourbières activement exploitées à Rivière-du-Loup, au Québec, du mois de mai à novembre 2022, chacune employant des stratégies de gestion distinctes. J'ai évalué les effets de la machinerie lourde sur la couche supérieure de la tourbe lors de la préparation des champs pour l'extraction, et j'ai quantifié les émissions des piles empilées de tourbe, récoltées et stockés sur place, les comparant à celles recouvertes d'une bâche réfléchissante imperméable à celles laissées à découvert.

À chambre fermée et munie d'un analyseur de gaz trace, J'ai mesuré les flux de dioxyde de carbone (CO_2) et de méthane (CH_4) durant quatre phases d'extraction: hersage, séchage, conditionnement et récolte par aspiration. Mes résultats démontrent une faible variance des taux d'émission de CO_2 entre les différentes phases d'extraction. Au même titre, les émissions de CH_4 étaient nettement plus élevées pendant les phases d'hersage, du conditionnement et de la récolte par aspiration comparativement à la phase de séchage, mais en généralement inférieures à celles des tourbières non perturbées. L'augmentation des émissions de CH_4 a été attribuée à un effet de perturbation causé par l'utilisation de machineries lourdes, indépendamment des conditions variables de la surface de la tourbe, le CH_4 atteignant un niveau le plus élevé immédiatement après la perturbation avant de se stabiliser au fil du temps.

Des mesures de flux sur la surface ont été effectuées à divers emplacements aux piles de stockage couvertes et non couvertes, de manière égale des échantillons de gaz prélevés à profondeurs des empilements ont été analysés par chromatographie en phase gazeuse afin d'évaluer le stockage de GES. Les effets des piles de stockage non couvertes présentaient de faibles émissions de CH_4, toutefois des émissions de CO_2 étaient supérieures à la moyenne comparativement aux champs d'extrait de tourbe, avec un taux d'émission moyen d'environ 5 g CO_2-C m^{-2} par jour. Les émissions des piles de stockage non couvertes étaient variables selon les saisons, et significativement plus élevées au sommet des empilements par rapport à leur base. Inversement, les émissions de CO_2 à travers la bâche des piles de stockage couvertes étaient dix fois plus faibles que celles des piles non couvertes. Cependant, les piles couvertes emmagasinaient plus de CH_4 (0.6 g CH_4-C m^{-3}) et de CO_2 (61.1 g CO_2-C m^{-3}) que les stocks non couverts (<0.005 g CH_4-C m^{-3}; 6.7 g CO_2-C m^{-3}). Comme les flux mesurés au-dessus des trous dans la bâche indiquaient la libération du CO_2 stocké, j'ai supposé, sans avoir pu prendre des mesures spécifiques, que les gaz stockés seraient libérés lorsque la bâche serait retirée et que la tourbe serait transportée afin d'être traitée. Bien que les stocks représentent moins de 1% de la zone totale de l'étude, ils sont à l'origine de 1 à 2 % des émissions totales du site incluant les flux de surface et les émissions libérées lors du retrait des piles.

Mes résultats contribuent à une compréhension plus complète des émissions de GES liées à l'utilisation des terres au Canada, offrant des perspectives pour améliorer la comptabilisation des GES et orienter l'industrie de la tourbe vers de meilleures pratiques de gestion.

Table of Contents

List of Figures

List of Tables

Abbreviations

GHG: Greenhouse gas

SD: Standard Deviation

SE: Standard Error

AIC: Akaike Information Criterion

CL: Confidence Level

C/N ratio: Carbon/Nitrogen ratio

NEE: Net Ecosystem Exchange

NPP: Net Primary Productivity

Glossary

Water table: Upper layer of underground surface below which soil is completely saturated by water

Aerobic: Process involving/requiring free oxygen

Anaerobic: Process involving/requiring an absence of free oxygen

Anoxic: Environment greatly deficient in oxygen

Heterotroph: Organisms that consume matter to produce energy and nutrients

Methanogens: Anaerobic archaea that produce methane as a byproduct of their energy metabolisms

Methanotroph: Bacteria or archaea that metabolize methane as their source of energy, producing CO_2 as a byproduct

Oxidation: Chemical reaction involving a substance losing electrons, resulting in the gain of oxygen and the loss of hydrogen

Carbon cycling: A cycle in which carbon is exchanged from the atmosphere into organisms in the Earth and back to the atmosphere again

Labile Carbon: Soil organic carbon that is easily broken down and serves as a primary food source for soil microbes

Q_{10} temperature coefficient: a value that measures how much the rate of a reaction increases when the temperature increases by 10°C

Carbon mineralization: A chemical process that converts carbon dioxide (CO_2) into solid carbonate minerals

Acknowledgments

I would like to express my gratitude to the many funders of this research: NSERC's Collaborative Research and Development Grant (CRD), awarded to Dr. Nigel T. Roulet (PI), the Canadian Sphagnum Peat Moss Association (CSPMA), and the Fonds de recherche du Québec – Nature et technologies (FRQNT) – Bourses de maîtrise en recherche for their generous support. Special thanks to Berger and Premier Tech for access to their sites, and to Dr. Pierre-Olivier Jean, Pierre-Olivier Sauvageau, and the field site operations supervisors for sharing their invaluable expertise in peatland management.

To my co-supervisors, Dr. Nigel T. Roulet and Dr. Ian B. Strachan: Thank you for your invaluable insights on both science and governance, and for your patience with my tendency to deep dive into details in my quest to realize the full potential of this project. Your trust allowed me the freedom to develop as an independent researcher, a quality I will carry forward in my career. I am also deeply grateful for the many opportunities you provided to engage with the broader scientific community, encouraging me to participate in the exchange of ideas and to develop my scientific communication skills at meetings and conferences. My sincerest thanks to Dr. Cynthia Kallenbach for allowing me to work in her impeccably organized lab and guiding me on my techniques, as well as to Dr. Maria Strack for helping shape my research direction. I would also like to thank Mike Dalva, the department's go-to for all things fieldwork related, from whom I learned to be an impromptu electrician. Thank you as well to Paula Kestelman, for her reliability and wisdom. I am also grateful to Dr. Mette Bendixen for her support and mentorship.

A huge thank you to my fieldwork assistant, Clara Schryer, who—despite being perpetually covered in peat—never once complained, embracing every challenge with enthusiasm and treating my work as if it were her own. I am incredibly lucky to have been part of "the triplets", sharing every step of my graduate school journey with Alice Watts and Nicolas Perciballi, my office/lab mates turned close friends. From my Mac Campus affiliations, I also thank Sophie Burgess and Laura Clark for their encouragement and insights. Additionally, I'm grateful to Dr. Bidya Sharma, Dr. Hongxing He, and Dr. James

Seward for their knowledge and guidance, and to all the other amazing people from the McGill Geography department that I had the privilege to meet along the way.

Special thanks to my lab and field helpers Angelina Nikolaeva, Andrew Kemp, Camille Jones, Michelle Wang, and Sara Negrin, who were instrumental in helping me process countless samples. I also want to acknowledge the wonderful team at McGill's Student Accessibility & Achievement and the Student Wellness Hub for helping me accelerate my personal development, which has been an invaluable complement to my academic journey.

Finally, I thank my partner, Benjamin Brunen, for his unwavering support and adaptability, stepping into every role I needed as a carpenter, field and lab assistant, life coach, coffee shop co-worker, and cheerleader. I am also endlessly grateful to my family and friends: Eddy Velosa, Lynda Dumouchel, Sandrina Velosa, Michelle Forrester, Olivia Vidmar, and Marta Kozlova, for being the best support network anyone could ask for—and for (hopefully) learning a thing or two about the importance of peatlands.

Contribution of Authors

I was responsible for the collection, processing, and analysis of the data presented in this thesis, as well as the production of the thesis itself. My co-supervisors Dr. Nigel T. Roulet and Dr. Ian B. Strachan were responsible for helping identify my research questions, contributing to the development of my research design, as well as reviewing my findings and written thesis chapters to provide me with feedback. Clara Schryer helped collect most of my data during fieldwork, at times with additional support from Nicolas Perciballi, Angelina Nikolaeva, and Alice Watts.

Chapter 1: Introduction

Wetlands are complex ecosystems characterized by saturated soils, creating an oxygen deficient (anoxic) environment that favours the growth of specialized plants adapted to wet conditions. Peatland ecosystems are a subtype of wetlands that are differentiated by the formation of peat, a carbon rich organic material made up of partially decomposed plant and animal constituents. Peat accumulates over time due to wet-anoxic conditions that limit microbial decomposition to anaerobic pathways, which have relatively slow decomposition rates and require the presence of more specialized microbial communities (Rydin & Jeglum 2013). As a result, carbon sequestration in peatlands is determined by the imbalance of net photosynthetic inputs from the net primary productivity of vegetation (the rate at which energy is converted to biomass by photoautotrophs), and outputs from decomposition by microorganisms to the atmosphere in the form of methane (CH_4), and carbon-dioxide (CO_2), as well as dissolved organic carbon losses in less significant amounts (Clymo et al. 1998; Page et al. 2011).

In their natural state, peatlands actively emit large amounts of methane from anaerobic decomposition. However, if left undisturbed, peatlands function as a net carbon sink due to carbon rich peat accumulation, which provides a global net-cooling effect over the span of the ecosystem's lifetime (Strack et al. 2008). As such, peatlands play an integral role in the cycling of carbon, as well as global CO_2 and CH_4 budgets.

Peatlands can undergo land-use change, including peat extraction for purposes such as horticulture and fuel. Most disturbances alter the ecosystem's biogeochemistry and carbon function. To prepare a peatland for peat harvesting, surface vegetation is removed, and ditches are dug around a perimeter to lower the water table of the area within. These modifications shift the ecological community to one dominated by heterotrophic respiration, in which microorganism, fungi, and archaea, decompose organic matter stored as peat following aerobic decomposition pathways (Page et al. 2011). Since there is no longer plant uptake of CO_2, this results in greater CO_2 emissions (while CH_4 is

still emitted in smaller amounts) to the atmosphere, shifting the ecosystem to a net carbon source.

Canada is one of the world's leading exporters of peat, having exported over 1.4 million tonnes of peat at a trade value of more than 525 million USD in 2022 (UN CommTrade 2022). Peatlands in Canada cover approximately 119.4 million hectares of land (UNEP 2022), of which 30,900 hectares (less than 0.03%) are actively harvested (CSPMA 2017). Under the United Nations Framework on Climate Change (UNFCCC) guidelines, Canada is required to report on anthropogenic greenhouse gas (GHG) emissions (mainly CO_2 and CH_4), which includes land-use change emissions, for which peat extraction falls under the wetland category (UNFCCC 2014). To facilitate this process, the Intergovernmental Panel on Climate Change (IPCC) has put forward three tier levels for estimating emissions.

The commonly used default Tier 1 emission factor (using spatially coarse area and activity data) for land use in this category may not always be representative of active peat extraction. A study in the United Kingdom by Wilson et al. (2015) quantified CO_2-C emissions from nine peat extraction sites and found the emission factor derived from their study (1.70 +/- 0.47 tCO_2-C ha^{-1} yr^{-1}) was considerably lower than the Tier 1 emission factor provided in the IPCC's Wetlands Supplement (2.8 +/- 1.7 tCO_2-C ha^{-1} yr^{-1}). Acknowledging this, the IPCC allows for Tier II country-based emission factors (using high-resolution land area data), which are improved upon with more national studies (IPCC 2006).

Previous work in Canadian extracted peatlands quantified average emissions from actively harvested peat fields in Riviere-du-Loup, Quebec. The emission rates of the drainage ditches were found to be greater than that of the fields, despite making up a much smaller portion of the extraction site (Clark et al. 2023). A later study by He at al. (2023) then used three years of CO_2 flux, soil moisture, soil temperature, and water table depth data collected by Clark et al. (2023) to verify the sensitivity of key parameters of an adapted CoupModel, showing high agreement with the measured values. The model also highlighted the importance of surface soil moisture availability on regulating CO_2 emissions

from heterotrophic respiration in extracted peat fields, which may have important implications for horticultural peat extraction processes that directly modify the peat surface (He et al. 2023).

Simulating annual fluxes using the adapted CoupModel, He & Roulet (2023) produced emission factors that were 50% lower than the current IPCC Tier 1, and 55% lower than the domestic Tier 2 currently used by Canada. Their results demonstrated that emission factors derived from empirical observations were biased towards higher emissions, because measurements were taken almost exclusively in summer months (He & Roulet 2023). The emission factor produced by He & Roulet (2023) is an example of Tier III emission factors, based on process-based modelling using inventory measurement systems and high-resolution activity data. While all tiers intend to provide unbiased estimates, uncertainties are expected to decrease from Tier 1 to Tier 3 (IPCC 2014).

Peat extraction can only take place in dry conditions. Therefore, extraction processes occur as frequently as possible during summer months to secure adequate supply. To prepare for harvest, the top layer of the peat field (top 3-6 cm) is harrowed to break the surface peat from the peat matrix below and allow it to dry. Vacuum harvesters are then used to collect the relatively dry peat surface layer. Harvested peat is kept in stockpiles in the field for up to 3 months before being shipped for further processing. During this time, peat in the stockpiles is subject to aerobic decomposition. Other studies have estimated that stockpiled peat emits CO_2 at higher rates than the fields (Nykanen et al. 1996; Alm et al. 2007b), but only one study in Finland has directly measured GHG fluxes from peat stockpiles (Ahlholm & Silvola 1990). Emissions from the stockpiles are likely to vary based on seasonality and management practices such as the use of an impermeable reflective tarp to cover the piles.

There is a need for further research to quantify GHG emission rates from peat stockpiles and to assess the effect of peat extraction management practices on field and stockpile emissions. My thesis aims to fill knowledge gaps for extracted peatlands in eastern Canada by asking: “**How do peat extraction management practices affect CO_2**

and CH_4 emissions in actively extracted peatlands?" Specifically, my research questions are **(1)** Do the operations involved in peat extraction impact field GHG emission rates? and **(2)** How do management practices surrounding the storage of peat in stockpiles impact emissions?

To answer these questions, I address the following research objectives: **(1)** Evaluate the impact of peat extraction operations (harrowing, conditioning, and vacuum harvesting) on field GHG emissions and surface peat layer conditions. **(2)** Quantify CO_2 and CH_4 emissions from uncovered peat stockpiles, assess the factors influencing these emissions (e.g., aspect, seasonality), compare them with emissions from stockpiles covered with an impermeable reflective tarp, and determine the overall contribution of stockpile emissions to site-wide GHG emissions. **(3)** Investigate how moisture and temperature relate to GHG emissions from the stockpiles and fields. Overall, my research aims to refine Canadian GHG accounting by filling key knowledge gaps, and report on land-use change carbon emissions from peat extraction. This work may help to inform policy and shift the industry towards more sustainable practices.

Correspondingly, I expect that: **(1)** Field emissions will be impacted by field extraction processes used to modify surface peat conditions (Table 1.1). **(2)** CO_2 emissions from peat stockpiles will be increased and CH_4 will be decreased compared to the fields due to the dry conditions of the piles; Flux rates will increase from spring to summer, then decrease again in the fall; Covered stockpiles will alter the microenvironment underneath the tarp causing differences in carbon dynamics when compared to uncovered piles; and Stockpiles will disproportionately contribute to site GHG emissions. **(3)** Temperature and moisture conditions will influence emissions from both fields and stockpiles.

Table 1.1: Predicted changes to peat conditions from extraction operations, and how these conditions may influence GHG fluxes (red indicates conditions that may increase fluxes, while blue indicates potential decreases).

Surface Layer Conditions	**Harrow/Condition**	**Vacuum-Harvest**
Depth	Loosened and temporarily increased.	Reduced since most of it was removed.
Soil Moisture Content	Temporarily increased due to the release of internal moisture from the breakup of peat when raking/tilling, Then begins to dry, increasing evaporation and decreasing moisture.	Could be temporarily increased due to compression from heavy machinery.
Temperature	Decreased due to evaporative cooling (especially post-harrow).	Increased due to removal of the surface layer and compression of the remaining peat.
Dry Density of Peat	Decreased due to air being introduced to the system.	Increased due to compression from machinery

This thesis presents my work in 7 Chapters, including this first introductory chapter. My **Literature Review** in **Chapter 2** explores the complexities surrounding peatlands in four parts. Part 1 focuses on peatlands in their natural state; Part 2 examines the impacts of peat extraction; Part 3 discusses the global context of peat extraction and use; and lastly, Part 4 identifies knowledge gaps in the literature, providing context for my research towards refining GHG accounting for managed peatlands in Canada. My **Methods** in **Chapter 3** introduce the study area, the field and laboratory methods used to collect and process data, statistical analysis, and calculations. The **Results** I present in **Chapter 4** include the reliability of volumetric water content measurements taken with a probe in the field, impacts of field operations, stockpile GHG fluxes, stockpile CO_2 and CH_4 storage, and the contribution of stockpiles to overall extraction emissions. My **Discussion** in **Chapter 5** synthesizes my results, highlighting important findings for field operations and stockpiles in the contexts of both biogeochemistry and GHG emissions accounting. I also discuss the limitations of my work, and directions for future research. **Chapter 6** is the **Conclusion** to my thesis, followed by my listed **References** in **Chapter 7**.

Chapter 2: Literature Review

In this literature review, I explore the complexities surrounding peatlands in four parts. Part 1 focuses on peatlands in their natural state; Part 2 examines the impacts of peat extraction; Part 3 discusses the global context of peat extraction and use; and lastly, Part 4 identifies knowledge gaps in the literature, providing context for my research towards refining greenhouse gas accounting for managed peatlands in Canada.

2.1 Peatlands in their Natural State

This section provides an overview of peatlands in their undisturbed state, focusing on natural decomposition processes and factors influencing carbon cycling. I discuss the methods used to measure GHG fluxes and carbon stores in natural peatlands, and their role in climate regulation. Lastly, I explore drivers for peatland loss and suggestions for future mitigation.

2.1.1 Introduction to Peatlands

Peatlands are a type of terrestrial wetland characterized by a high-water table near the ground surface, leading to water-saturated soils. These oxygen-deficient soil conditions favour plants and organisms that thrive in acidic, waterlogged environments and are highly resistant to decay (Rydin & Jeglum 2013). One of the key peatland species is *Sphagnum* moss, a bryophyte that plays a major role in peatland formation, especially in boreal regions (Rydin & Jeglum 2013).

Peatlands are characterized by the accumulation of peat, an organic material made from partially decomposed plant and animal matter (Rydin & Jeglum 2013). Soils covered with at least 30 cm of peat are classified as peatlands (Gorham 1995), though this threshold can vary by country (IUCN UK 2019). Peatlands are further subdivided by water sources and trophic status. Ombrogenic peatlands receive water only from precipitation, while minerogenic peatlands also receive lateral and subsurface inflows. Oligotrophic peatlands are nutrient poor, while minerotrophic peatlands are richer in mineral elements and possibly nutrients (Rydin & Jeglum 2013; Charman 2009). Peat soil has an average pH of approximately 4.5, which is typically lower in bogs and higher in fens (Rinaldi et al. 2019).

In addition to traditional ecosystem carbon pools such as biomass, litter, and mineral soils, the peat in peatlands—comprising more than 50% carbon—serves as an additional carbon stock, (Joosten & Couwenberg 2008). Peatlands accumulate peat through net primary production (NPP: the balance between photosynthesis by organisms converting atmospheric CO_2 into biomass, and respiration releasing CO_2 to the atmosphere). The fact that peatlands secure long-term carbon storage is not necessarily because NPP is large, but rather that decomposition rates are slowed by anoxic conditions, preventing peat from breaking down (Rydin & Jeglum 2013; Strack et al. 2008). As a result, global peatlands store approximately 550 gigatons of carbon, accounting for 30% of the world's soil organic carbon, more than any other terrestrial system (Byrnes et al. 2004; Joosten & Couwenberg 2008; Strack et al. 2008). However, any decomposition of organic matter in peatlands also results in carbon losses in the form of GHG emissions and dissolved organic carbon (DOC) (Strack et al. 2008).

2.1.2 Decomposition Pathways

In natural peatlands, decomposition occurs through both aerobic and anaerobic processes. Above the water table, where oxygen is available in the upper peat profile, heterotrophic bacteria and fungi decompose organic matter via aerobic pathways, releasing CO_2 to the atmosphere (Page et al. 2011). Below the water table, where oxygen is scarce, heterotrophic methanogens break down organic matter at reduced rate, releasing CO_2 and CH_4 (Page et al. 2011). The remaining undecomposed organic matter accumulated by NPP (i.e., tree litter, leaves, mosses) becomes incorporated into the surface peat layer.

Due to the high-water table, the prevalent form of decomposition in natural peatlands is anaerobic, involving a specialized group of archaea known as anaerobic methanogens (Andersen et al. 2013). However, when the methane produced below the water table diffuses through the oxygen-rich upper peat layers, it may be metabolized by methanotrophic bacteria (methanotrophy), converting CH_4 into CO_2 via oxidation (Andersen et al. 2013). The balance between aerobic and anaerobic decomposition governs carbon cycling in natural peatlands (Figure 2.1).

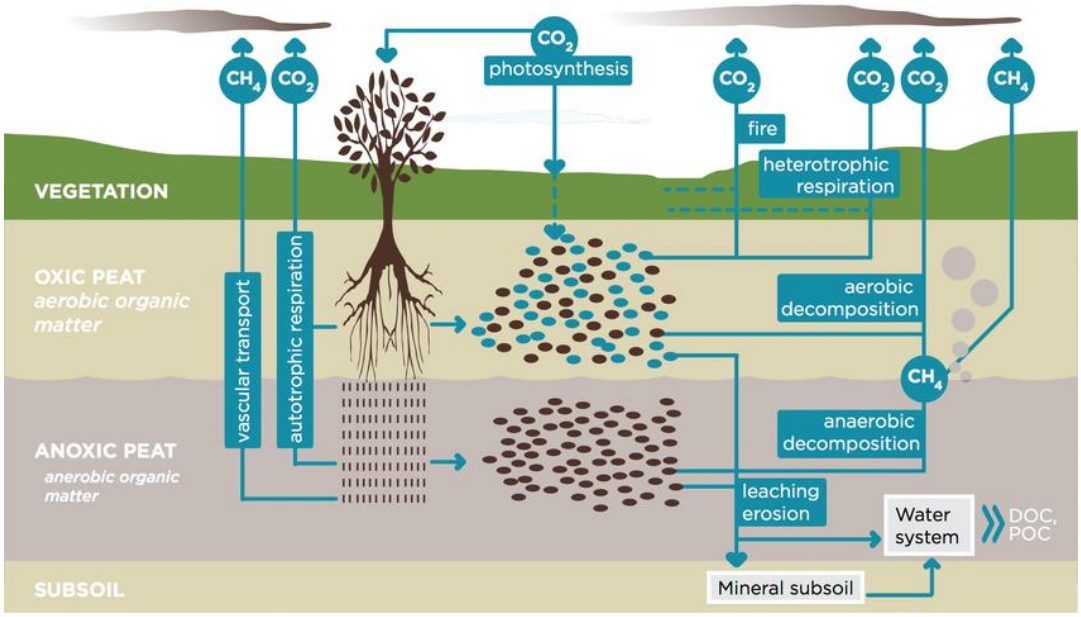

Figure 2.1. Carbon cycling in natural peatlands (Figure from Page et al. 2011).

2.1.3 Factors Affecting Peat Decomposition and Carbon Exchange

Peatland methane emissions tend to increase when the water table rises, as more organic matter from fresh biomass and labile carbon becomes available to methanogens, and methanotrophy is reduced due to waterlogged conditions (Page et al. 2011 and references therein). However, methanogenic communities have been shown to be diverse in both high and low CH_4 emitting sites. Therefore, sites with low CH_4 emissions are likely due to inactive microbial populations or high rates of methanotrophy in the aerobic peat layer (Winsborough & Basiliko 2010).

Key processes beyond microbial presence can affect peat decomposition and the exchange of carbon with the atmosphere. These include microbial population dynamics, the availability and decomposability of organic matter, and microbial response to hydrology and temperature (Page et al. 2011; Andersen et al. 2013). Additionally, land use, land cover, vegetation, and nutrients may also impact microbial enzymatic activity levels, influencing emission rates (Oertel et al. 2016).

2.1.4 Flux Data Collection Methods

Gas exchange between a surface and the atmosphere can be quantified using scientific instruments, where the chosen measurement method must reflect the ecosystem's

physical structure. Areas with low or absent vegetation can use portable chamber methods, while areas with taller vegetation and trees that exceed chamber headspace dimensions can opt for eddy covariance towers (Alm et al. 2007a). Thus, chambers measure at the plant community scale (for vegetated soils), while eddy co-variance measures at the ecosystem scale.

2.1.4.1 Chamber Measurements

Gas outflows from a surface to the atmosphere can be measured using commercially available portable infra-red gas analysers (IRGA) (Carbone et al. 2019). IRGA systems measure gas concentrations in real time and allow data to be streamed or downloaded and then visualized on a computer. These analyzers are robust and durable, allowing them to be used in field-based applications and measure data at up to 2 Hz with reliable precision (Carbone et al. 2019).

In a closed chamber system, the air is circulated between the chamber headspace and an IRGA. Opaque chambers are used to measure ecosystem respiration (from plant and microbial communities), while transparent chambers measure the net ecosystem gas exchange (Carbone et al. 2019). Gas fluxes are calculated as changes in gas concentration in the chamber over time as a function of chamber volume, air temperature, and air pressure according to the ideal gas law (Alm et al. 2007a). The chamber should be sealed to prevent external airflow, and ambient gas concentration readings should be recorded before placing the chamber onto the surface for measurement. Fluxes may have high spatio-temporal variability, resulting in large uncertainties in extrapolated flux estimates. Wangari et al. (2022) found that increasing the number of chamber measurement locations and taking measurements across seasons significantly reduced uncertainties in landscape-scale GHG fluxes. The authors recommend taking multiple CO_2 and CH_4 flux measurements at a minimum of two locations per km^2 for forest ecosystems and six locations per km^2 for cropland (arable) ecosystems. They also observed significant differences between measurements taken in spring, summer, and fall, indicating that measuring across multiple seasons provides a more accurate representation of temporal variability.

2.1.5 Carbon Stores and Fluxes in Natural Peatlands

Peatlands play an integral role in the Earth's CO_2 and CH_4 budgets through their carbon storage capacity. Two mechanisms have major effects on these exchanges, climate change and land-use change (Harris et al. 2021), where the latter is the focus of this thesis.

The amount of carbon accumulated reflects soil organic matter (SOM) and soil organic carbon (SOC) ratios, which vary based on peat type, conditions, and soil horizons (Klingenfuß et al. 2014). Carbon accumulation in near-surface peat cannot be directly compared to long-term rates in deeper layers (Young et al. 2019). In Finland, the long-term average accumulation was 17 g C m^{-2} yr^{-1} in minerotrophic fens and 21 g C m^{-2} yr^{-1} in ombrotrophic bogs over the Holocene (Alm et al. 2017b). Similarly, in northeastern Canada's Hudson Bay Lowlands, two peat cores recorded a long-term average of 24.2 g C m^{-2} yr^{-1}, with lower rates during colder periods and recent increases attributed to warming (Lamarre et al. 2012). More recently during the 2000s, the mean carbon accumulation rate from five northern peatland sites was estimated at 32.3 ±7.8 g C m^{-2} yr^{-1} (Yu 2012). This highlights the need to consider the ecosystem's entire lifespan in carbon budgets.

Peatlands are estimated to hold the equivalent of 77% of atmospheric carbon, while only occupying approximately 3% of the Earth's land surface (Yu et al. 2010). Paradoxically, the same water saturated conditions that allow peat to accumulate and store carbon, also make global wetlands (predominantly peatlands) the largest single source of atmospheric methane, even when anthropogenic emissions are included (Byrne et al. 2004). Peatlands emit approximately 0.8 Gt CO_2 equivalent of methane per year (Huang et al. 2021), at an average rate of 7.6 to 15.7 g CH_4-C m^{-2} yr^{-1} for northern peatlands (Abdalla et al. 2016). Carbon also exits peatland systems as DOC, with annual DOC exports ranging from 1.4 to 94.8 g C m^{-2} yr^{-1}, with an average of 18.5 ± 19.3 g C m^{-2} yr^{-1} for undisturbed sites (Rosset at al. 2022). Despite large methane emissions, when the ecosystem's lifetime is considered (i.e., >100 years), undisturbed peatlands provide a net-cooling effect and act as a net carbon sink (Strack et al. 2008).

Yu (2012) found large variations in the carbon balances of four natural northern peatlands monitored for different periods between 1998 and 2009 (Table 2.1). Despite carbon losses from the ecosystem in the form of methane and DOC, the net ecosystem carbon balance (NECB) and net ecosystem carbon exchange (NEE) resulted in net carbon uptake for these natural peatlands.

Table 2.1: Average site means for NECB, NEE, CH_4, and DOC, for four northern peatlands (adapted from Table 4 in Yu 2012). Negative values represent an influx from the atmosphere to the ecosystem, while positive values represent an outflux from the ecosystem.

Site Name *Peatland Type* *Reference*	**NECB** (g C m^{-2} yr^{-1} ± SD)	**NEE CO_2** (g CO_2-C m^{-2} yr^{-1})	**CH_4** (g CH_4-C m^{-2} yr^{-1})	**DOC** (g C m^{-2} yr^{-1})
Mer Bleue, Canada *Ombrotrophic bog* *Roulet et al. 2007*	-21.5 ± 39.0	-40.2 ± 40.5	3.7 ± 0.5	14.9 ± 3.1
Degerö Stormyr, Sweden *Minerogenic Fen* *Nilsson et al. 2008*	-24 ± 4.9	-51.5 ± 4.9	11.5 ± 3.5	17.7 ± 3.7
Glencar, Ireland *Blanket bog* *Koehler et al. 2011*	-29.7 ± 30.6	-47.8 ± 30	4.1 ± 0.5	14.0 ± 1.6
Stordalen, Sweden *Permafrost palsa mire* *Olefeldt et al. 2012*	-44.5 ± 16.3	-50 ± 17.0	2.0	3.2 ± 0.6

Fluxes are sensitive to variations in environmental conditions with immediate responses to changes in solar irradiance, and lagged responses to changes in temperature and moisture in the air or soil (Alm et al. 2007a; Kettunen 2003).

The sensitivity of biological processes such as heterotrophic respiration is widely measured by the Q_{10} temperature coefficient (Mundim et al. 2020). A study by Liu et al. (2024), found that the Q_{10} of peat respiration differed significantly by climate zone (with boreal peatlands being the highest), as well as peatland type and C/N ratio. The authors noted that peat respiration in bogs had an average Q_{10} of 3.2 ± 0.3 (which was significantly higher than that of fens 2.4 ± 0.2), and that Q_{10} within the top 10 cm of peat was significantly lower than Q_{10} at greater depths. Wet conditions can reduce the Q_{10} of peat respiration if soil moisture content exceeds optimal conditions for microbial community functioning (Liu et al. 2024), which is estimated at 64% to 89% for peat soils (Kechavarzi et al. 2010).

2.1.6 Drivers of Peatland Loss and Future Mitigation

A study by Loisel et al. (2021) reported expert assessment on the importance of relevant drivers on the global peatland carbon balance over time, cross referenced with main findings from the literature. Drivers leading to rapid loss of peatlands included fire, land-use change, and permafrost thaw, while gradual drivers included temperature increase, water table draw down, sea-level rise, and nutrient addition. The authors found that the main causes of peatland carbon loss in the Anthropocene were land-use change (-23 to 0 Gt C in northern latitudes, and -14 to -2 Gt C in the tropics) and fire (-8 to 0 Gt C in northern latitudes, and -10 to 0 Gt C in the tropics) (Loisel et al. 2021).

It is anticipated that carbon loss drivers will be amplified during the remainder of this century (Loisel et al. 2021). Warmer and dryer conditions pose a risk for increased wildfire extents and frequencies across northern regions, disturbing peatland carbon stores (Harris et al. 2021). To mitigate peatland loss due to fires, wetland area reduction, and land-use change, better fire management practices should be implemented, and efforts to conserve and restore peatlands should be prioritized (Loisel et al. 2021).

2.2 Peat Extraction and Land-Use Impacts

In this section, I examine the consequences of peat extraction on peatland ecosystems, including changes in decomposition pathways, carbon stores, and biogeochemical processes. I also explore efforts to restore degraded peatlands, and the influence of restoration on carbon dynamics and GHG emissions. Understanding these impacts is critical to evaluating the broader environmental implications of peat extraction.

2.2.1 Land-Use Change

Peatlands can undergo land-use change through conversion to agricultural land, burning, or extraction of peat for fuel and horticultural purposes (IUCN 2021). The repurposing of these landscapes typically involves draining the peatland and removing the surface vegetation and upper peat layer, fundamentally altering the peatland's ecology and carbon cycling (Charman 2009).

Peatlands are selected for active harvesting of peat moss for anthropogenic use (details in §2.3.1) based on quality, peat depth, surface area, and other social, economic and cultural factors (e.g., proximity to infrastructure) (CSPMA 2022). Peat was traditionally harvested through block cutting, a method where human labour or machinery removes 200 m x 10 m peat blocks from large trenches (Waddington et al. 2009). Over the past four decades, vacuum harvesting has become more common, particularly in Canada (Waddington et al. 2009). To prepare a site for vacuum-harvest, a main drainage ditch is dug along the site's perimeter, along with shallower parallel drainage channels that subdivide the site into fields. The surface vegetation is removed to expose the underlying peat, and the top layer of peat is loosened, dried, and extracted using specialized machinery (see Methods §3.1 for more details) (CSPMA 2022).

2.2.2 Decomposition and Changes to Peatland Biogeochemistry

In both natural and disturbed peatlands, microorganisms decompose organic matter to drive the biogeochemical cycling of carbon. Altering the ecological and environmental conditions of a peatland also alters the presence of microorganisms and their functioning, which in turn impacts GHG emissions.

When peatlands are drained to lower the water table and dry the surface peat layer for extraction, previously saturated peat becomes more aerated, and historically stable carbon is released to the atmosphere via aerobic decomposition (Hooijer et al. 2011). While CO_2 emissions rise due to this rapid decomposition, CH_4 emissions from slower anaerobic decomposition decrease due to reduced methanogen activity and increased methanotrophy in the drained oxic peat layer (Huang et al. 2021). Figure 2.2 demonstrates a timeline of the effects of peat drainage (Page et al. 2011), where aerobic decomposition becomes the dominant decomposition pathway (Trettin et al. 2006).

CO_2 emissions are generally highest in the first 5 years following site drainage, after which sites emit CO_2 at a lower rate regardless of their age (Clark et al. 2023; Hooijer et al. 2011). The reduction in emissions is due to diminished peat depth, decreased availability

of easily decomposed substrates, and the loss of microbial biomass from the extracted layers (Andersen et al. 2006).

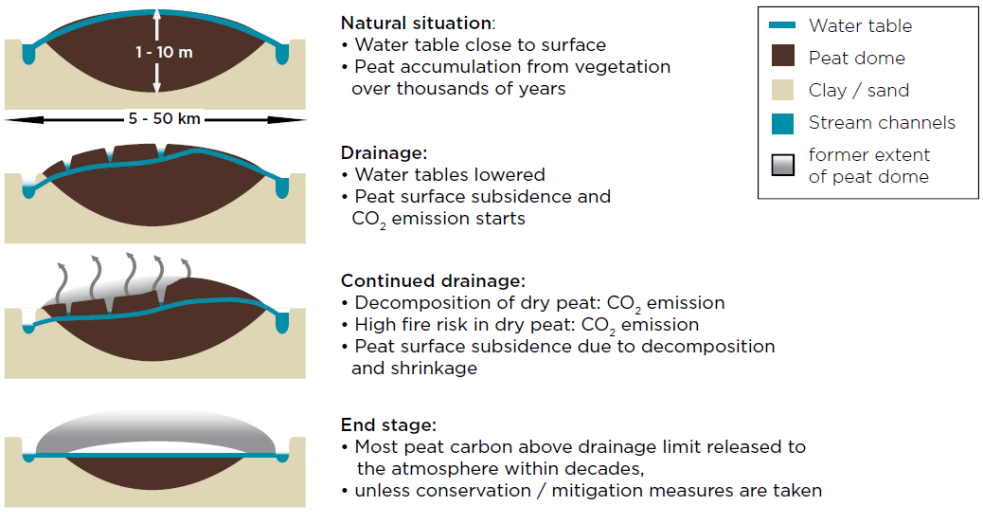

Figure 2.2: Effect of peat drainage on a peatland dome (Page et al. 2011 adapted from Delft Hydraulics 2006).

Basiliko et al. (2013) found horticultural peat extraction strongly impacted substrate availability and rates of carbon mineralization, enforcing that changes in conditions brought about by land-use change are important considerations in peat decomposition. In extracted peat sites, it is primarily the biogeochemical properties of peat such as the C/N ratio (or quality), soil pH, nutrients, and the humification index, as well as environmental conditions such as temperature, moisture, and oxygen availability that affect the decomposition rate of peat (Waddington et al. 2009).

2.2.3 Carbon Stores and Fluxes in Extracted Peatlands

The vegetation removed to prepare a peatland for extraction results in a one-off loss of the carbon stored in plant biomass (Hooijer et al. 2011). As biomass production is eliminated and heterotrophic respiration dominates, NPP becomes zero and the ecosystem shifts from a net carbon sink to a carbon source (McNeil & Waddington 2003).

Drained peatlands are responsible for approximately 1.9 gigatons of CO_2 annually, which corresponds to 5% of global anthropogenic greenhouse gas emissions (IUCN 2021). One study found no detectable methane emissions from extracted sites (Andersen et al.

2006), while another reported some, though in much smaller quantities than CO_2 from extracted sites and CH_4 from natural peatlands (Clark et al. 2023). Nitrous oxide (N_2O) emissions are generally low in natural peatlands. However, drainage and other anthropogenic disturbances can trigger greater releases of N_2O, another potent GHG (Joosten & Couwenberg 2008; Strack 2008).

A study in Finland estimated the range of total fluxes from an actively harvested peatland area to be between 1928 to 2635 g CO_2 eq m^{-2} yr^{-1} for summer months, and 2459 to 3697 g CO_2 equivalent m^{-2} yr^{-1} for winter months (Alm et al. 2007b). However, emissions can be up to 3000 g CO_2 m^{-2} yr^{-1} higher than average when high temperatures are coupled with adequate soil moisture conditions (e.g., wet, warm summers) (Alm et al. 2017b). Wilson et al. (2015) advanced the understanding of greenhouse gas emissions from peatlands managed for extraction in temperate regions, specifically Ireland and the UK. The study derived region-specific emission factors for carbon dioxide (CO_2-C), highlighting significant variations compared to the default Tier 1 values provided by the IPCC. By demonstrating lower emissions (1.70 ± 0.47 and 1.64 ± 0.44 t CO_2-C ha^{-1} yr^{-1} for industrial and domestic sites, respectively) than the Tier 1 factor (2.8 ± 1.7 t CO_2-C ha^{-1} yr^{-1}), the authors emphasized the need for refined Tier 2 reporting to reduce uncertainties and improve accuracy. Moreover, the work highlighted the role of site-specific variables (such as soil temperature and land use) in controlling emissions, and expanded the global data set for peatland emission factors by incorporating nine sites in a previously underrepresented region (Wilson et al. 2015).

2.2.4 Peatland Restoration

Mined and extracted peatlands can continue to be carbon sources for years following operations if left abandoned without restoration efforts (Rankin et al. 2018). Through the re-introduction of key vegetation, including species within the *Sphagnum* genus, nutrient enrichment in surface layers, and the use of integrated structures to re-establish water retention, restored peatlands can return to a carbon functioning ability similar to that of an undisturbed peatland within 15 years of restoration (Nugent et al. 2019).

Extracted and restored sites tend to share similarities in their physiochemical characteristics (Andersen et al. 2006). Most of the microbial biomass found in the upper oxic peat layers is removed when the field is actively extracted, resulting in a 2 to 5-fold decrease in post-harvested sites (Croft et al. 2001) The remaining microbial communities differ greatly from their original structure (Croft et al. 2001; Artz et al. 2007), with profound long-term changes to methanogen and methanotroph communities (Andersen et al. 2006).

Enriching the surface layers with nutrients and easily metabolized compounds during restoration causes active microbiota to re-colonize the surface horizons, metabolizing the new organic material so quickly that subsurface layers remain more humified (made up of low quality, decomposed substrate) (Anderson at al. 2006). The microbial community can be restored in approximately three years post-restoration, as opposed to 20 years after abandonment (Anderson at al. 2006; Croft et al. 2001).

From an atmospheric perspective, these results are reflected in higher CO_2 emissions linked to the decomposition of newly added organic material, and very low CH_4 emissions during the initial years of restoration (Nugent et al. 2019). Approximately four years after the start of restoration efforts, Nugent et al. (2019) observed a decline in decomposition losses, increased productivity, and increased CH_4 emissions. This demonstrates a time lag between restoration and the return to pre-disturbance CH_4 emissions. During this time, carbon accumulation rates (biomass production) exceed GHG emissions (from respiration), transitioning the system back to a carbon sink (Nugent et al. 2019). Therefore, post-extraction peatland restoration is key to minimizing carbon loss to the atmosphere, while continuing to gain the economic benefits of peat extraction (Rankin et al 2018).

2.3 Prevalence of Global Peat Extraction and Use

This section explores the widespread use of peat as a natural resource, with a particular focus on its importance in horticulture. I discuss global peat extraction trends, with special attention to the Canadian context, and consider the importance of accurate GHG accounting.

2.3.1 Peat as a Natural Resource

The anthropogenic use of peat can be separated into three main categories: energy peat, horticultural peat, and other (Figure 2.3).

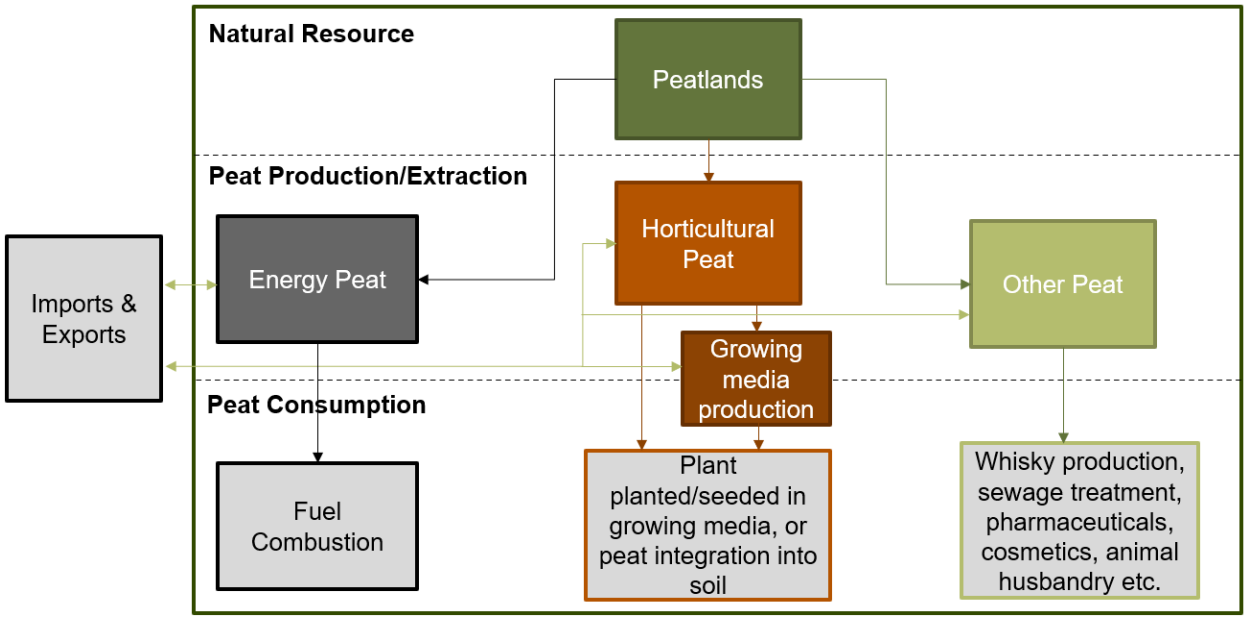

Figure 2.3: Overview of peat-flows for natural resource extraction and use.

Energy peat, which has decreased substantially in recent years, refers to peat being extracted as an energy source. Energy peat is considered consumed once it has been combusted (Hirschler & Osterburg 2021). However, since peat is the first step in the formation of coal, it is a relatively inefficient fossil fuel (Peters & von Unger 2017).

Horticultural peat production (also referred to as extraction) refers to peat being extracted for use as a growing substrate (i.e., for food production and ornamentals) or for soil fortification in the professional and hobby horticulture market. Peat can be further processed to produce growing media in an intermediate step. This type of peat is considered consumed when a plant is planted or seeded in the growing media, or when peat is integrated into the soil (Hirschler & Osterburg 2021).

Lastly, other peat production refers to peat being extracted for purposes other than horticulture or energy. This represents the smallest percentage of peat production that is consumed for whisky production, bio-filtration, cosmetics, pharmaceutical products, animal husbandry etc. (CSPMA 2022b).

2.3.2 Importance of Horticultural Peat

The substrate industry has its origins in the early 20th century, but large-scale extraction began in the 1960s (Kitir et al. 2018). Thanks to its physical, chemical, and biological properties, peat offers unique reliability in crop cultivation that is currently unmatched by other raw materials (IPS 2021). Notably, its high-water retention, nutrient-holding capacity, and favorable particle size distribution contribute to enhanced biomass production, particularly under controlled cultivation conditions (Blok et al. 2021; Choi et al. 2019). Peat can also be tailored to meet specific crop needs (Cleary et al. 2005). For example, the composition of peat can be altered with different sieving techniques, its pH can be precisely adjusted through lime addition, and nutrient ratios can be adjusted (IPS 2021).

Although there are existing alternative substrate options such as green compost, wood fibre, perlite, and coconut coir, peat-based substrates consistently outperform alternatives in maintaining shoot and root growth (Choi et al. 2019), supporting beneficial microbial populations that enhance plant growth, and providing an ideal balance between water retention and aeration for overall plant performance (Block et al. 2019). Peat's consistency across batches ensures uniform physical and chemical properties, reducing variability in cultivation outcomes compared to alternative substrates (Blok et al. 2019). However, studies also highlight the potential for partial peat substitution (i.e., up to 40%) with sustainable alternatives while still achieving reasonable plant performance, albeit with some compromises in growth metrics such as shoot biomass and reproductive output (Choi et al. 2019; Campos Mota et al. 2007). In fact, many alternative growing substrates are hybrid mixtures, of which peat is still a major constituent (Fascella 2015).

Ireland is one of the few countries that has reported on specified values of horticultural peat use by various sectors, distinguishing between mushroom casing (approximately 70 kt yr^{-1}, 29% total Irish horticultural peat use), professional horticulture (12.7 kt yr^{-1}, 15%), and hobby market use (158 kt, 56%) (Prasad 2021; units converted from m^3 using Hirschler & Osterburg 2022 density factor of 0.338 t m^{-3} for Ireland). The same report also estimates that within professional horticulture peat requirements, 71.4% is used for ornamentals, while 28.6% is used to for fruits and vegetables (Prasad 2021).

2.3.3 Global Context

Almost all energy-peat produced (98%) is consumed within the borders of the country that produced it, while the opposite is true for horticultural and other peat, where 97% is exported to be consumed outside of the producing countries borders (Hirschler & Osterburg 2021). From 2012-2020, more than 80% of global peat extraction took place in the EU (Hirschler & Osterburg 2022; verified with USGS 2020; USGS 2022; USGS 2024 data), and a large majority (89%) was traded within it for consumption (Hirschler & Osterburg 2021). Other notable peat producers included Canada (approximately 4.5% of global production) and Russia (approximately 3.3%) (calculated from USGS 2018 & USGS 2020 data). From 2013 to 2017, major energy-peat producing/consuming countries included Finland (39% of total EU peat-energy production and consumption) and Ireland (37% of EU production and consumption), producing/consuming more than 2.5 times as much energy-peat than other EU countries (calculated from Hirschler & Osterburg 2022 data). Major non-energy peat producing countries included the Baltic states (40% of total non-energy peat production in the EU) and Germany (25%) (Hirschler & Osterburg 2022). Germany was also a top non-energy peat consumer (17% of total non-energy peat consumption) along with the Netherlands (15%) (Hirschler & Osterburg 2022).

The carbon content of decomposed peat is considered irrecoverable in the 30 years required to prevent major climate impacts (Goldstein et al. 2020). Increasing recognition of the biogeochemical role of peatlands in global carbon cycling and their importance in climate mitigation has sparked backlash from NGOs, governing agencies, and the public to limit further land-use change in natural peatlands, especially for energy-peat production (Peters & von Unger 2017). Commercial horticulture still heavily relies on peat worldwide (Prasad 2021), but initiatives to phase out peat use have been launched across the entire EU, with the aim of extending regulations to eliminate its use as a growing media over time (IPS 2021).

Ireland (the second largest producer/consumer of energy-peat after Finland) has become particularly attentive to its peat extraction and use within the last decade. In 2019, they began requiring Environment Impact Assessment and planning permission for peat

production on areas greater than 30 hectares, which had historically been exempt from these regulatory processes. Then in 2021, all formal peat mining operations in Ireland ended (IPS 2021; USGS 2022). Germany, with only 5% of its natural peatlands remaining, has also adopted new policies to stop additional peatland degradation and phase out horticultural peat (Peters et al. 2019).

By compiling USGS yearly reports on the worldwide flow of peat (Table 2.2), I've estimated that increased regulations and pushback on peat extraction have resulted in a 24% reduction in annual global peat extraction in 2024 relative to 2018 (data from USGS 2020; USGS 2022; USGS 2024). However, these changes have had major implications for the global peat extraction landscape, and not all countries have decreased production. Notably, peat extraction increased by 94% in Canada, 75% in Russia, and 57% in Poland in 2024 relative to 2018. In Ireland, Finland and Germany, 2024 production decreased by 100%, 42%, and 32% relative to 2018, respectively.

Table 2.2: Peat production for top peat producing countries and world total from 2018-2023 in thousand metric tons (kt), ordered by largest positive percent change to largest negative percent change over the period.

Country	**2018**	**2019**	**2020**	**2021**	**2022**	**2023**	**% change over period**
Canada	1240	1300	1400	1300	2390	2400	94
Russia	800	800	1000	1000	1400	1400	75
Poland	700	700	900	900	1100	1100	57
Latvia	1900	1900	2000	2100	2440	2400	26
Estonia	1030	1000	1060	1100	1130	1100	7
Sweden	2450	2500	2400	2400	2560	2500	2
Belarus	2620	2600	2590	1900	2300	2300	-12
World total	30400	30000	28900	27000	23600	23000	-24
Germany	3800	4000	2300	2300	2600	2600	-32
Finland	9970	10000	12000	12000	5870	5800	-42
Ireland	3000	3000	1300	0	0	0	-100

2.3.4 Canadian Context

Peatlands in Canada cover approximately 119.4 million hectares, representing 12% of the country's total land area (UNEP 2022). Globally, Canada holds 25% of the world's peatlands, a proportion surpassed only by Russia (29%) and far exceeding that of other countries, with the closest being the U.S. (8%), Brazil (5%), and Indonesia (4%) (UNEP

2022). Approximately 30,900 hectares of Canadian peatlands are actively harvested, equating to less than 0.03% of the total peatland area (CSPMA 2017). Despite this relatively small proportion of extracted peatlands, there is a need to include GHG emissions from Canadian peatlands in Earth system models to predict future climate change (Harris et al. 2021). The sample size for GHG flux measurements for peatland types and disturbances across Canada is limited (Harris et al. 2021; Webster et al. 2018). Therefore, improved quantification and reporting of peatland carbon stocks and emissions are required to fill key knowledge gaps (Harris et al. 2021).

In 2022, Canada exported 1,458,055 kt of peat worldwide, valued at over 500 million USD (UN Comtrade Database 2024). Although peat extraction has decreased or ceased in several European countries, their imports of horticultural peat from Canada have risen. For example, average annual peat imports from Canada to Ireland between 2020 and 2022 (9,673 kt) were more than double the average annual imports between 2016 and 2018 (3,847 kt) (UN Comtrade Database 2024). Similarly, Finland saw its average annual peat imports from Canada increase from 18–40 kt in previous years to 200 kt in 2020–2022 (UN Comtrade Database 2024; Hirschler & Osterburg 2022). Despite the reduction in peat extraction within the EU, demand for peat remains high, with Canadian extraction companies increasingly stepping in to meet this need.

2.3.5 Greenhouse Gas Accounting

Under the United Nations Framework on Climate Change (UNFCCC) guidelines, countries must report on anthropogenic greenhouse gas emissions (mainly CO_2 and CH_4), which includes changes due to land use, of which peat extraction for horticultural purposes falls under the wetland category (UNFCCC 2014). Accounting for GHG emissions originating from disturbances to biogeochemical cycles is challenging. To ease this process, the Intergovernmental Panel on Climate Change (IPCC) has put forward three tier levels for estimating emissions: Tier 1 uses default IPCC emission factors with spatially coarse per area and activity data; Tier 2 uses the same approach as Tier 1, but with country-specific emission factors and high-resolution land area data; and Tier 3 uses models, inventory

measurement systems, and high-resolution activity data (IPCC 2006). Countries are encouraged to use Tier 2 and 3 whenever possible for more accurate accounting.

2.4 Towards Refined Greenhouse Gas Accounting

This final section focuses on improving GHG accounting in extracted peatlands through direct measurements, particularly by addressing overlooked emission sources. I review recent studies on field and ditch fluxes, discuss the complexities of stockpile emissions, and emphasize their contribution to overall GHG outputs. The goal of this section is to identify gaps in current knowledge that provide context for my research objectives.

2.4.1 Direct Measurement of Extracted Peatland Field and Ditch Fluxes

A major source of uncertainty in carbon flux accounting for extracted peatlands is the differing temperature sensitivity of heterotrophic soil respiration in the northern and southern hemispheres, which can lead to inaccuracies when extrapolating fluxes based on regional weather patterns (Alm et al. 2007b). To address this, a number of studies have been undertaken to provide a more comprehensive assessment of regional net changes in GHG fluxes and carbon stores in extracted peatlands (summarized in Supplementary Data 1 in He & Roulet 2023). GHG emissions from extracted peatlands are composed of the peat fields ("extraction site"), drainage ditches, and stockpiled peat (Wilson et al. 2015). Below I discuss four studies from actively harvested sites, where emissions from both fields and drainage ditches were quantified.

Nykanen et al. (1996) measured fluxes at two mined peatlands in Finland. From 1991 to 1992, they measured emissions from the fields ("site") only, using clear chambers (typically used for sites with vegetation) over the span of a full year. From 1993-1994, they measured emissions at a new peat mining site subdivided into recently started, old, and cut-away, using an opaque chamber over summer months. Sundh et al. (2000) collected flux data at six different harvested peatlands (including both an old and newly opened site) every second week from June to September in Sweden in 1995. Clark et al. (2023) measured fluxes at an actively vacuum-harvested site near Riviere-du-Loup, Quebec between June and September in 2018, 2019, and 2020. This study assessed spatial

differences in GHG fluxes within peat fields separated by ditches, and between sectors that had been in active harvesting for a range of years. Following the methodology of Clark et al. (2023), Hunter et al. (2024) measured flux data at an actively vacuum-harvested site near Drayton Valley, Alberta, twice a week between the months of May and August in 2019, 2021, and 2022.

In all four studies, CO_2 emissions from fields and ditches were comparable, while methane emissions were higher for the ditches relative to the fields (Table 2.3).

Table 2.3. Comparison of carbon emissions from fields and drainage ditches from four actively extracted peatland studies using closed chamber measurements.

Location	**CO_2 emissions** ($g\ CO_2\text{-}C\ m^{-2}\ day^{-1}$)	**CH_4 emissions** ($mg\ CH_4\text{-}C\ m^{-2}\ day^{-1}$)	**Source**
Fields	0.13–2.95	0.7 (average)	Nykanen et al. 1996
	0.40–1.49	0.2–18.0	Sundh et al. 2000
	0.9 (± 0.06)	9.2 (± 4.0)	Clark et al. 2023
	1.22	3.13	Hunter et al. 2024
Drainage ditches	0.17–0.60	7.5–897.6	Nykanen et al. 1996
	-0.73–1.05	19.8–449.4	Sundh et al. 2000
	2.05 (± 0.12)	72.0 (± 18.0)	Clark et al. 2023
	0.93 (wet), 2.93 (dry)	762 (wet), 3.13 (dry)	Hunter et al. 2024

Sundh et al. (2000) reported slightly higher methane fluxes at the newly opened site than at the old one. Similarly, Clark et al. (2023) found that CO_2 fluxes were highest at the most recently opened sector (with no differences in methane fluxes). They also found a spatial effect for the 2016 (youngest) sector, where CO_2 emissions were highest from the center of the field and decreased towards the drainage ditches. Hunter et al. (2024) did not find a significant spatial effect on CO_2 or CH_4 emissions along the transect at their 2017 (youngest) site, and differences in emissions between sector ages were inconsistent between study years. Differences in precipitation between eastern and western Canadian regions leads to eastern peat fields being contoured whereas western peat fields are kept flat. Clark's results pointed out that age of exposed peat influences the GHG fluxes measured. Hunter's was the first study to compare the fluxes based on ditch moisture levels, finding dry (without standing water) ditch CO_2 and CH_4 emissions significantly greater than those from wet ditches and fields (Hunter et al. 2024).

While ditches emit 2 to 10 times more methane than the fields, they account for only 2-6% of total site area (Clark et al. 2023; Hunter et al. 2024), contributing approximately 1-3% of total site emissions (Nykanen et al. 1996; Sundh et al. 2000).

2.4.2 Convoluted Documentation of Stockpile Fluxes in the Literature

Another major source of uncertainty comes from a lack of data on the contribution of peat stockpiles to overall extracted site emissions (Penman et al. 2003). Only the study by Ahlholm & Silvola (1990) in Finland quantified and reported emissions from extracted peat stored in stockpiles directly, finding average emission rates of 19.66 g CO_2-C m^{-2} day^{-1}. The study by Nykanen et al. (1996) directly measured field and ditch emissions in harvested peat areas, but also considered stockpiles in their annual site emission estimates using Ahlholm & Silvola's (1990) stockpile CO_2 fluxes. A later study by Alm et al. (2007b), simulated annual emissions from peat harvesting areas and stockpiles using data from Ahlholm & Silvola (1990), Nykanen et al. (1996), and their own data for stockpile emissions. Details surrounding their data collection, how winter stockpile emissions were derived, and how annual stockpile emissions were extrapolated in their simulation are not included in the manuscript. Stockpile methane emission rates were reported at 0.002 g CH_4-C m^{-2} day^{-1} in the summer and 0.16 g CH_4-C m^{-2} day^{-1} in the winter, and N_2O values from stockpiles were very small (<0.1 g CO_2-eq m^{-2} day^{-1}) (Alm et al. 2007b).

A more recent study by Waddington et al. (2009) simulated peat stockpile characteristics in a laboratory incubation experiment (using various anticipated moisture and temperature levels) to estimate stockpiles emissions from vacuum harvesting and block cutting extraction methods. They found that stockpiles emitted approximately 0.198 g CO_2-C m^{-2} day^{-1}, which was greater than vacuum-harvested field emissions, and greater than block cutting stockpile emissions. However, since these values were not directly measured from stockpiles, they are not easily comparable to those from Ahlholm & Silvola (1990).

There appears to be some disparities in the limited literature regarding stockpile CO_2 emission rates centered around the studies by Ahlholm & Silvola (1990), Nykanen et al.

(1996), and Alm et al. (2007b) (Table 2.4), which may have led to errors in estimating the contribution of stockpiles to overall site emissions and GHG accounting.

Table 2.4: Comparison of peat stockpile fluxes in the literature (non-exhaustive). The table presents data from key studies on reported stockpile flux rates, converted flux rates in common units (g CO_2-C m^{-2} day^{-1}), and the source attributed for each reported value.

Study	**Reported Flux Rate & Units** (as stated in text)	**Converted Flux Rate** (g CO_2-C m^{-2} day^{-1})	**Source Attributed** (for reported value in text)
Nykanen et al. 1996	3000 mg CO_2 m^{-2} hr^{-1}	19.66	Ahlholm & Silvola 1990
Waddington et al. 2009	3 g CO_2 m^{-2} hr^{-1}	19.66	Ahlholm & Silvola 1990
Alm et al. 2007b	2.12–3.12 g CO_2 m^{-2} hr^{-1}	13.89–20.44	"New data in Finland" (uncited)
Alm et al. 2007b	83 g CO_2 m^{-2} day^{-1} Average (summer)	22.66	Ahlholm & Silvola 1990, Nykanen et al. 1996 & their own study
Alm et al. 2007b	139 g CO_2 m^{-2} day^{-1} Average (winter)	37.95	Nykanen et al. 1996 & their own study
Statistics Finland 2006	1750 kg CO_2 eq ha^{-1} yr^{-1}	0.13	Nykanen et al. 1996, corrected with IPCC 1995 GWP
Lapvetelainen et al. 2007	1750 kg CO_2 eq ha^{-1} yr^{-1}	0.13	Statistics Finland 2006
Statistics Finland 2024 *1. 1990-2014* *2. 2015 onwards*	1. 293,955 kg CO_2 eq ha^{-1} yr^{-1} 2. 325,125 kg CO_2 eq ha^{-1} yr^{-1}	1. 21.99 2. 24.32	Based on Nykänen et al. 1996 & Alm et al. 2007b

The 2006 report on Finland GHG emissions from 1990-2004 cites Nykanen et al. (1996) for the reported stockpile emission factor. However, the value listed is two orders of magnitude smaller than the value used by Nykanen et al. (1996), originally from Ahlholm & Silvola (1990). A 2007 study then used this value in its system for estimating peat-based emissions for the Finland Greenhouse Gas Inventory (Lapveteläinen et al. 2007). In the most recent Statistics Finland GHG inventory report from 2024, both Nykanen et al. (1996) and Alm et al. (2007) are cited, and more details regarding how annual calculations were extrapolated are provided. These revised emission estimates are more aligned with others from the literature.

According to Nykanen et al. (1996), stockpiles contributed approximately 16% to total site emissions. Based on findings from Alm et al. (2007b), where 5-10% of the harvest

area was considered occupied by stockpiles, I calculated that the contribution of stockpiles to overall emissions ranged from 41% to 60%. This calculation used the average CO_2-eq totals for fields and stockpiles, alongside the estimates for total site CO_2-eq during the summer and winter. Lastly, Statistics Finland (2024) estimates that stockpiles occupy 2% of the harvest area and contribute around 40-46% to CO_2 emissions from harvested areas.

In summary, all direct measurements of stockpile fluxes trace back to a single study conducted in 1990, revealing a significant gap in our understanding of peat stockpile emissions. Additionally, specifics on what was measured, or indication that units were converted, are not always clearly outlined. As such, conversion errors in flux units may contribute to the variations reported in the literature, resulting in confusion about what is known for certain regarding stockpile emissions and their contribution to overall extraction site emissions.

2.4.3 Literature Review Summary and Filling Knowledge Gaps

In their natural state, peatlands serve as net carbon sinks. However, human alterations to peatlands, particularly through drainage and the removal of vegetation, significantly impact biogeochemical processes, transitioning them into net carbon sources.

Growing acknowledgment of the importance of peatlands in mitigating the climate crisis has led to increased regulations on peat extraction, especially in the EU, where many peatlands have been degraded. While energy-peat is slowly being phased out of the top producing/consuming EU countries, demands for horticultural peat are being met by increased imports from other countries, such as Canada and Russia.

Canada is home to 75% of all North American peatlands (UNEP 2022) where approximately 0.03% (30,900 hectares) of these peatlands have been or are currently being harvested (CSPMA 2017). Canada is required to report on land use emissions, which includes peat extraction. New research stemming from collaboration between the peat industry (CSPMA), academic institutions, and the government, is accelerating the move towards Tier 3 emission factors for Canadian GHG accounting (He & Roulet 2023).

To date, studies quantifying GHG emissions from actively extracted peatlands have primarily focused on fields and ditches. As a result, the effects of peat extraction management practices on overall site emissions remain unclear. Specifically, the influence of field operations (i.e., before and after harrowing and vacuum harvesting) on surface peat and field GHG emissions has yet to be quantified. Stockpile emissions are also poorly understood, with many reports identifying them as a significant knowledge gap (e.g., Penman et al. 2018; Wilson et al. 2015; Sundh et al. 2000). Moreover, the effects of covering peat stockpiles with impermeable reflective tarps—a common management strategy—have not been scientifically investigated.

My research addresses these gaps by evaluating the impacts of peat extraction management practices, including timing of operations and stockpile management, on GHG emissions. Through direct flux measurements and an investigation of decomposition drivers, my work aims to refine Canada's GHG inventory reporting for managed peatlands under the UNFCCC, and guide the peat industry toward more sustainable practices.

Chapter 3: Methods

In this chapter, I outline the methods used to address all three of my research objectives, including data collection, processing, and statistical analysis. I begin with a detailed overview of the study area and peat extraction management practices. Following that, I describe the methods for measuring and evaluating fluxes from both field operations and stockpiles, along with stockpile CO_2 and CH_4 storage. Finally, I explain my approach to estimating the contribution of stockpiles to overall site CO_2 emissions.

3.1 Study Area

In this section, I provide the regional context for peat extraction history, site preparation, and operations. I also introduce the two study sites and describe differences in their management practices. Lastly, I present the weather conditions during the study period along with the historical climate data for the region.

3.1.1 History of Regional Peat Extraction

The study was conducted at two actively extracted peatlands 450 km northeast of Montreal, near Rivière-du-Loup, Quebec, Canada. The area, east and south of the town, was once characterized by a large treed ombrotrophic bog ecosystem complex. Known to be one of the largest and most important peat deposits in Quebec, its area and depth were documented as early as 1864 (Risi et al. 1953). By 1914, the bog covered 7,220 acres with an estimated 3,926 acres of peat litter suitable for agricultural use (Anrep 1914, as cited in Risi et al. 1953). Peat extraction began in 1939, with the establishment of the first agricultural peat moss harvesting plants assigning economic importance to the bog (Risi et al. 1953; Robert 1965).

Currently, two companies extract peat to be used as growing media in horticulture from this altered bog, referred to here as Company A and Company B to maintain partial anonymity. Both enterprises have been in operation for over 60 years, significantly contributing to the region's economy.

3.1.2 Site Preparation

Both companies prepare fields for extraction by stripping surface vegetation and creating a drainage network of ditches to reduce surface peat water content to approximately 85% of the pre-disturbance value (CSPMA 2022). A main drainage ditch surrounds the perimeter of the extraction area, directing water to a settling pond adjacent to the site. Shallower, parallel drainage channels connect to the main ditch to further drain subsections of the extraction area, referred to as fields. Company A's fields are 500 m in length and 30 m in width, while Company B's field dimensions vary, but are on average 500 m by 25 m. At both sites, fields are contoured in a convex shape to enhance drainage, a common practice in eastern Canadian peat extraction (CSPMA 2022). Fields are grouped into sectors based on the year they were first prepared for extraction (commonly referred to as “opened”). The peat in each sector is graded by the industry based on a qualitative assessment of the level of humification (using a simplified Von Post Humification Scale). Higher grades are used in industrial horticulture, while lower grades are used in gardening mixes or water filtration.

3.1.3 Peat Extraction Operations

Peat extraction at the study sites occurs in four phases. First, a tractor drags a large rake to harrow the fields, separating the surface peat from the peat matrix below, creating what is referred to in this study as the surface layer or harrowed layer. Next, the surface peat is left to dry in its harrowed state. The drying phase duration depends on weather conditions and can last from six hours to several days. Once the upper layer is sufficiently dry (to approximately 50%; CSPMA 2022), a tractor with a different rake overturns the top layer of peat to further loosen it for harvest, a process known as conditioning. The conditioned phase also varies from one hour to several days, typically lasting 1-3 hours in good weather. Finally, large vacuum harvesters extract the loose top layer of peat. Fields are ideally harrowed immediately after harvest, but can be left in the vacuum-harvested phase for up to six hours. All phases are then repeated.

Due to the dependence on hot and dry weather conditions, the peat industry extracts as much as possible when conditions permit, necessitating storage until it can be

moved for further processing. The extracted peat is stored by dumping it from the vacuum harvesters, forming a pile at the edge of the fields near the access road, which is further structured by a tractor. Fields in the same sector are extracted simultaneously and stockpiled together. Peat from different sectors (with different industry qualities) is never mixed.

3.1.4 Study Sites and Management Practices

The study was conducted at two extraction sites, one owned and managed by Company A (Site A), and another by Company B (Site B), where data collection took place from May 22nd to November 5th, 2022. Site A was south of Highway A85, while Site B was northeast of the highway (Figure 3.1). Despite only being approximately 6 km apart, the management practices differed between the two sites, which benefited the study.

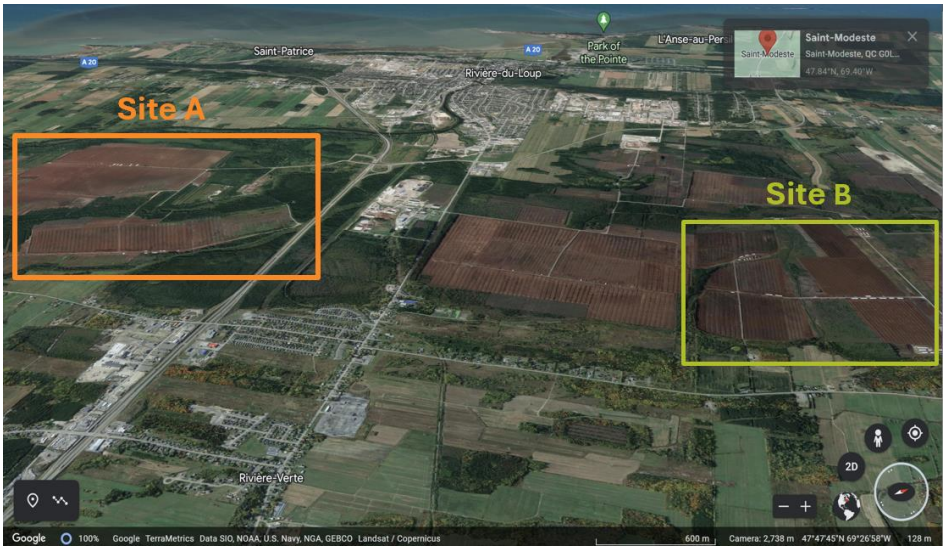

Figure 3.1: Study Sites A and B in Rivière-du-Loup, Quebec.

The operations at Company B are smaller, making it more feasible to coordinate with the Field Operations Supervisor on the timing of extraction operations to address my first objective. Consequently, data collection on field emissions for each extraction phase took place exclusively at Site B.

The main difference in management practices between the two companies pertains their stockpiles. The internal temperature of stockpiles must be closely monitored to ensure that they do not heat up past approximately 40 °C, avoiding the risk of spontaneous

combustion. Company A prefers to keep their stockpiles uncovered, allowing them to easily break up the pile to dissipate heat if it begins to build up at the center of the pile. Conversely, Company B covers their stockpiles with a tarp, believed to be impermeable to both liquids and gases. They aim to slow down the internal heating of stockpiles by increasing their albedo, covering the dark brown piles with a white tarp to reflect solar radiation rather than absorb it. With the outcomes of either strategy previously untested, this study collected data on uncovered stockpiles at Site A, and covered stockpiles at Site B.

3.1.5 Weather and Climate

Weather data was downloaded from the Riviere-du-Loup weather station, 2.3 km northwest from Site A (Environment and Climate Change Canada 2024a). From the beginning of May to the end of November 2022, the region experienced a total of 541 mm of precipitation. August and September were the dryest months, which was reflected through increased extraction activities. The warmest months were July and August, where hourly temperatures remained within a range of 9 to 29 °C. For the months of May to November, total precipitation and average daily temperatures in 2022 were compared to reported regional normals (Figure 3.2). These normals were calculated using data from 1981-2010 from the St. Arsene weather station (Environment and Climate Change Canada 2024b), approximately 21 km northeast of Site A.

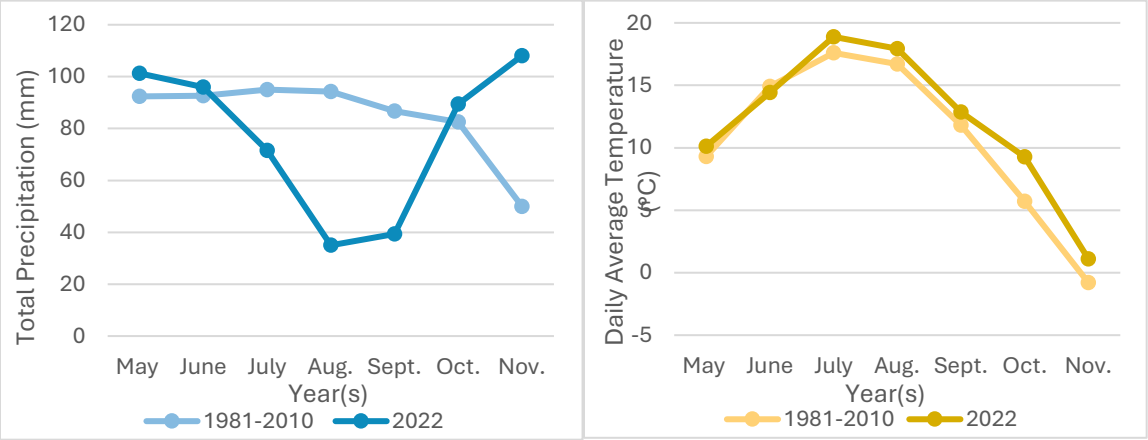

Figure 3.2: Comparison of 2022 weather data and normals calculated from 1981-2010 data, from May to November in the study region (Environment and Natural Resources Canada 2024). Left: total precipitation (mm), and right: average daily temperature (°C), by month.

Dominant wind speeds during the study period were between 15 to 24 km hr^{-1} in the southwest and south directions (Figure 3.3), with gusts up to 41-61 km hr^{-1}.

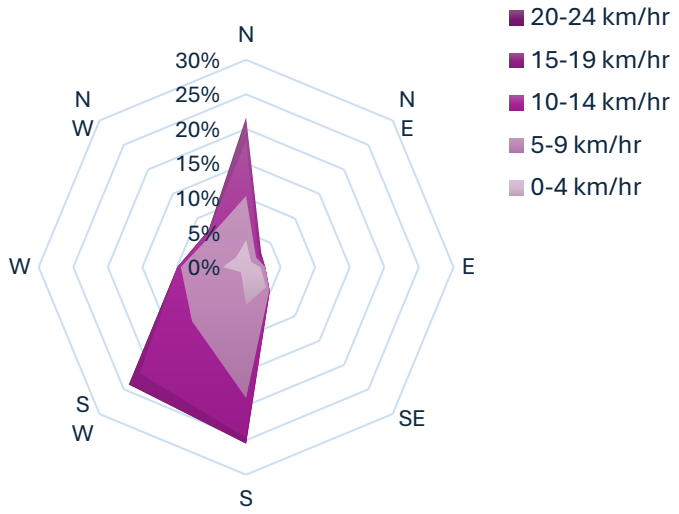

Figure 3.3: Windrose depicting average daily wind speed and direction in Rivière-du-Loup during the study period. Data from ECCC (2024).

3.2 Field Operations and Stockpile Fluxes

In this section, I outline the data collection methods used to measure fluxes and ancillary variables in extracted peat fields, as well as in uncovered and covered stockpiles. I then explain how this data was processed, and describe subsequent statistical analyses.

3.2.1 Field Operations Data Collection

3.2.1.1 Sampling Strategy

Due to frequent rainfall from May to July, field operations were limited at the start of the season, resulting in concentrated field flux data collection between August 21st and September 12th, 2022. Each sampling day, I coordinated with the Field Operations Supervisor to learn about scheduled operations and plan safe field flux measurements on available fields. On some occasions, measurements were taken immediately after a processing step (e.g., harrowing) by standing by the field during the operation. At other times, measurements were conducted hours or even days later. The ranges of time elapsed since the last operation for each extraction phase are shown in Figure 3.4.

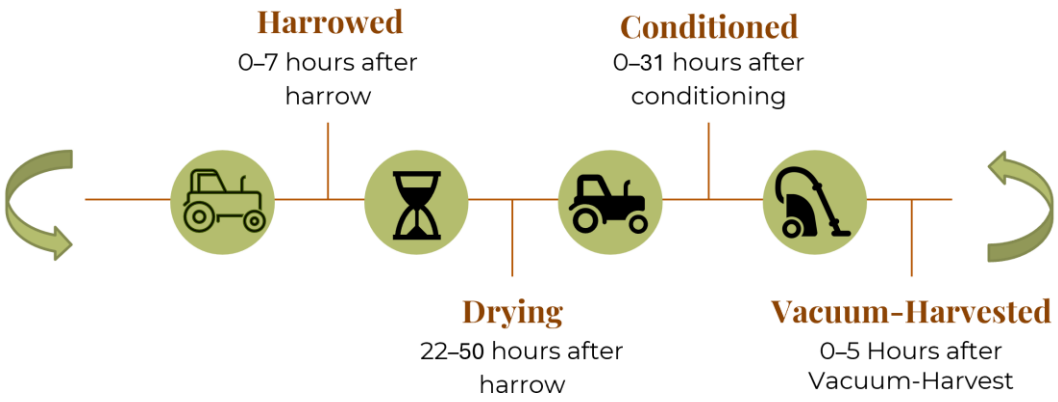

Figure 3.4: Peat extraction processing steps, and the ranges of time when fluxes were measured relative to the most recent operation.

Measurements were taken at five positions on each field, arranged in a cross pattern starting 30–40 m into the field (Figure 3.5). Each field required approximately 30 minutes to complete all five measurements. Typically, 3–6 adjacent fields in the same extraction phase and sector were sampled in succession, adding to variation in the time of measurement relative to the last operation. The sampled sectors were opened in 1960, 2011, 2012, 2013, and2015. This approach was informed by Clark et al. (2023), who found that CO_2 emissions in the most recently opened sector included in their study (in production for 2–4 years when sampled), were highest at the center of the field and gradually declined toward the ditches.

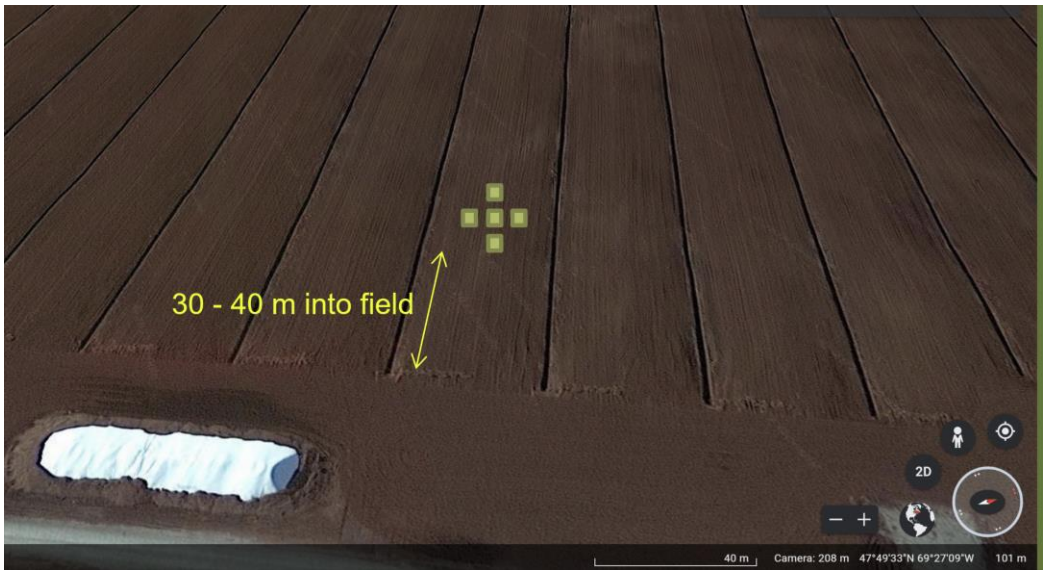

Figure 3.5: Example of the five measurement positions taken on a given field.

3.2.1.2 Closed Chamber Flux Measurements

To measure CO_2 and CH_4 fluxes from the peat field surface to the atmosphere, I employed the closed chamber method using an infrared gas analyzer (IRGA) (LI-7810, LI-COR Biosciences, Lincoln, NE).

At each measurement location, a metal collar was hammered into the field using a rubber mallet. Since the fields were actively undergoing extraction, collars could not be left in place. An opaque aluminum chamber (64 x 64 x 20 cm) equipped with an internal fan was held up to the atmosphere until ambient CO_2 and CH_4 levels for that day were reached. Ambient levels were determined using the lowest concentrations of CO_2 and CH_4 reported by the IRGA mobile software, which provided live readings as the chamber was held aloft for several minutes. Once ambient levels were established, the chamber was placed atop the collar, allowing air to flow from the chamber through tubing to the trace gas analyzer for a duration of four minutes. The initial air temperature, as well as the starting and ending CO_2 and CH_4 concentrations, were recorded. After completing the flux measurement, the chamber was removed, and the collar was relocated to the next measurement position in the field.

3.2.1.3 Ancillary Measurements

During the chamber measurement period, several ancillary measurements were taken, including the height from the ground to the top of the chamber and collar structure, the surface layer thickness, soil temperature and moisture, and samples for bulk density and gravimetric moisture content analysis.

At each chamber measurement: the distance from the ground to the top of the chamber and to the collar was measured at all four corners to calculate chamber-collar volume for each measurement; the surface layer thickness was determined using a transportable square grid; ten points were selected (five coinciding with surface layer peaks and five with troughs), and the depth at each point was measured with a ruler. After removing the collar, soil temperatures (°C) at 0, 10, 20, and 40 cm depths were recorded at every measurement position using a portable soil/compost thermometer (G1791,

Greisinger, Germany). Surface moisture was also measured as volumetric water content (VWC, %) at both a peak and a trough (denoted as 0 cm in depth) using a handheld soil moisture sensor (HydroSense II, Cambell Scientific, Edmonton, AB). At the center measurement location of each field (see Figure 3.5), additional temperature measurements were taken at 60, 80, and 100 cm depths, and moisture was measured at 20, 40, 60, and 80 cm depths. However, it was rarely possible to reach 80 cm of depth with the moisture probe. Therefore, it was excluded from subsequent analysis. As the soil moisture probe measures along two rods that extend 12 cm past the tip of the instrument (see §3.2.3.3 for more details), measurements at the surface represent the VWC integrated for the top 12 cm of the field, the depth of 20 cm represents the VWC from 20-32 cm in depth from the surface of the field, and so on.

Finally, for each sampled field, three surface peat samples were collected from within areas where the collar had been removed. Care was taken to minimize compression. A circular metal ring was inserted into the field (volume: 63.7 m^3) and a knife used to remove excess soil from overflowing from the top of the ring. A flat metal spatula was inserted directly underneath the ring when retrieving it from the ground. Samples were placed in labeled plastic bags and stored on ice in a cooler until they could be transferred to a refrigerator. Photos of the field equipment and setup can be found below (Figure 3.6).

Figure 3.6a: Field equipment used in field operations data collection (left probe: HydroSense II Handheld Soil Moisture Sensor, right probe: Greisinger G1791 Soil/Compost Thermometer, collar-chamber structure, & rubber mallet).

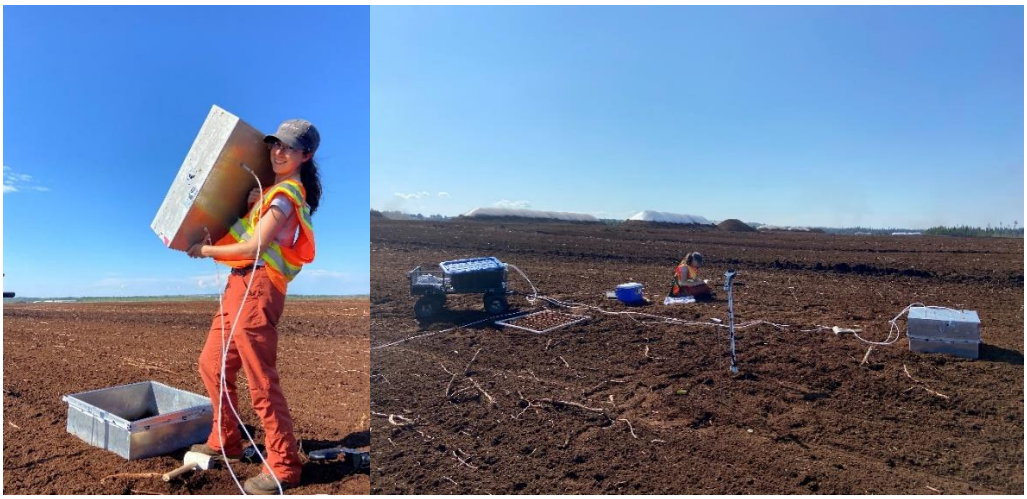

Figure 3.6b: Left: field assistant (C. Jones) holding up the chamber in preparation for a flux measurement. Right: example of flux measurement field setup.

3.2.2 Stockpile Data Collection

3.2.2.1 Uncovered Stockpiles

Uncovered stockpile flux measurements were collected from July 20th to November 3rd, 2022. Stockpiles were primarily selected at random, with a preference for those away from active operations and of regular size and shape. The piles varied in industry-designated grades, including Grades 2, 3, and 5. Fluxes were measured at the top and bottom positions at the center of each of the four pile faces, totalling eight flux measurements per pile (Figure 3.7). During each flux measurement, temperature (°C) at 0, 20, 40, 80, and 100 cm depths, and volumetric water content (%) at 0, 20, 60, 60, and 80 cm depths, were measured with the probes inserted perpendicularly to the surface of the stockpile.

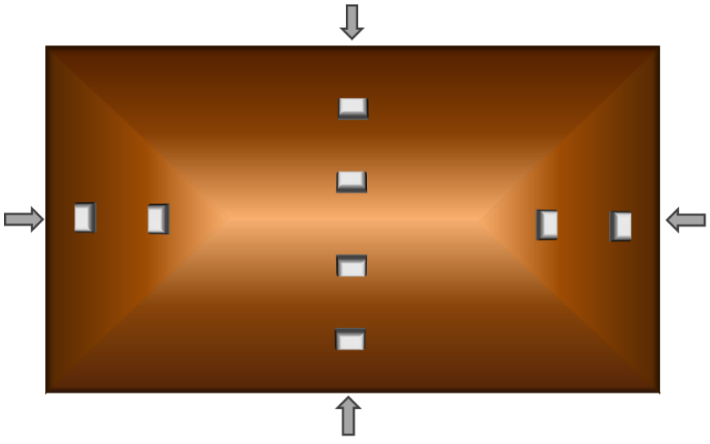

Figure 3.7a: Bird's eye view of eight uncovered stockpile flux measurement positions.

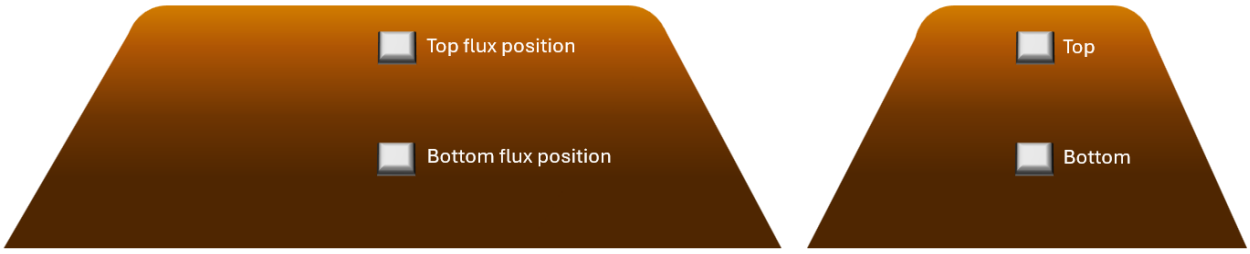

Figure 3.7b: Side view of flux measurement positions on the long (left) and short (right) faces of uncovered stockpiles.

Measurements were taken by a team of two. One person took notes and monitored equipment readings while dictating the workflow, and the other climbed the pile with the necessary equipment (flux chamber and probes), wearing snowshoes to minimize disturbance (Figure 3.8). The bottom position was always sampled first as climbing to the top position caused some disturbance below.

Figure 3.8: Uncovered stockpile flux measurements. Left: holding up the chamber to obtain ambient GHG concentrations, and right: taking temperature measurements next to chamber during a 4-minute flux measurement.

From July 22nd to August 24th, a metal collar was inserted by hand (and if necessary, hammered) into the stockpile, and the chamber was placed on the collar during measurements. However, due to challenges in achieving an even seal to prevent leakage, and the acquisition of a new chamber (61 x 61 x 22.5 cm) with an additional metal rim welded on an angle around the bottom 5 cm, we discontinued using the collar as of August 24th. Instead, the chamber was directly pushed into the stockpile. The dry, fluffy nature of

stockpiled peat allowed for a sufficient seal between the chamber and the stockpile to prevent leakage. Since chamber or chamber-collar dimensions were taken with each flux measurement, and their volumes are represented in the flux equation, fluxes from both methods can be treated similarly.

As with the field flux measurements, an opaque aluminum square chamber with an internal fan was held up to the atmosphere until ambient CO_2 and CH_4 levels for the day were reached. The chamber was then positioned (either atop the collar or directly on the stockpile) for air to flow from the chamber through tubing to the trace gas analyzer for four minutes. Initial air temperature, as well as starting and ending CO_2 and CH_4 concentrations, were recorded.

3.2.2.2 Covered Stockpiles

The sampling strategy for covered stockpiles differed because of their design. The steep and slippery surfaces, covered with a plastic-like tarp, made climbing difficult and posed a risk of damaging the covering. Additionally, taking measurements over a tarp required the closed chamber to be held in place for the full duration of the four-minute measurement, requiring the researcher to have secure footing. As a result, the top position was inaccessible for flux measurements. The bottom position was also inaccessible due to the tarp being anchored by peat piled over the edges at the bottom of the pile. Measurements were therefore taken from positions where the researcher could stand on the anchoring peat and hold the chamber against the tarp securely. This position was typically between where the top and bottom positions would be on uncovered stockpiles, although covered stockpiles were on average 1 m taller than uncovered ones. Covered stockpiles were also 15 to 30 m longer than uncovered ones, so three flux measurements were taken on each of the two long faces of the piles, in addition to one flux measurement on each of the short faces, totaling eight measurements per pile (Figure 3.9).

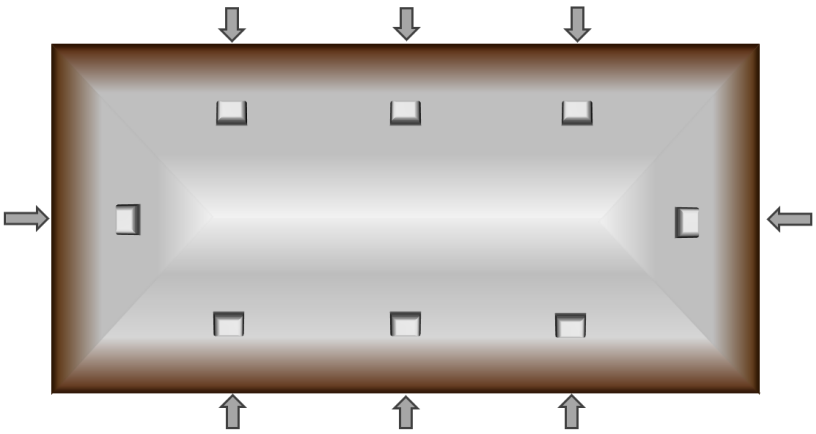

Figure 3.9a: Bird's eye view of eight covered stockpile flux measurement positions.

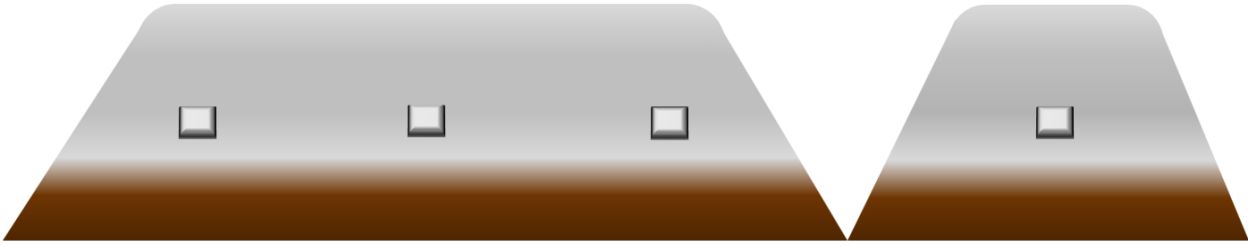

Figure 3.9b: Side view of flux measurement positions on the long (left) and short (right) faces of covered stockpiles.

Covered stockpile flux measurements were conducted between May 13th to July 13th, 2022. For each position, a measurement was first taken over the intact tarp. Holes are made on covered stockpiles to measure the internal temperature of the pile, after which they are left covered with tape. If a covered hole was present, a measurement was then taken over the covered hole, followed by a measurement over the open hole after removing the tape. If no covered hole was present, a hole was punctured (with the company's permission), and a measurement was taken over the new hole, which was then covered with industry-standard tape. Most regular sized covered stockpiles have a minimum of three covered holes.

Fluxes were measured using a different chamber than the fields and uncovered stockpiles. To avoid damaging the tarps, I covered a lightweight plastic container in aluminum foil, and used insulation foam to line the rim to create an airtight seal over the tarp when the researcher applied light pressure to keep it in place (Figure 3.10). Flux measurements then proceeded the same way as for uncovered stockpiles.

Figure 3.10: Left: flux measurement on covered stockpile, and right: chamber used for flux measurements on covered stockpiles.

Covered stockpile measurements were discontinued after July due to low average emissions (< 1 g m^{-2} day^{-1}) with little variation over the tarp. In contrast, open hole measurements indicated very high average emissions (> 450 g m^{-2} day^{-1}) with significant variation between measurements. However, these high values represented gases trapped under the tarp escaping from a small hole rather than true surface fluxes, and it was not possible to estimate the area underneath the tarp contributing to the leakage. Therefore, the study shifted focus to prioritize sampling the gas storage underneath the tarp (see §3.3) rather than continuing flux measurements for covered stockpiles.

3.2.3 Data Processing

3.2.3.1 Flux Measurement Adjustments

Flux data was downloaded from the IRGA at the end of each sampling day. Due to the length of the tubing between the chamber and the analyzer (which allowed greater mobility on stockpiles), there was a 22-24 second delay between the chamber being positioned and the start of the recorded measurement on the analyzer. I accounted for this delay as best as possible in my field notes, and the change in concentration over time for each flux measurement in this study was visually inspected and adjusted as needed.

Adjustments included removing erroneous data points caused by the tubing delay at the start and end of a measurement. Additionally, in a few instances where chamber leakage was observed (due to the chamber and collar not being fully sealed together), the slope from the first half of the measurement was used in subsequent calculations. All adjustments were documented, and they varied between measurements (including no adjustments necessary). In a small number of cases where the slope was very unstable, the measurements were excluded from the study. Examples of adjustments made based on graphs depicting change in concentration over time can be seen in Figure 3.11. The adjusted rates were used in subsequent flux calculations.

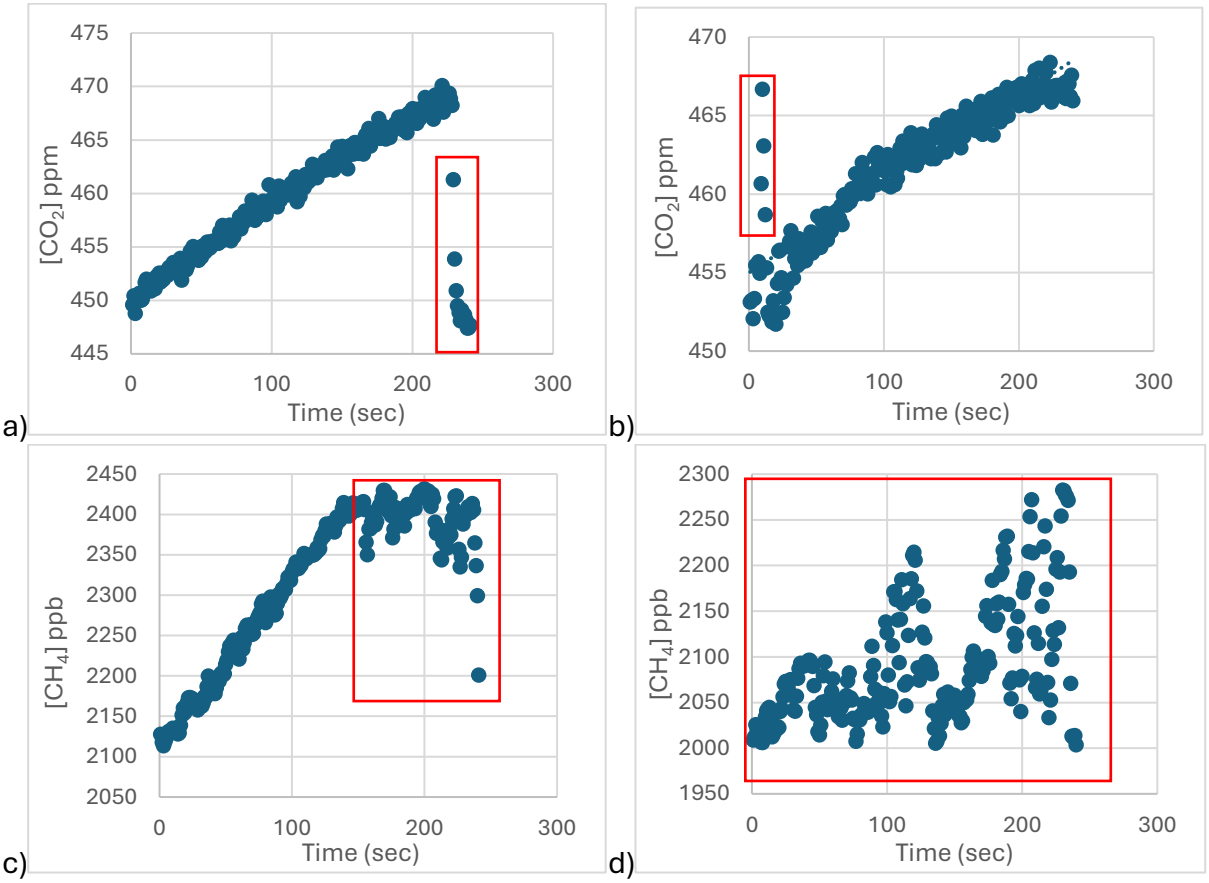

Figure 3.11: Examples of erroneous data points identified through visual inspection with excluded data points framed in red: a) last few seconds removed due to tubing delay, b) first few seconds removed due to tubing delay, c) last 1.5 min of measurement excluded due to chamber leakage, d) entire measurement excluded due to suspected error.

3.2.3.2 Flux Calculations

The flux (*F*; g CO_2-C m^{-2} day^{-1}; mg CH_4-C m^{-2} day^{-1}) was calculated following (Pelletier et al. 2011) using:

$$F = \left(\frac{f_x \cdot \left(\frac{V}{R \cdot T} \right) \cdot n \cdot t}{SA} \right) \cdot P_C \quad (3.1)$$

where f_x is the change in storage over time (ppm min^{-1} CO_2; ppb min^{-1} CH_4), R is the ideal gas constant (0.0821 L · atm $mol^{-1} \cdot k^{-1}$), T is the air temperature in the chamber at the time of measurement (Kelvin), n is the molecular mass of the gas (44.01 g mol^{-1} CO_2; 16.02 g mol^{-1} CH_4), t is the number of minutes in a day (1440 min day^{-1}), SA is the GHG emitting surface area contributing to the flux measurement (m^2; equivalent to either SA of chamber, or SA of collar if chamber-collar was used), Pc is the proportion of Carbon (0.273 for CO_2-C; 0.749 for CH_4-C) and V is the volume of chamber or chamber-collar (m^3). The volume (*V*) of the collar-chamber structure or the volume of the chamber alone when a collar was not used (e.g., for stockpile fluxes) was calculated as

$$V\ (m^3) = (SA \cdot h)_{collar} + \ (SA \cdot h)_{chamber} \quad (3.2)$$

where *h* is the average height (m) from measuring the four corners of the chamber and collar. In cases where a collar was used, the 2 cm of overlap between the chamber and collar were accounted for in the collar volume and subtracted from the chamber height.

3.2.3.3 Reliability of VWC Probe Measurements

The Hydrosense II probe estimates VWC by measuring the dielectric permittivity of the soil within a 3% error margin (Campbell Scientific 2020). This technique works by emitting an electromagnetic pulse that travels along two parallel 12 cm rods inserted into the soil. The time taken for the pulse to travel along the rods and return reflects the average water content over the volume between the rods (Jones & Or 2003). The probe also detects electrical conductivity between the rods and adjusts the permittivity measurements accordingly (Campbell Scientific 2020).

The unique physical properties of peat, such as its high porosity and carbon content, can affect detection of the reflected signal in the sensor electronics, affecting the

reliability of the probe's measurements (Campbell Scientific 2020; Gnatowski et al. 2018; Jones & Or 2003). To evaluate the accuracy of the Hydrosense II in measuring VWC in peat, a calibration experiment was conducted. Moisture measurements were taken from both a field and an uncovered stockpile of industry Grade 5 peat at random positions with varying moisture levels. For each position, three probe readings were taken alongside three peat samples collected using copper rings (volume: 15 cm^3). The samples were stored in labeled plastic bags and kept in a cooler until they could be refrigerated.

In the laboratory, the samples were weighed and then dried in an oven at 60 °C for 48 hours. To ensure complete drying, five randomly selected trays were re-weighed after an additional 4-6 hours in the oven. If the weight change was less than 0.1 g, the samples were deemed fully dried, and the remaining trays were weighed. Volumetric water content (θv) was then calculated using

$$\theta v = \frac{\theta g \cdot P_{soil}}{P_{water}} \tag{3.4}$$

where θg (grams) is the gravimetric water content $\left(\frac{m_{wet} - m_{dry}}{m_{dry}}\right)$, P_{soil} (g cm^{-3}) is the soil bulk density $\left(\frac{m_{dry}}{Volume_{sample}}\right)$, and the bulk density of water (P_{water}) is ~1 g cm^{-3}.

The average VWC obtained from the lab analysis and the probe readings were plotted against the average travel time (period) of the electromagnetic pulse, corresponding to the three samples taken around the same location.

3.2.4 Statistical Analysis of Flux Data

All statistical analyses were performed using either R software package (R Core Team 2024) for advanced statistical modeling, or Microsoft Excel with the Real Statistics Resource Pack (Release 8.9.1; Zaiontz 2023) for basic statistical procedures.

3.2.4.1 Preliminary Assessments

To determine the appropriate statistical method for assessing differences, preliminary assessments on randomly sampled categorized data were conducted to determine if ANOVA assumptions were met:

The Shapiro-Wilk test assessed data normality. If the p-value was less than 0.05, indicating non-normality, and the sample size was small ($n < 35$), ANOVA assumptions were deemed unmet. Levene's test checked for homogeneity of variance between categories. If the p-value was less than 0.05, indicating non-homogeneous variance, ANOVA assumptions were considered unmet.

If the Shapiro-Wilk test indicated non-normality ($p < 0.05$) but the sample size was large ($n > 35$) and Levene's test indicated homogeneous variance ($p > 0.05$), ANOVA assumptions were considered met.

3.2.4.2 Field Operations

Since field measurements were taken in randomized sectors, fields, and positions around the center of each field, they were considered independent of one another. This independence is supported by Clark et al. (2023).

When ANOVA assumptions were met, ANOVA was used to identify differences in means, followed by Tukey's HSD test to determine specific differences between extraction phases. When assumptions were not met, Kruskal-Wallis non-parametric test was used to identify differences in the medians, followed by Pairwise Mann-Whitney tests to determine specific differences. Assessed differences between the harrowed, drying, conditioned, and vacuum-harvested phases, including the corresponding primary and secondary tests, are summarized in Table 3.1.

Table 3.1: Primary and Secondary tests to assess differences between extraction phases.

Assessed differences between extraction phases	**Primary Test**	**Secondary Test**
CO_2 fluxes	One-way ANOVA	Tukey's HSD
CH_4 fluxes	Kruskal-Wallis	Pairwise Mann-Whitney
Surface layer temperature	Kruskal-Wallis	Pairwise Mann-Whitney
Surface layer moisture	One-way ANOVA	Tukey's HSD
Surface layer thickness	One-way ANOVA	Tukey's HSD
Surface layer dry bulk density	Kruskal-Wallis	Pairwise Mann-Whitney
Temperature profile	Unbalanced 2-factor ANOVA with regression	Tukey's HSD
Moisture profile	Unbalanced 2-factor ANOVA with regression	Tukey's HSD

Given the variability in sampling times relative to the last extraction operation, I could not control for the time since treatment. Therefore, I aimed to assess whether the flux measurements were independent of time. Notably, during the drying phase, the field is left undisturbed for an extended period, allowing moisture in the harrowed surface layer to evaporate into the atmosphere.

To evaluate the disturbance effect, I reorganized the field flux measurements based on the time elapsed since the last disturbance, regardless of the field phase, and grouped them into time categories that best fit the data while minimizing sample size variation. It is important to note a time gap (from 10 to 22 hours) in the bin categories, corresponding to the overnight period when site access was restricted.

After the preliminary data assessment, a one-way ANOVA, followed by Tukey's HSD test, was conducted to evaluate differences in mean CO_2 and CH_4 emission rates (independently) in relation to time since the last disturbance.

3.2.4.3 Uncovered Stockpiles

Unlike field flux measurements, which were taken at random positions, flux measurements for uncovered stockpiles were strategically sampled from the top and bottom positions on the four faces of each stockpile. Given this approach, these measurements could not initially be considered independent. However, due to the high spatial variability of flux measurements, I hypothesized that there would be no significant relationship between individual stockpiles and flux measurements. This would imply that flux measurements from different positions on the same stockpile could be treated as independent. To test this hypothesis, I employed two separate approaches to assess differences in uncovered stockpile fluxes based on position (top vs. bottom), seasonality, aspect, and industry grade.

Approach 1: Stockpile Fluxes Considered Independent

In the first approach, flux measurements from uncovered stockpiles were treated as independent, regardless of the stockpile from which they were taken. To evaluate differences between fluxes at the top and bottom positions, I conducted paired sample t-

tests for CO_2 and CH_4 fluxes separately. Significant differences were found between the top and bottom positions for CO_2 fluxes only, leading to the separate consideration of these positions in subsequent CO_2 analyses. For CH_4, the top and bottom positions were combined for further analysis.

To assess seasonal differences, fluxes were grouped by the month in which they were measured (July, August, September, and November), and a one-way analysis of variance (ANOVA), followed by Tukey's HSD test, was conducted (separately for fluxes from top and bottom positions). The same approach was used to evaluate differences based on aspect and industry grade. For CH_4 fluxes, a one-way ANOVA was used for month and industry grade, while differences by aspect were assessed using a Kruskal-Wallis test followed by Pairwise Mann-Whitney tests.

Temperature and moisture profiles corresponding to each flux measurement were also analyzed based on the same categories (position, month, aspect, and industry grade) using an unbalanced two-factor ANOVA with regression.

Approach 2: Stockpile Fluxes Clustered by Pile

In the second approach, which was applied only to CO_2 fluxes (since CH_4 fluxes were relatively small), I treated the measurements associated with each stockpile as clustered data, assuming that observations within the same stockpile were correlated, while observations from different stockpiles were independent. I used a Linear Mixed Effects (LME) model to account for both random effects (differences between piles) and fixed effects (differences based on position, seasonality, aspect, and industry grade), using the following R packages: "tidyverse," "viridis," "lme4," "lmerTest," "readxl," "emmeans," and "car." To ensure the residuals fit a normal distribution, the CO_2 flux data were log-transformed. This step was unnecessary in Approach 1 due to the preliminary assessment of the data distribution.

The initial model showed a singular fit, indicating overfitting and suggesting that the random effects (differences between piles) were too complex for the data to support.

Consequently, the random effect was removed from the model. The final model was a standard linear regression of the form:

$$\log(flux_{CO_2}) = \beta_0 + \beta_1 \cdot Position + \beta_2 \cdot Month + \beta_3 \cdot Aspect + \beta_4 \cdot Grade + \epsilon \quad (3.5)$$

where β_0 is the fixed intercept, $\beta_{1,2,3,4}$ are the fixed effects and ϵ is the residual error.
I present and compare the results of both approached in Results §4.3.

3.2.4.4 Covered Stockpiles

For covered stockpiles, fluxes measured over the tarp (n=31), over covered holes (n=15), and over open holes (n=31) were compared. After assessing the data distribution using preliminary tests, I applied the non-parametric Kruskal-Wallis test to determine differences in the median CO_2 and CH_4 fluxes (separately), followed by the Pairwise Mann-Whitney test to identify specific differences.

Further analysis of factors like seasonality, aspect, and grade was not conducted due to the small sample size (see §3.2.1.5).

3.3 Stockpile CO_2 & CH_4 Storage

In the following section, I explain how stockpile GHG storage data was collected in the field, and how this data was subsequently analyzed using gas chromatography.

3.3.1 Storage Sampling

Gas samples were taken from both covered and uncovered stockpiles throughout the study period to estimate stockpile GHG storage. Sippers (thin metal poles with mesh on one end to prevent substrate entry, and tubing on the other end connected to a syringe for gas extraction) were inserted into piles from two to four different positions, to extract gas samples from various depths. Syringes were used to draw out air samples from pore spaces within the piles, which were then stored in 12 ml exetainers to later be analyzed in the laboratory.

Exetainers needed for gas sample storage were evacuated in advance, either using a vacuum pump or by manually removing the air with a syringe. Exetainers evacuated by a

vacuum pump were used within two weeks, while those evacuated manually were prepared 1-2 days before use by repeatedly drawing out air until a vacuum was achieved.

In the field, a sipper was pushed to the first depth, typically 25 cm, and using a 60 ml syringe, 1-2 gas samples (depending on the sipper size) were drawn and discarded to remove any ambient air from the sipper. Using a 20 ml syringe, the next sample was drawn/discarded to prime the syringe. The following three samples drawn were transferred to their respective labeled exetainers by removing the closed syringe filled with gas from the sipper, and using a needle attachment to pierce through the exetainer caps and release the samples within. Once filled, nail polish was used to cover the caps to prevent gas leakage.

The sipper was then pushed to the next depth, typically 50 cm, and the process was repeated, including the discard of 2-3 samples to remove any gases from the previous positions from the sipper and syringe.

3.3.2 Sampled Stockpiles

Between July 23 and September 27, 2022, samples were taken from six different stockpiles, from up to four different positions (Figure 3.14), and from depths ranging from 25-300 cm. Relevant sampling information for each stockpile included in the study is summarized in Table 3.2.

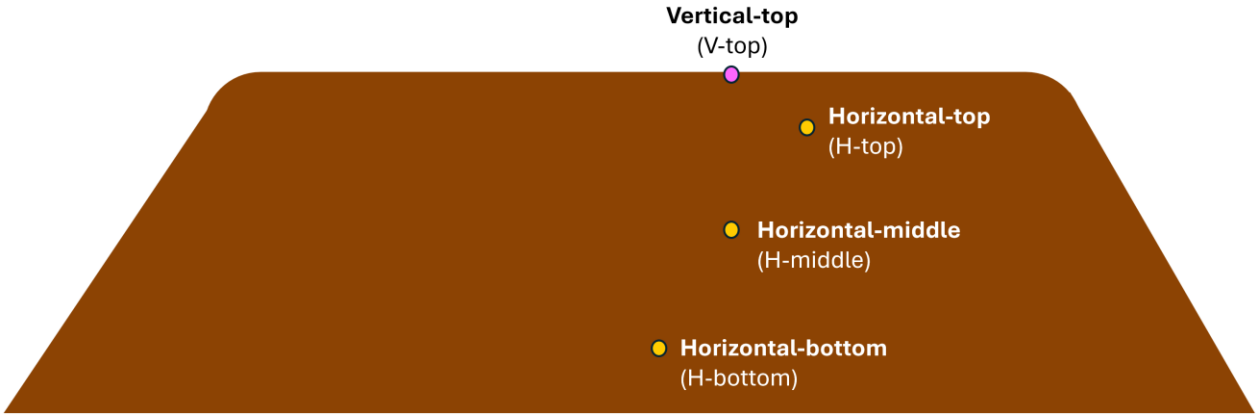

Figure 3.14a: Sampling positions for GHG storage on the long face of stockpiles. For four of the six piles, only the Vertical-top and Horizontal-middle positions were sampled.

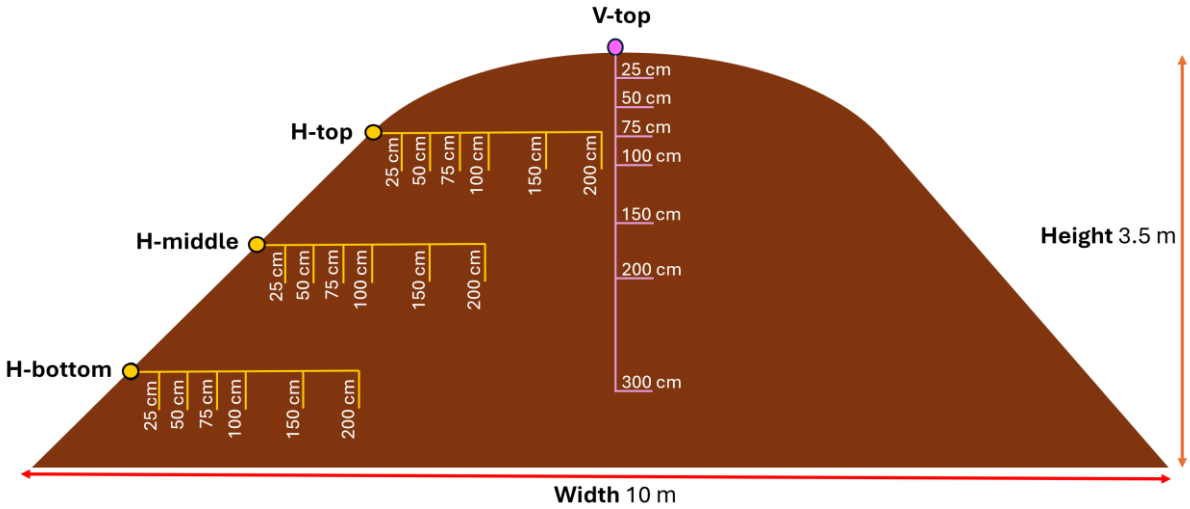

Figure 3.14b: Sipper orientations and depths corresponding to the four positions of GHG storage sampling (shown on a pile cross section). The diagram is to scale and uses the approximate dimensions of uncovered Pile 253, which has similar dimensions to other uncovered stockpiles. Note that covered stockpiles were larger, with an average height of 4 m and average width of 15 m.

The number of depths sampled increased throughout the summer, as gas chromatography results confirmed the effectiveness of sipper sampling for gas storage. During the final round of sampling in September, a longer sipper was used to reach a depth of 200 cm. Additionally, samples were taken from the 300 cm depth exclusively at the V-top position of uncovered Pile 253; however, the 300 cm sipper was subsequently damaged and could not be used further.

For all gas samples, temperature measurements at depths of 25, 50, 75, and 100 cm and moisture measurements at depths of 25, 50, and 75 cm were taken using the previously mentioned probes. Measurement depths were limited by the length of the probes.

Table 3.2: Information for stockpiles sampled for GHG storage.

Pile ID # *(industry grade)*	**Covered/ Uncovered**	**Positions**	**Dates sampled** (2022)	**Depths sampled (cm)** (corresponding to date)
Pile 86 *(Gr. 2)*	Uncovered	H-middle V-top	Aug-26	25, 50, 75, 100, 150
Pile 253 *(Gr. 5)*	Uncovered	H-bottom H-middle H-top V-top	a) Aug-16 b) Sept-27	a) 25, 50, 75, 100, 150 b) 25, 50, 75, 100, 150, 200 (300 at V-top only)

Pile 2 *(Gr. "humide")*	Covered	H-middle V-top	a) July-23 b) Aug-23 c) Sept-26	a) 50, 150 b) 25, 50, 75, 100, 150 c) 25, 50, 75, 100, 150, 200
Pile 10 *(Gr. 3)*	Covered (atop of gravel instead of field)	H-middle V-top	a) July-23 b) Aug-23 c) Sept-26	a) 50, 150 b) 25, 50, 75, 100, 150 c) 25, 50, 75, 100, 150, 200
Pile 14 *(Gr. 5)*	Covered	H-middle V-top	a) July-23 b) Aug-23 c) Sept-26	a) 50, 150 b) 25, 50, 75, 100, 150 c) 25, 50, 75, 100, 150, 200
Pile "McGill" *(Gr. 5)*	Covered	H-bottom H-middle H-top V-top	Aug 3	25, 50, 75, 100, 150

3.3.3 Sample Analyses

In gas chromatography, a sample is injected into a port where it is vaporized and carried by an inert gas. The sample passes through a column where different components of the gas are separated and exit the column at different times. Once separated, the components continue to a detector where their presence is recorded as peaks on analyzing software. The retention time (the time taken for a compound to travel through the column) results in an area under each peak, which is used to identify the concentrations (in ppm) of CO_2 and CH_4 in the sample.

Gas samples were analyzed on a GC-2014 gas chromatograph (GC) (GC-2014, Shimadzu, Japan). The carrier gas was ultra high purity nitrogen (UHP N_2) at a pressure of 600 kPa. The packed columns included: one 1.0m Hayesep T, 80/100 mesh, two 2.0m Hayesep D, 80/100 mesh, two 1.5m Hayesep N, 80/100 mesh, and one 0.7m Shimalite Q, 100/180 mesh. GHG concentrations were detected using a Methanizer at 380 °C for CO_2, and a Flame Ionization Detector (FID) at 250 °C (using air and H_2 at 350 kPa for the FID flame) for CH_4.

Three standardized samples of known concentrations (each of CH_4 5.1 ppm; CO_2 5000 ppm) were injected at the start of every analysis. The average ratio of concentration to area under the curve of the standards was used to calculate the unknown concentrations of samples based on the area under the CH_4 and CO_2 peaks.

Gas sample concentrations were very high (>100,000 ppm CO_2 and >1000 ppm CH_4). Therefore, to avoid the columns quickly becoming saturated, N_2 gas (not analyzed by the machine) was used to dilute the samples at a ratio of approximately 2:1. Exact dilution ratios were recorded to calculate the multiplier of each sample. Both the concentrations given by the software, and the calculated concentrations were then multiplied by that number, and their values were cross referenced to check for any major disparities that could indicate an error.

For each of the samples, I used molar mass ratios and the ideal gas law to convert from ppm (CO_2 or CH_4) to g C m^{-3}. The adjusted Molar Volume (V_m) was calculated using the re-arranged ideal gas law, temperature measurements, and assuming that: the temperature of the air in pore spaces was the same as the temperature of the surrounding substrate; the standard atmospheric pressure existed in pore spaces (1 atm); and that temperatures at the 100 cm depth were representative of deeper temperatures (at 150, 200, and 300 cm). Although deeper temperatures were likely warmer than those measured at 100 cm, the difference would have minimal impact on molar volume, making this a reasonable assumption for the purposes of these calculations.

Triplicate samples at any given depth were averaged and reported, to make comparisons between positions, depths, and the management of stockpiles.

3.3.4 Change in Storage Over Time

The change in storage (ΔS) over time (Δt) was estimated for piles sampled on multiple dates. The change is storage from the day a pile was first formed (or the day the pile was first tarped for covered stockpiles), and the first round of sampling was calculated ($\Delta S/\Delta t_1$). I assumed the stockpile had no stored CO_2 in pore spaces when it was first formed, and that CO_2 storage increased at a constant rate per day to normalize the change in storage by time passed.

Storage concentrations measured during the first round of sampling were also subtracted from those measured during the second round, and the difference in storage was divided by the number of days between the 2 sampling dates ($\Delta S/\Delta t_2$).

For cases with a third round of sampling, the difference in storage concentrations between the third and second rounds of sampling were divided by the number of days between the sampling dates ($\Delta S/\Delta t_3$).

3.4 Contribution of Stockpiles to Overall Site CO_2 Emissions

Overall stockpile emission estimates are a function of stockpile surface area, flux, and the number of stockpiles present in the field. In this section, I elaborate on the methods used to calculate stockpile geometry. Next, I explain how I quantified the changing number of stockpiles in the field over the study period and estimated the surface area exposed to the atmosphere. Lastly, I estimate the contribution of stockpiles to extraction emissions.

3.4.1 Stockpile Geometry Calculations

To estimate the average surface area of stockpiles exposed to the atmosphere, I measured the dimensions of 17 stockpiles (13 at Site A and 4 at Site B) using a surveyor tape measure and an Abney level. For each pile, I used geometry and trigonometry to determine the specific lengths needed to calculate surface area, treating the main body as a triangular prism and the ends as oblique pyramids (Figure 3.15).

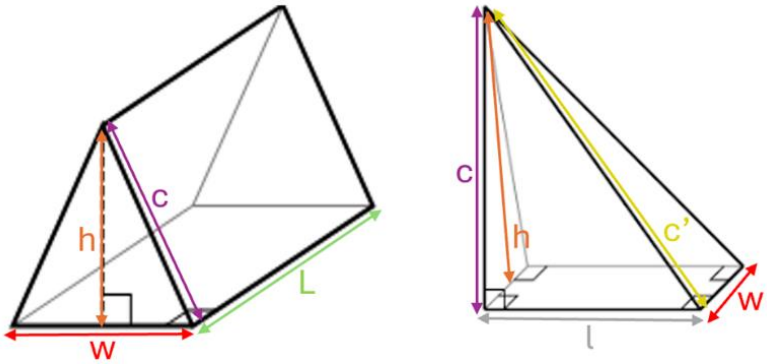

Figure 3.15a: Geometric shapes used to estimate surface area of stockpiles. Left: triangular prism used to represent the main body of a stockpile, and right: oblique pyramid used to describe both ends of a stockpile. Image source: www.khanacademy.org.

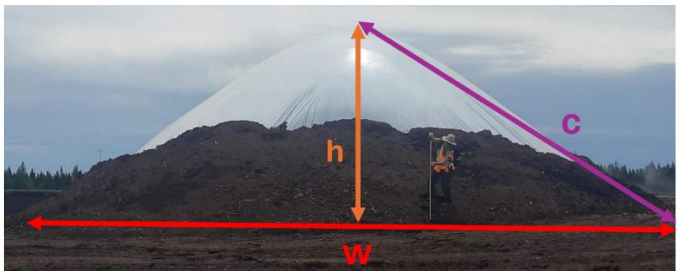

Figure 3.15b: Geometry superimposed on stockpile images. Top image: long face of stockpile corresponding to length. Bottom image: short face of pile corresponding to width. Length of main body *(L)*, length of end 1(l_1), length of end 2(l_2), and width (*w*) were measured in the field.

To collect data needed to calculate the height (*h*) of a given stockpile, an observer walked along the length of the pile, stopping at 3-5 different points to look through the Abney level to the top of the pile, recording the angle measures given by the instrument. The distance of the observer to the center of the pile's width and the observer's eye height were also noted (Figure 3.16). The average of the measured angles was used to calculate the height of the pile according to

$$h = d \cdot \tan(a) + o \tag{3.6}$$

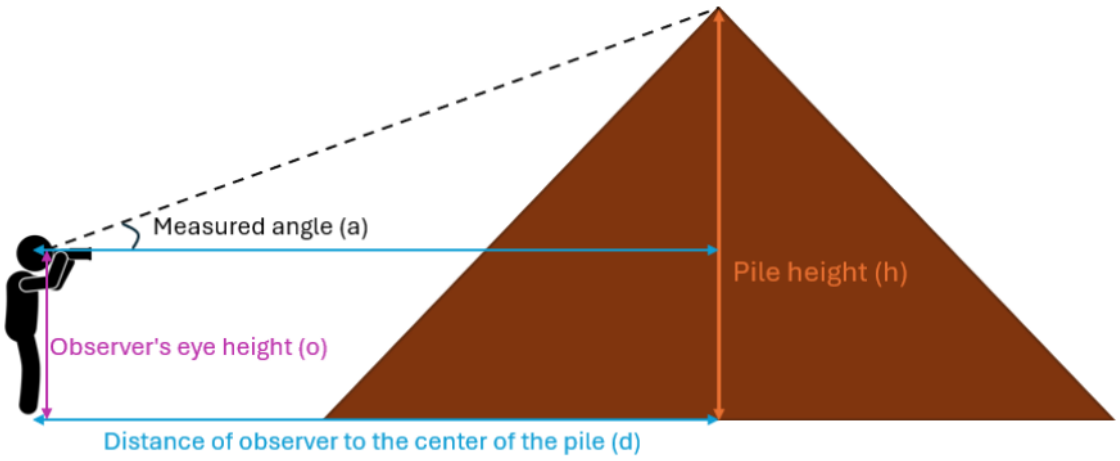

Figure 3.16: Measurements used to calculate stockpile height, where the measured angle (*a*) is the average of 3-5 angles. Image source for stick figure: www.Vecteezy.com

To calculate length *(c)* using trigonometry, I treated the width of the pile as a flat triangular face of a triangular prism (see Figure 3.15) using

$$c = \sqrt{h^2 + \left(\frac{1}{2}w\right)^2} \tag{3.7}$$

Similarly, to calculate lengths *(c'₁)* and *(c'₂)* (separately), the end lengths of the pile (l_1 & l_2) were treated as right-angled triangular faces of an oblique pyramid (see Figure 3.15) using

$$c'_{(1,2)} = \sqrt{h^2 + l_{(1,2)}^2} \tag{3.8}$$

Stockpile surface area *(SA)* exposed to the atmosphere was then calculated using

$$SA = 2(L \cdot c) + (l_1 \cdot c) + (l_2 \cdot c) + \left(\frac{w \cdot c'_1}{2}\right) + \left(\frac{w \cdot c'_2}{2}\right) \tag{3.9}$$

Stockpile rectangular base area *(BA)* was calculated from

$$BA = (L + l_1 + l_2) \cdot w \tag{3.10}$$

For covered Piles 2, 10, and 14, stockpile volume ($V_{covered}$) was calculated as

$$V_{covered} = \left(\frac{l_1 \cdot w \cdot h}{3}\right) + \left(\frac{l_2 \cdot w \cdot h}{3}\right) + \left(\frac{L \cdot w \cdot h}{3}\right) \tag{3.11}$$

3.4.2 Stockpile Accounting and Area Estimates

To capture changes in the number of stockpiles over time, I analyzed Planet satellite imagery in the form of GeoTiff files (Planet Team 2018) on ArcGIS Pro 3.1.0 (Esri 2023). For both Sites A and B, I used manual visual processing to determine the number of stockpiles on a given date. Stockpiles were distinguished based on size (full-sized or half-sized), covering (covered, uncovered, or half-covered), and confidence level.

For total stockpile surface area and base area on a given date, slightly different methods were used for Sites A and B due to management differences impacting the feasibility of the analysis (more details below).

3.4.2.1 Site B – Mostly Covered Stockpiles

Company B covers their stockpiles with white reflective tarps, making them easily distinguishable from the fields in satellite images due to the contrast of white against brown. Given the high certainty of pile observations, I analyzed satellite images for 75 clear days (i.e., no cloud or fog interference) between May 1st and November 30th, 2022, when stockpiles could be easily distinguished. This represents approximately 35% of the days within this period.

To estimate the total surface area of the stockpiles, I quantified the average number of stockpiles in the field for every month. Next, I selected a date from each month where the number of stockpiles in the field was approximately equal to the average number of stockpiles for that month. For each of the selected dates, I used the "Create Feature" tool in ArcGIS Pro to outline the perimeters of the stockpiles visible in the imagery. Subsequently, I used the "Measure Feature" ArcGIS tool to calculate the base area for every stockpile outlined. Lastly, I used the linear relationship between the base area and the surface area of stockpiles (Figure 3.17) established using the 17 stockpiles whose geometry was measured in the field (see §3.4.1) to estimate the surface area of those stockpiles.

The total stockpile surface area emitting to the atmosphere for each month was the sum of the surface areas of stockpiles on the relevant date (representing the average emitting stockpile surface area for that month). Similarly, the average total stockpile base area was the sum of the base areas of stockpiles.

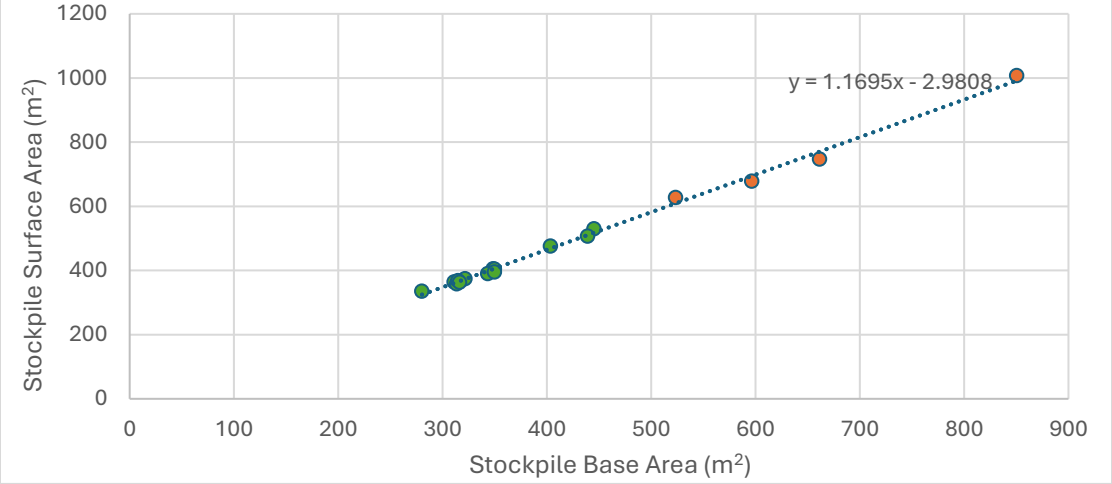

Figure 3.17: Linear relationship between stockpile base area and stockpile surface area for 17 stockpiles measured in the field. In green: uncovered stockpiles at Site A, and in orange: covered stockpiles at Site B.

3.4.2.2 Site A – Mostly Uncovered Stockpiles

Company A leaves most of its stockpiles uncovered in extracted fields, making them more difficult to distinguish due to subtle colour differences. Stockpiles were primarily identified in the satellite images by a change in texture and colour (i.e., lighter brown from dryer peat

in the piles) in areas where stockpiles were in the field. Due to greater uncertainty in the observations at Company B, only the clearest images from months with flux measurements (July, August, September, and the first five days of November 2022) were selected for stockpile accounting. I analyzed images from 21 dates, representing approximately 20% of days within this period.

The lack of contrast between the stockpiles and the fields made it impossible to trace the perimeter of stockpiles accurately; therefore, the base area polygon method could not be used to estimate surface area. Instead, total stockpile surface area (representing the average for each month) was estimated by multiplying the average number of piles for that month by the average stockpile surface area calculated for measured uncovered stockpiles at Site A. Similarly, total stockpile base area for each month was calculated by multiplying the number of piles by the average stockpile base area for measured stockpiles at Site A.

3.4.2.3 Area Calculations

I once again used area polygons (using Planet satellite imagery in ArcGIS) to measure the site study area comprising of a portion of extracted fields with stockpiles at Sites A and B (separately), followed by the extracted field area (without stockpiles) for each relevant month. Since most stockpiles are located on extracted fields, the proportion of extracted field area exposed to the atmosphere was calculated using

$$Extracted\ Field\ Area\ \% = \frac{(Site\ study\ area - Total\ stockpile\ base\ area)}{Site\ study\ area} \cdot 100 \quad (3.12)$$

The proportion of stockpile area (%) was calculated by simply using "Total stockpile base area" as the numerator in equation 3.12.

3.4.3 CO_2 Contribution Estimates

3.4.3.1 Approach and Assumptions

Uncovered stockpile fluxes were measured at Site A in July, August, September, and November, while covered stockpile fluxes were measured at Site B in May, June, and July 2022. Accordingly, the average monthly ratio of stockpile area to field area, and stockpile

emissions to field emissions, were calculated for the months of July to September and November at Site A, and May to July at Site B (see Results §4.6.3.3). Since stockpile sizes varied, a date from each month with approximately the same number of stockpiles as the monthly average was used as a proxy to estimate average daily emissions for that month (described in more detail below). Due to relatively low methane emissions from stockpiles, the contribution of stockpiles to overall methane emissions was not quantified.

To quantify stockpile CO_2 emissions and estimate their relative contribution to site CO_2 emissions from extraction operations, I made assumptions based on operating procedures observed in the fields. I assumed that the site study area (and stockpiles in that area) were representative of other extracted peatland sectors for Company A and Company B. Since site access was limited to the designated study areas, detailed analysis of the other sectors was not possible.

I assumed that the surface area of each full-sized covered stockpile included holes from the insertion of a temperature probe, and that all holes were taped over (covered) between sporadic temperature readings. I excluded instantaneous CO_2 emissions from open holes in the tarp, because the duration of open hole fluxes is both variable and unknown. The surface area included in flux measurements over covered holes was greater than the surface area of the covered holes themselves. Since flux measurements were calculated on a per m^2 basis, I assumed that a full-sized covered stockpile included three covered holes, representing 3 m^2 of surface area emitting at the average flux for covered holes. For half sized piles, I assumed there would be one covered hole and therefore, 1 m^2 of the surface area emitting at the average flux for covered holes. For half covered stockpiles, I assumed there were no holes since this often represents a pile in the process of being covered with a fresh tarp.

For uncovered stockpiles, fluxes measured at the top and bottom positions were found to have significantly different emissions rates (see Results §4.3.1.1). Based on visual inspection of stockpiles in the field, I assumed that 25% of the total uncovered surface area was emitting at a rate corresponding to the average top position flux, while 75% of the surface area was emitting at the average bottom position flux.

I confirmed this assumption by superimposing equal sized squares, and half sized triangles and rectangles, over a few photos of stockpiles taken in the field. An example of the delineated boundary between the two positions, and the verification of their relative proportions is shown in Figure 3.18.

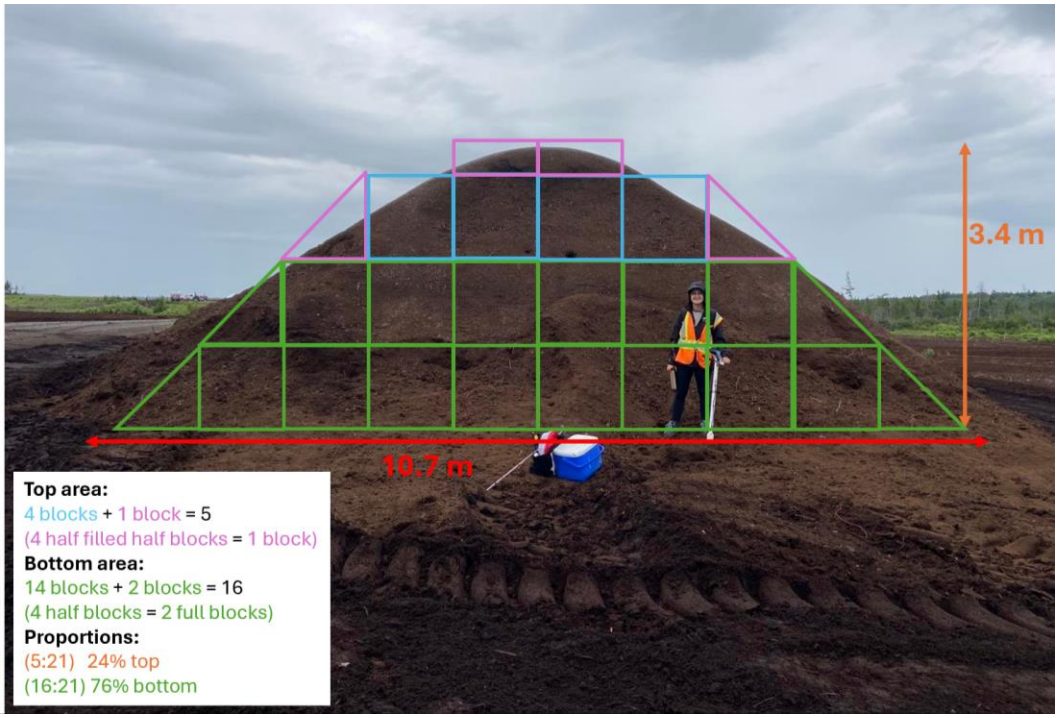

Figure 3.18: Example of delineation between top and bottom positions of stockpile surface area, and verification of their relative proportions.

3.4.3.2 Calculations

I estimated the relative contribution of stockpiles and fields to the overall emissions for my extracted study sites.

The total CO_2 emissions from uncovered stockpiles ($Total\ E_{uncovered}$) at Site A were calculated using

$$Total\ E_{uncovered} = (SA_u \cdot 0.25 \cdot Etop_{month}) + (SA_u \cdot 0.75 \cdot Ebottom_{month}) \qquad (3.13)$$

where SA_u (m^2) is the total surface area of uncovered stockpiles on a given date, $Etop_{month}$ (g CO_2-C m^{-2} day^{-1}) is the average flux at the top position for a given month, and $Ebottom_{month}$ (g CO_2-C m^{-2} day^{-1}) is the average flux at the bottom position for a given month.

The total CO_2 emissions from covered stockpiles ($Total\ E_{covered}$) (g CO_2-C day^{-1}) is

$$Total\ E_{covered} = E_{ch} \cdot (3 \cdot full\ piles + half\ piles) + E_{tarp} \cdot [SA_c - (3 \cdot full\ piles + half\ piles)] \quad (3.14)$$

where E_{ch} (g CO_2-C m^{-2} day^{-1}) is the average covered hole stockpile flux, *full piles* is the number of full piles in the field on the proxy date, *half piles* is the number of half piles in the field on the proxy date, E_{tarp} (g CO_2-C m^{-2} day^{-1}) is the average tarp stockpile flux and SA_c (m^2) is the total covered stockpile surface area on a given date.

Although Company A kept most of their stockpiles uncovered, they sometimes covered stockpiles, especially in preparation for winter. Company B covered all stockpiles, however, the process of creating and covering a pile can sometimes take several days, leaving some stockpiles uncovered in the field for shorter periods. Piles were also sometimes left half covered during the processes of pile formation or retrieval.

To account for the underestimation of emissions from covered stockpiles at Site A in August, September, and November (when covered fluxes were not measured), and from uncovered stockpiles at Site B in May and June (when uncovered stockpile fluxes were not measured), I calculated adjustment factors. These factors were derived for the month of July when both covered and uncovered flux measurements were collected (using July 18th as a proxy for the monthly average). I calculated emissions from the total uncovered stockpile surface area at Site B using equation 3.13 (previously used for uncovered stockpile emissions at Site A).

Next, since stockpiles sizes varied between Sites A and B, and the size of the stockpile influences the number of covered holes on each pile, I calculated the average monthly proportion of m^2 area including covered holes in the total stockpile surface area at Site B from May-November. I averaged the proportions, finding that 0.39% of the total covered stockpile surface area (from May-November at Company B) included covered holes.

Next, I recalculated the emissions from uncovered stockpile surface area at Site B, treating it as though it were covered, using the average covered hole area proportion (rather than the number of large and small piles used in equation 3.14).

I then quantified the multiplier needed to adjust these emissions (treating uncovered stockpile area at Site B as covered) to those quantified for the total uncovered stockpile surface area at Site B (using the formula for Site A's uncovered stockpile emissions) using

$$Adjustment\ factor_{Site\ B\ uncovered} = \frac{Site\ B\ Total\ E_{uncovered}}{(SA_u \cdot 0.0039 \cdot Ech) + (SA_u \cdot 0.9961 \cdot Etarp)} \quad (3.15)$$

The adjustment factor for uncovered stockpiles at Site B was 5.15. Accordingly, the adjustment factor for covered stockpiles at Site A was $\frac{1}{5.15}$.

For covered stockpiles at Site A in August, September, and November (there were no covered stockpiled at Site A in July), emissions were calculated according to

$$Site\ A\ Total\ E_{covered} = (SA_c \cdot 0.25 \cdot Etop + SA_c \cdot 0.75 \cdot Ebottom) \cdot \left(\frac{1}{5.15}\right) \quad (3.16)$$

For uncovered stockpiles at Site B in May and June, emissions were calculated according to

$$Site\ B\ Total\ E_{uncovered} = (SA_u \cdot 0.0039 \cdot Ech + SA_u \cdot 0.9961 \cdot Etarp) \cdot 5.15 \quad (3.17)$$

For half covered stockpiles at either site, the covered half was considered in the total covered stockpile surface area and the uncovered half was considered in the total uncovered stockpile surface area for the site.

Average monthly field emissions for both sites were calculated by multiplying the extracted field area (m^2) by 0.9 g CO_2-C m^{-2} day^{-1}, in accordance with Clark et al. (2023), reaffirmed by my results for average CO_2 field emissions.

Evidence in the literature suggests that ditches emit at a higher rate than the fields but take up significantly less area (Clark et al. 2023; Hunter et al. 2024). For this analysis aimed at determining the relative importance of stockpiles in GHG accounting, drainage ditches within the site study area were considered to emit at the same rate as the fields, and therefore were not distinguished as separate features. This implies a slight underestimation in total extraction emissions, and a slight overestimation of extracted field area.

The CO_2 emitted to the atmosphere when the tarp is removed from covered stockpiles contributes to overall stockpile emissions. To calculate this, bulk density and porosity is required. To evaluate the bulk-density of stockpiles at depth, samples were collected from two uncovered stockpiles (industry Grade 3 and 5) with exposed cross sections (created by a bulldozer to prevent overheating). Cross sections of covered stockpiles were not available, therefore density at depth was assumed to be similar for both types of piles. Sampling was conducted along vertical, angled, and horizontal axes at 50 cm intervals, from the center (0 cm) outwards towards the surface (Figure 3.19).

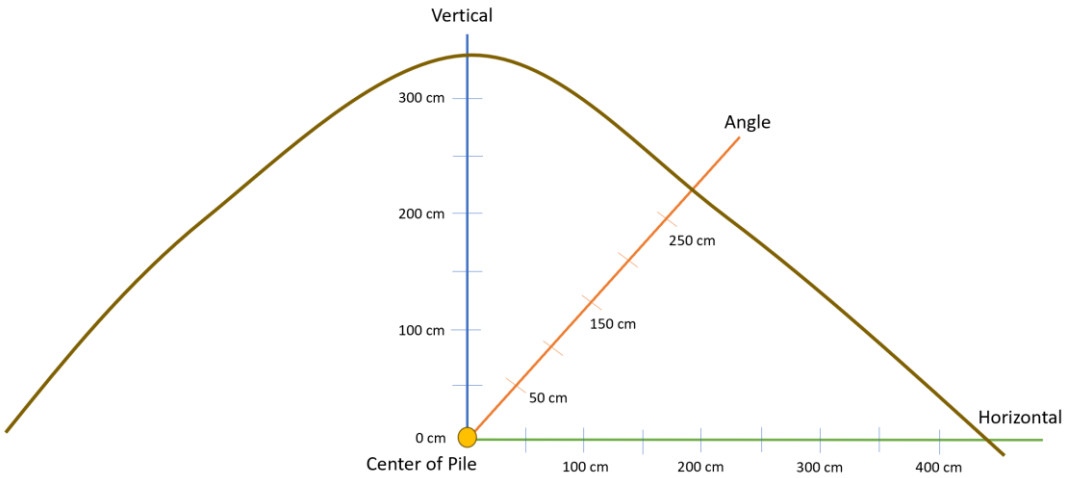

Figure 3.19: Density sampling positions along three axes of a stockpile cross-section.

At each sampling position, three peat samples were taken using copper rings (volume: 15 cm^3). In the laboratory, the samples were weighed and dried in an oven at 60 °C for 48 hours, with checks to ensure complete drying.

Solid bulk density (P_{soil}) was calculated by dividing the sample dry weight, by the sample volume. The three samples collected from the same position and axis were then averaged. The range of measured bulk densities did not differ significantly with depth (see Results §4.6.3.1 for more details), and corresponded with field surface peat densities measured by Lai (2022) on fields within Site A of this study. Using a pycnometer test with kerosene, Lai calculated the particle density and subsequent porosity of the surface layer. The top 10 cm of peat, with bulk densities ranging from 110-200 kg m^{-3}, was found to have a porosity of approximately 82% (Lai 2022).

The amount of CO_2 stored within the pore spaces of covered Piles 2, 10, and 14 (see Table 3.2) that would be instantaneously emitted upon tarp removal (*Instantaneous E*) was estimated using

$$Instantaneous\ E = (Volume_{covered} \cdot porosity - Volume_{covered} \cdot porosity \cdot VWC) \cdot [CO_2] \quad (3.18)$$

where $Volume_{covered}$ is the stockpile volume (m^3, calculated using equation 3.11), porosity was 0.82 (from Lai 2022), and $[CO_2]$ is the measured CO_2 concentration (g CO_2-C m^{-3}) (as described in §3.3.2).

The calculation first used averaged *VWC* and *[CO_2]* values across H-mid and V-top positions measured throughout the study[1] (for Pile 2, 10, and 14, respectively). The calculation was then repeated with the lowest CO_2 concentration and highest VWC recorded for that pile (at either position throughout the study[1]) to estimate minimum CO_2 emissions upon tarp removal. Conversely, the highest CO_2 concentration and lowest VWC were used to estimate maximum instantaneous CO_2 loss. The instantaneous emissions (*Instantaneous E*) for Piles 2, 10, and 14 were then averaged to provide an estimate of CO_2 lost from stockpile removal. The maxes and mins described above were also averaged to provide a confidence interval.

To further assess differences in emissions between stockpile management techniques, I simulated the lifespan (daily fluxes) and removal (instantaneous emissions) of Piles 2, 10, and 14, as both covered and uncovered piles. Details on this can be found in Appendix A.

[1] Since stockpiles are not usually removed from the field within the first 2 weeks of being covered, VWC and [CO_2] measurements from the first round of sampling for Piles 10 and 14 were excluded.

Chapter 4: Results

In this chapter, I first assess the reliability of VWC measurements from the moisture probe by comparing them to laboratory analyses of samples from fields and stockpiles. I then present the impact of field operations on GHG fluxes, surface peat properties, and temperature and moisture profiles across the four extraction phases. Next, I analyze flux trends on uncovered stockpiles, considering positional differences, seasonal variations, aspect, and peat industry grades using two approaches, and I quantify emissions from covered stockpiles. I then review GHG storage dynamics for uncovered and covered stockpiles, comparing their diffusive patterns. Finally, I quantify stockpile geometry and track the number of stockpiles during the 2022 extraction season to estimate their contribution to total CO_2 emissions. I also simulate cumulative emission differences between covered and uncovered stockpiles.

4.1 Reliability of VWC Probe Measurements

In the field, the Hydrosense II probe consistently overestimated VWC by an average of 10% compared to the laboratory measurements (Figure 4.1). While the slopes of the regression lines were within the 3% error margin of the instrument, the discrepancy in intercepts indicated a consistent overestimation by the probe. However, the linear equation relating period and VWC derived from probe readings fell within the standard error of the corresponding equation derived from lab data for field measurements (standard error of slope=11.0%; standard error of y-intercept=22.5%).

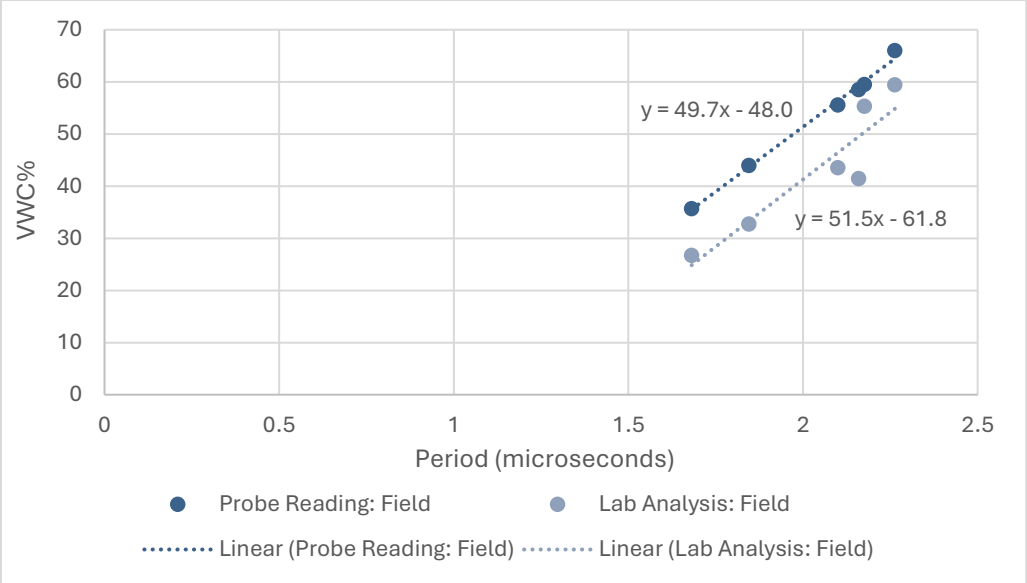

Figure 4.1: Comparison of averaged WVC (%) from probe readings and averaged VWC (%) from corresponding samples analyzed in the laboratory for extracted peat fields, relative to averaged period (microseconds) given by the probe.

For stockpiles, the probe consistently underestimated VWC relative to lab measurements, particularly at lower moisture levels (Figure 4.2). This discrepancy is likely due to the higher porosity of dry peat, which may interfere with the probe's accuracy. On average, probe measurements underestimated laboratory VWC by 9% for stockpiles. While the slope of the probe-derived equation was within the standard error of the lab-derived equation, the y-intercept was outside of the standard error range (standard error of slope=8.1%; standard error of y-intercept=11.9%).

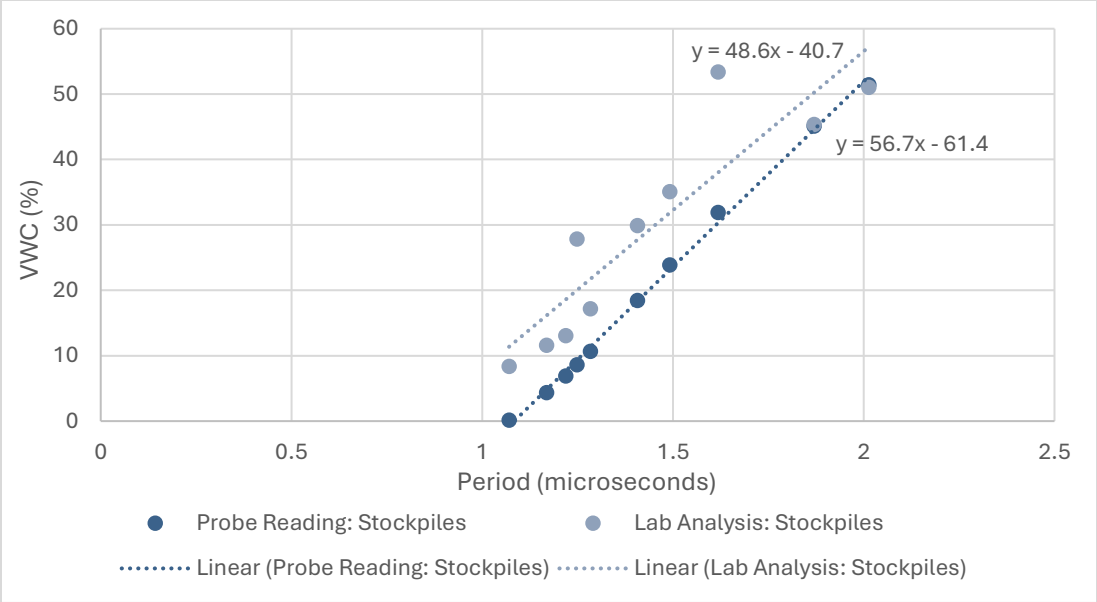

Figure 4.2: Comparison of averaged WVC (%) probe readings and averaged VWC (%) from corresponding samples analyzed in the laboratory for stockpiles, relative to averaged period (microseconds) given by the probe.

Despite these differences, the VWC values obtained using the Hydrosense II were considered adequate given that the moisture measurements in this study were primarily used for relative comparisons. As such, the VWC values presented correspond to unadjusted values measured by the probe on site unless otherwise specified.

4.2 Field Operations

The following section presents comparative changes in peat fields throughout the four phases of extraction: harrowed, drying, conditioned, and vacuum-harvested. First, I examine CO_2 and CH_4 emissions trends. Next, I compare physical changes to the loose surface layer properties, as well as temperature and moisture profiles. Lastly, I explore how time since the last disturbance affected flux measurements.

4.2.1 Aggregated Field Fluxes

To assess differences in field CO_2 fluxes during the four phases of peat extraction, I conducted a one-way analysis of variance (ANOVA). Although the flux data was not normally distributed, parametric testing assumptions were met due to the large sample size (n>35) and homogenous variance of the four categories. The results indicated no

significant differences in mean CO_2 flux between the four phases of peat extraction (Table 4.1, Figure 4.3).

Table 4.1: Summary statistics for extraction phase CO_2 field flux measurements.

Phase	**Count** (n)	**Mean CO_2 flux** (g CO_2-C m^{-2} day^{-1})	**Median CO_2 flux** (g CO_2-C m^{-2} day^{-1})	**Standard Deviation**
Harrowed	50	0.94	0.82	0.53
Drying	38	0.92	0.84	0.41
Conditioned	39	0.94	0.84	0.43
Vacuum-Harvested	42	0.85	0.76	0.39

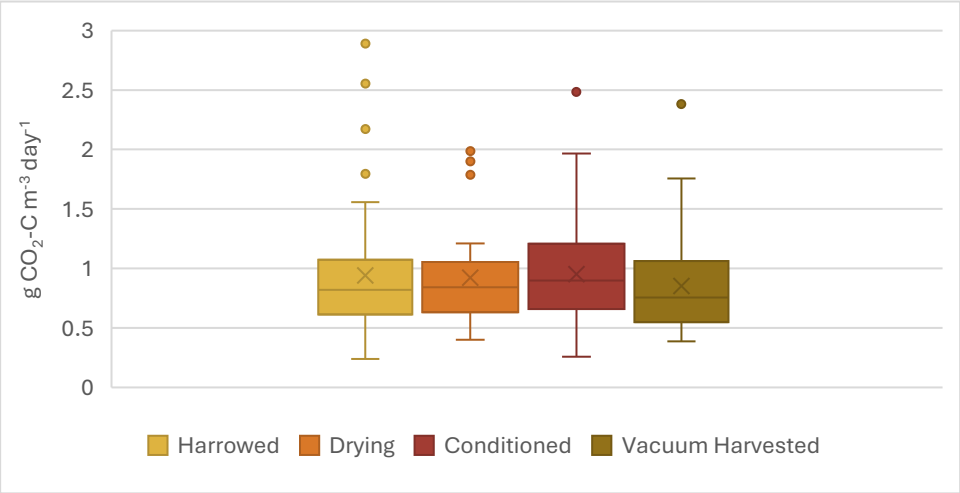

Figure 4.3: Distribution of CO_2 field fluxes by peat extraction phase.

A Kruskal-Wallis test indicated significant differences in median CH_4 fluxes between the phases of peat extraction ($p<0.0001$), and a subsequent Pairwise Mann-Whitney test revealed that the drying phase had a significantly lower median CH_4 flux than the harrowed ($p<0.0001$), conditioned ($p<0.001$), and vacuum-harvested ($p<0.005$) phases (Table 4.2, Figure 4.4).

Table 4.2: Summary statistics for extraction phase CH_4 field flux measurements.

Phase	**Count** (n)	**Mean CH_4 flux** (mg CH_4-C m^{-2} day^{-1})	**Median CH_4 flux** (mg CH_4-C m^{-2} day^{-1})	**Standard Deviation**
Harrowed	50	265.0	45.0	697.2
Drying	38	15.6	9.3	19.8
Conditioned	39	72.8	39.0	110.5
Vacuum-Harvested	42	55.7	28.0	68.9

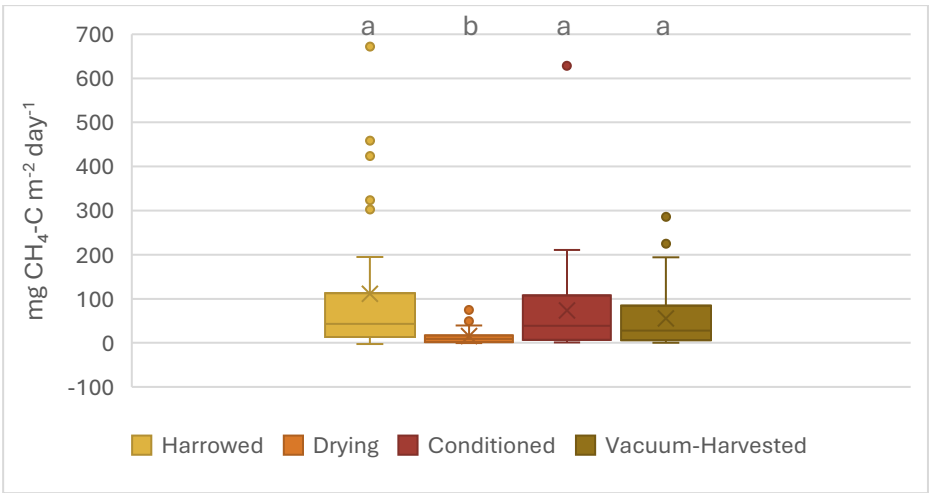

Figure 4.4: Distribution of CH_4 field fluxes by peat extraction phase. To improve visualization, three large values from the harrowed category were not plotted: 1118.2, 2985.3, and 3909.6 mg CH_4-C m^{-2} day^{-1}. Groups sharing the same letter are not significantly different.

4.2.2 Comparison of Surface Peat Layer Properties

The peat extraction cycle begins with harrowing, when a tractor pulls a large rake over the field, breaking up the surface peat layer and disconnecting it from the underlying peat matrix. This disturbance releases some internal moisture, resulting in a thicker and cooler surface layer and moister profile, particularly when compared to the vacuum-harvested phase that comes before, marking the end of an extraction cycle. Next, the field enters the drying phase, where the surface layer continues to thicken and cool due to increased evaporation, resulting in the dryest surface layer and profile observed across all phases. Once the peat is sufficiently dried, a conditioner passes over the field to further loosen the surface layer for harvest. This additional disturbance increases the surface moisture content relative to the drying phase, while other conditions return to average. Lastly, vacuum harvesters extract the prepared surface peat, leaving behind a thin, compacted surface layer with increased moisture content only at the surface, likely due to compression by the heavy machinery.

Apart from bulk density, which remained stable across all phases, these results align with the initial hypotheses regarding the effects of extraction processes on the surface peat layer. They confirm that the phases of extraction are achieving their intended outcomes. Although several statistically significant differences in peat surface conditions

were observed these differences were not substantial enough to meaningfully alter microbial activity (further discussed in §5.1.2).

4.2.2.1 Surface Temperature

A Kruskal-Wallis test revealed differences in median surface temperature between extraction phases ($p<0.0001$) (Figure 4.5). A Pairwise Mann-Whitney test confirmed that the drying phase was significantly cooler than the harrowed ($p<0.0005$), conditioned ($p<0.05$), and vacuum-harvested ($p<0.0001$) phases. Additionally, the surface temperature for the vacuum-harvested phase was significantly warmer than the harrowed phase ($p<0.05$).

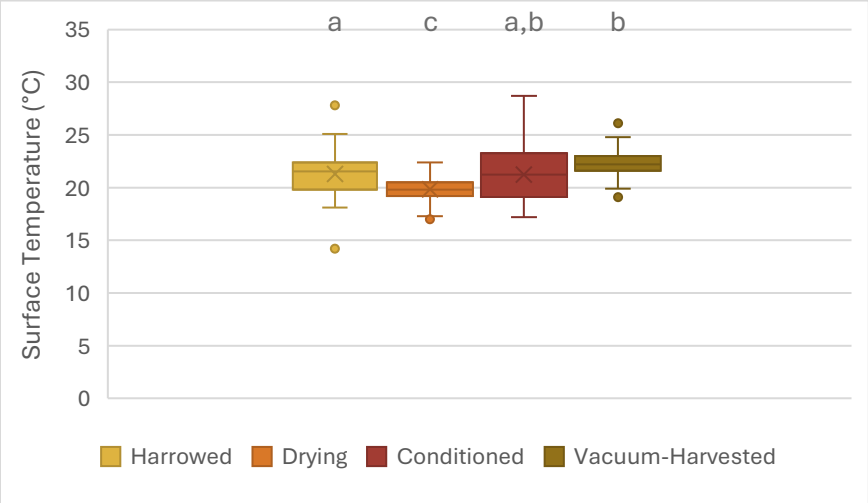

Figure 4.5: Distribution of surface layer temperature taken during conditioned (median=21.3°C, n=40), drying (median=19.8°C, n=35), harrowed (median=21.3°C, n=50), and vacuum-harvested (median=22.2°C, n=40) phases. Groups sharing the same letter are not significantly different.

4.2.2.2 Surface Gravimetric Water Content

The gravimetric soil water contents of the surface layer throughout the four extraction phases were compared using a one-way analysis of variance (ANOVA) (Figure 4.6). The results indicated significant difference in mean percent soil water ($p<0.005$). Tukey's HSD identified that the drying phase was significantly less moist than the vacuum-harvested phase ($p<0.005$). There is also an observable trend that the surface moisture during drying is generally less moist than the other phases, with the vacuum-harvested phase being the moistest, and the harrowed and conditioned phases being somewhere in between.

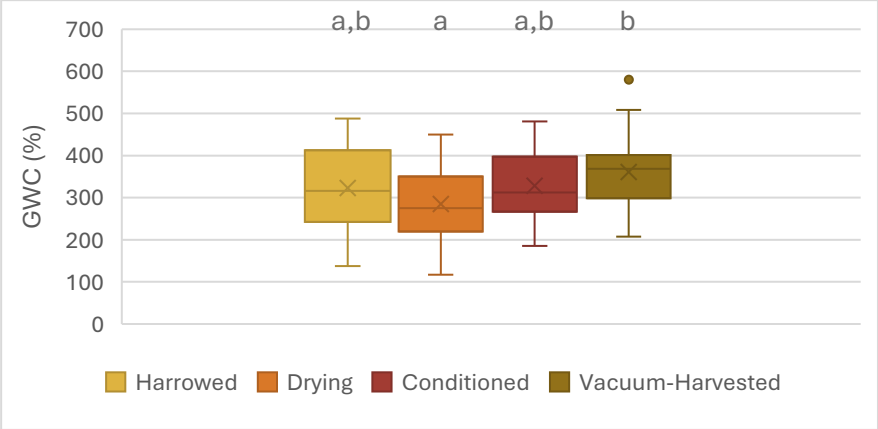

Figure 4.6: Distribution of surface layer gravimetric water content (%) from samples taken during the harrowed (mean=322.8%, n=49), drying (mean=285.1%, n=35), conditioned (mean=328.3%, n=32), and vacuum-harvested (mean=361.0%, n=39) phases. Groups sharing the same letter are not significantly different.

4.2.2.3 Surface Layer Thickness

Mean surface layer thickness varied by extraction phase (Figure 4.7). The data was not normally distributed (Shapiro-Wilk, $p<0.05$), but ANOVA assumptions were upheld due to homogenous variance and a large sample size ($n>35$). The results indicated significant differences ($p<0.0001$), with a thicker surface layer during drying, than during the conditioned ($p<0.05$) and vacuum-harvested ($p<0.0001$) phases (Tukey's HSD). The harrowed surface was also significantly thicker than its vacuum-harvested counterpart ($p<0.005$).

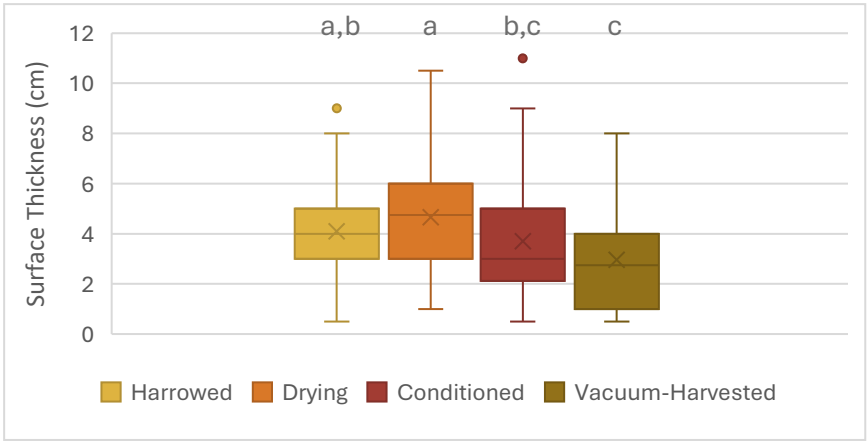

Figure 4.7: Distribution of peat surface layer thickness measurements (cm) taken during harrowed (mean=4.10, n=100), drying (mean=4.66, n=70), conditioned (mean=3.70, n=80), and vacuum-harvested (mean=2.96, n=70) phases. Groups sharing the same letter are not significantly different.

4.2.2.4 Bulk Density of Surface Layer

The dry bulk density of the surface peat layer did not vary greatly across extraction phases. A Kruskal-Wallis test was used to assess differences between group medians, finding no significant differences in bulk densities between the harrowed (median=122 kg m^{-3}, n=49), drying (median=126 kg m^{-3}, n=35), conditioned (median=113 kg m^{-3}, n=32), and vacuum-harvested (median=113 kg m^{-3}, n=39) phases. These densities are within the estimated range of the extracted peat fields (Lai 2022).

4.2.3 Comparison of Field Temperature and Moisture Profiles

To investigate whether the effects of operations on temperature and moisture observed at the surface extended into the peat matrix below, I compared the mean temperature and moisture profiles of the fields. An unbalanced two factor ANOVA using regression was used to evaluate the effects of depth, extraction phase, and the interaction between them on temperature and moisture profiles.

4.2.3.1 Temperature Profile

Temperature profiles were significantly different at depth ($p<0.0001$), but remained relatively uniform throughout the phases of extraction, finding no significant difference between phases or in the interaction of depth and phase (Figure 4.8). Tukey's HSD follow-up test confirmed that all depths were significantly different from each other ($p<0.05$).

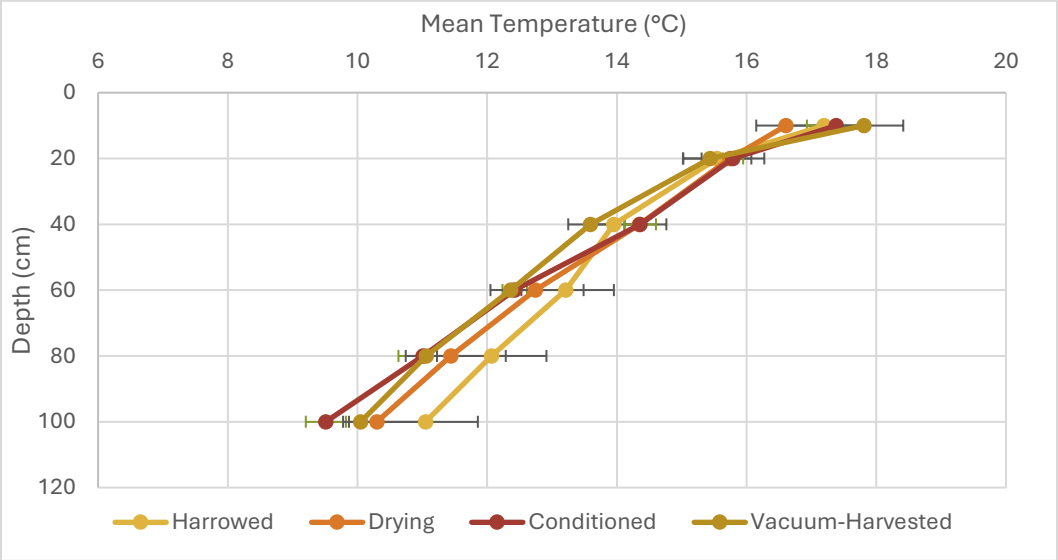

Figure 4.8: Average field temperature reading (°C) at depth compared across phases of extraction, with standard error bars.

Despite significant differences in surface layer temperatures between phases, subsurface temperatures were unaffected by mechanical disturbances at the surface, suggesting that temperature variations in the surface layer were driven primarily by human operations rather than by natural biogeochemical processes.

4.2.3.2 Moisture Profile

Field moisture significantly differed between phases and depths ($p<0.0001$) (Figure 4.9). Tukey's HSD follow-up test found that the moisture profile of the drying phase was significantly reduced compared to the harrowed ($p<0.005$) and conditioned ($p<0.05$) phases, which follow processes that release internal moisture from peat. The moisture profile of the harrowed and vacuum-harvested phases also differed significantly ($p<0.005$). Apart from the 40 and 60 cm that were found to be similar, there were significant differences between all depths ($p<0.005$). These differences are likely due to the effect of surface processes on capillary action. However, these moisture differences were biogeochemically insignificant, as levels at each depth remained within 5% of each other.

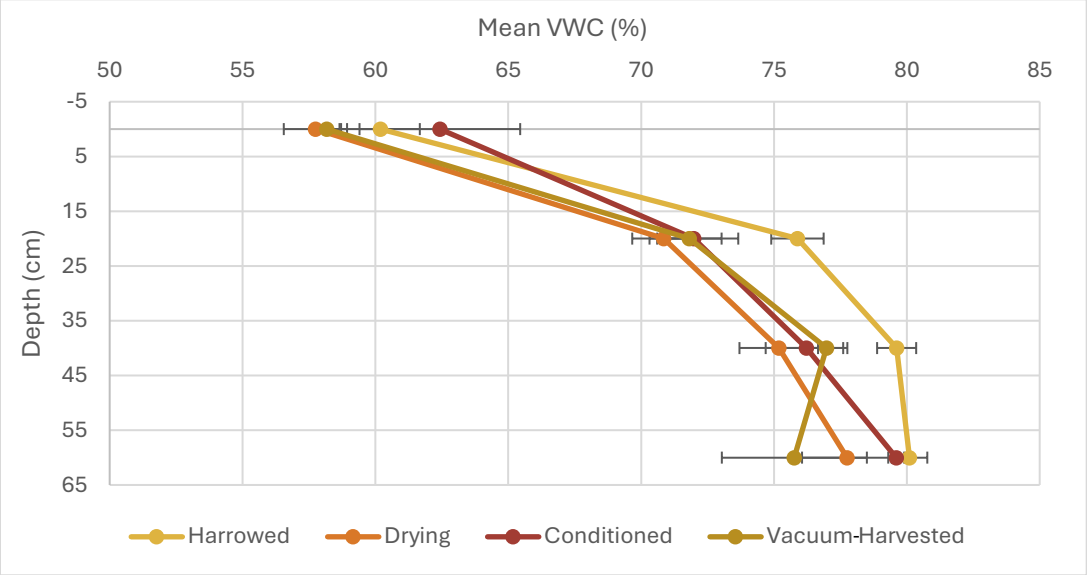

Figure 4.9: Average field moisture reading at depth (VWC%) compared across phases of extraction, with standard error bars. Note that readings represent an average taken from a 12 cm layer starting at each indicated depth.

4.2.4 Disturbance Effect

To assess differences in field CO_2 emissions based on time since last disturbance (Figure 4.10), I conducted a one-way analysis of variance (ANOVA) across time-elapsed categories. Although the flux data was not normally distributed (Shapiro-Wilk, $p<0.05$), parametric testing assumptions were met due to large sample size ($n>35$) and homogenous variance of the six categories. The results indicated no significant differences in mean CO_2 emission rates based on time since disturbance.

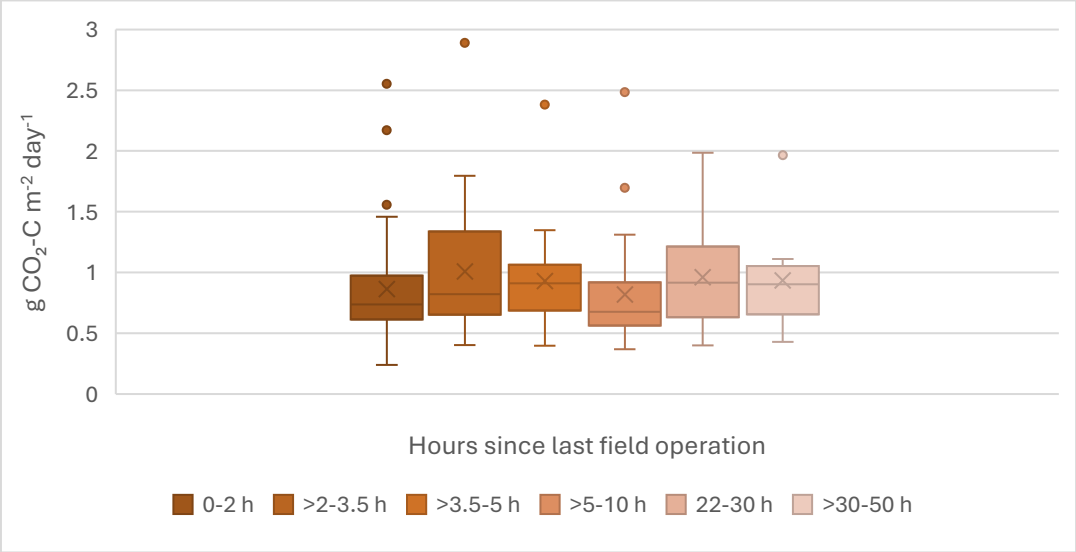

Figure 4.10: Distribution of CO_2 field fluxes based on time-elapsed since the field was last disturbed relative to the time of measurement (n= 30, 28, 30, 29, 29, 23 respectively).

CH_4 emissions based on time since last disturbance (Figure 4.11) were not normally distributed (Shapiro-Wilk, $p<0.0001$) and variance between categories was not homogenous (Levene's test, $p<0.0001$). A Kruskal-Wallis test identified significant differences in CH_4 emission rates between time-elapsed categories ($p<0.0005$). A subsequent Pairwise Mann-Whitney test identified that flux measurements taken between 0-2 hours after the disturbance had significantly higher CH_4 emissions than flux measurements taken later after the disturbance (>3.5-5 h, >5-20 h, 22-30 h, >30 hours) at the $p<0.05$ significance level. Fluxes from the next two most recent time categories (>2-3.5h and >3.5-5 hours) had significant differences from the two final time categories (22-30 h and >30 hours; $p<0.05$)

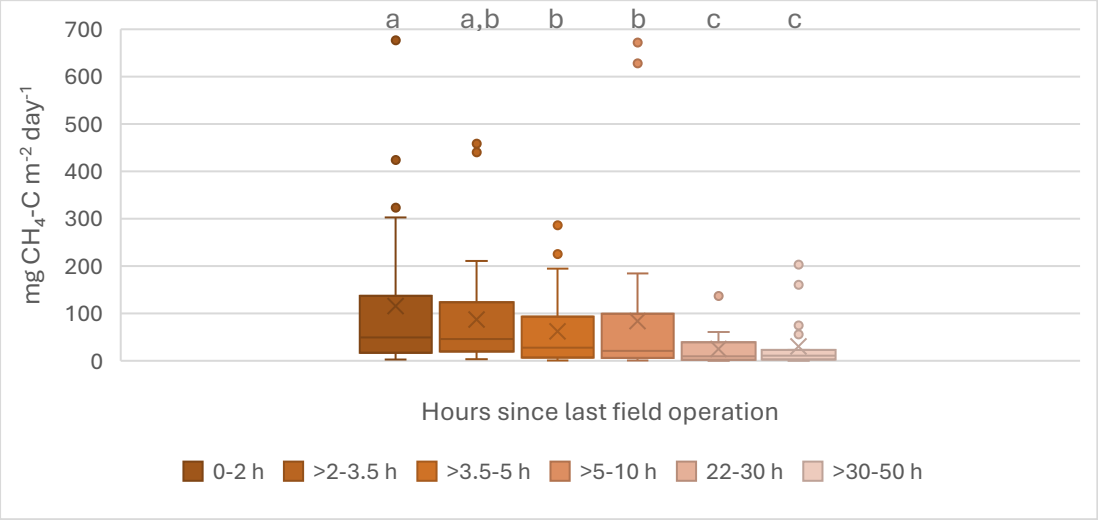

Figure 4.11: Distribution of CH_4 field fluxes grouped by the time-elapsed between measurement and the last disturbance (n= 27, 28, 28, 29, 29, 23 respectively). Groups sharing the same letter are not significantly different. To improve visualization, three large values from the 0–2-hour category were not plotted: 1118.2, 2985.3, and 3909.6 mg CH_4-C m^{-2} day^{-1}.

Based on visual inspection of the data, methane field emissions were at their peak and most variable closest to the time of disturbance. They later stabilized at a lower emission rate sometime between 10 and 22 hours since the disturbance. Pairing the time categories based on the similarity assessment above, I found that the mean CH_4 flux decreased by approximately 88.5% over time, and median flux decreased by 78.7% (Table 4.3).

Table 4.3: Time since disturbance summary statistics with similar groups merged.

Descriptive Statistics	**0-3.5 hours since disturbance**	**>3.5-10 hours since disturbance**	**>22-50 hours since disturbance**
Count *(n)*	57	57	52
Mean flux *(mg CH_4-C m^{-2} day^{-1})*	235.9	73.0	27.3
Median flux *(mg CH_4-C m^{-2} day^{-1})*	47.0	23.0	10.0
Standard deviation	652.1	128.2	44.1

The disturbance effect could not be properly explored by phase due to inadequate sample sizes for time-categories. This reflects the aim of operations management to minimize the amount of time between extraction processes to maximize production.

4.3 Uncovered Stockpile Fluxes

The following section presents the results from uncovered stockpile fluxes based on flux measurement position, seasonality, aspect, and grade. Temperature and moisture profiles are then compared. Lastly, covered stockpile flux results are presented.

A total of 140 flux measurements were taken across 18 different piles between the months of July and November 2022. Measurements were taken on the four faces of the stockpile at the bottom and top positions in the center of the face. The piles alternated between three industry designated peat grades throughout the study; these were: Grade 2 (six piles), Grade 3 (five piles) and Grade 5 (seven piles). The overall mean emission rate for CO_2 was 4.99 g CO_2-C m^{-2} day^{-1} (SD=7.65) and for CH_4 was 4.87 mg CH_4-C m^{-2} day^{-1} (SD=18.71).

4.3.1 Approach 1: Independent Fluxes

4.3.1.1 Positional Differences

To assess the difference in mean between the two positions, I conducted a paired sample t-test for CO_2 and CH_4 fluxes separately (Figure 4.12) The CO_2 fluxes measured at the top position of piles (Mean=8.10 g CO_2-C m^{-2} day^{-1}, SD=9.70) were significantly greater ($p<0.0001$) than those measured at the bottom (Mean=1.88 g CO_2-C m^{-2} day^{-1}, SD=2.10). There was no difference between positions for CH_4 fluxes. As such, the top and bottom positions were considered separately for all subsequent CO_2 analyses and grouped together for subsequent CH_4 analyses (Mean=4.9 mg CH4 m^{-2} day^{-1}, SD=18.7).

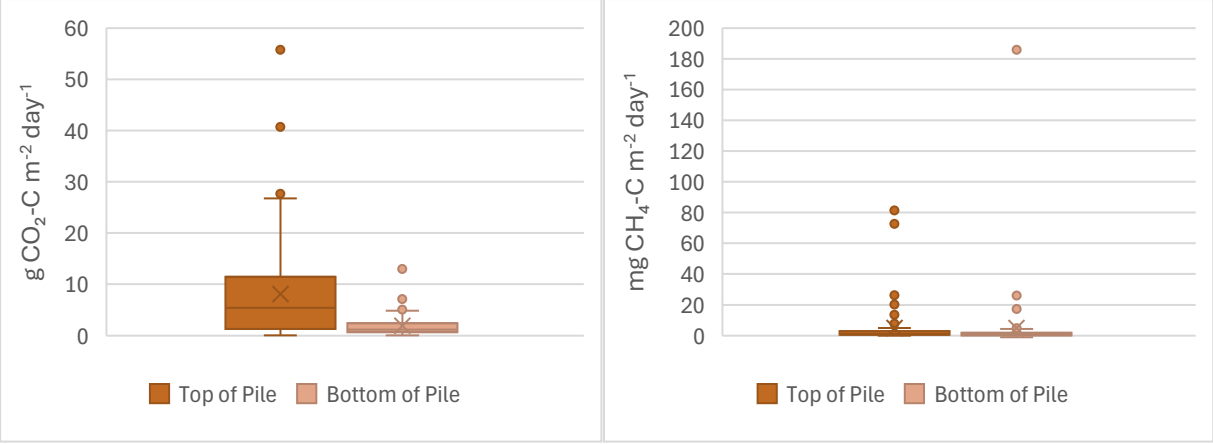

Figure 4.12: Distribution of CO_2 (left) and CH_4 (right) fluxes by measurement position on the stockpile.

4.3.1.2 Seasonal Trends

To determine the presence of seasonality in flux emission trends, fluxes were averaged over the month within which they were taken. CO_2 emissions taken at the top position increased during the summer months, peaked in September, and then decreased in late fall (Figure 4.13). However, these differences were not statistically significant. For CO_2 emissions at the bottom position, a one-way analysis of variance (ANOVA) revealed that the differences between means were significantly different ($p<0.005$). Tukey's HSD follow-up test then confirmed that bottom CO_2 flux measurements in November were lower (Mean=0.76 g CO_2-C m^{-2} day^{-1}, SD=0.62) than in July ($p<0.05$), August ($p<0.0005$), and September ($p<0.0005$) (Means=2.60, 2.15, & 2.35 g CO_2-C m^{-2} day^{-1}, SD= 2.60, 1.73, 1.42, respectively). No seasonal trends were observed for CH_4 fluxes on uncovered stockpiles.

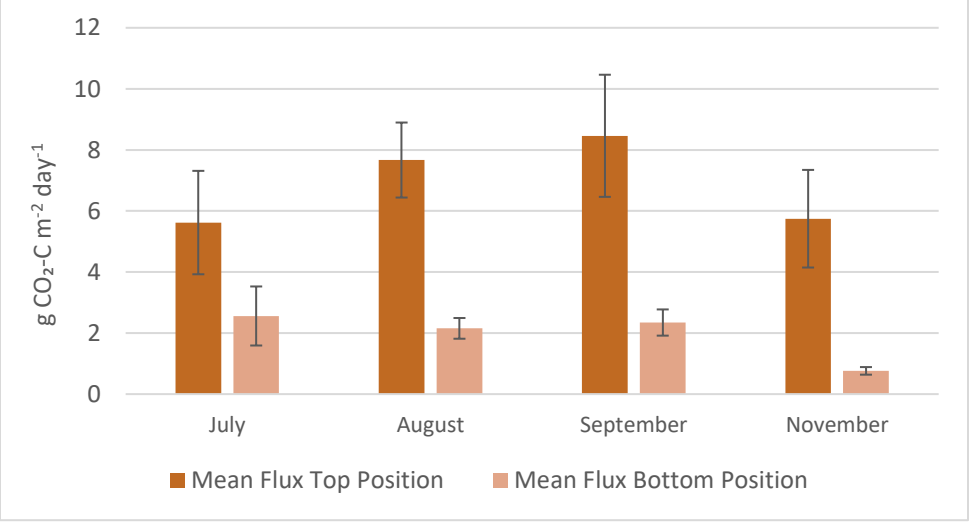

Figure 4.13: Seasonality of mean stockpile CO_2 fluxes at top and bottom positions. Note that no flux measurements were taken during the month of October.

4.3.1.3 Influence of Aspect

To determine whether the direction of the stockpile face had an influence on flux, measurements were grouped by aspect. Due to the orientation of the site, most stockpiles at Site A had their long axis facing the Northeast (45°) and Southwest (225°) directions, with the short axis facing Southeast (135°) and Northwest (315°) as depicted in Figure 4.14.

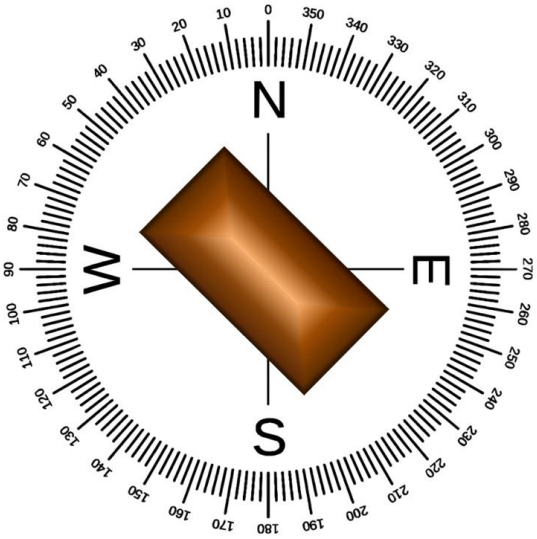

Figure 4.14: Orientation of most stockpiles at Site A. Other stockpiles were oriented with a 90-degree rotation, with lengths facing the Northwest and Southeast directions.

Two separate one-way analysis of variance (ANOVA) tests were conducted for fluxes at the top and bottom positions (Figure 4.15). These revealed that while there were no differences in flux between aspects at the bottom position, there were significant differences between aspects at the top position ($p<0.05$). A subsequent Tukey's HSD specified that top flux measurements facing Southwest had lower emissions (Mean=2.50 g CO_2-C m^{-2} day^{-1}, SD=2.64), than those facing Northwest ($p<0.005$), Northeast ($p<0.005$), and Southeast ($p<0.05$) (Mean=11.04, 10.23, & 8.58 g CO_2-C m^{-2} day^{-1}, SD=13.28, 10.61, & 7.20, respectively).

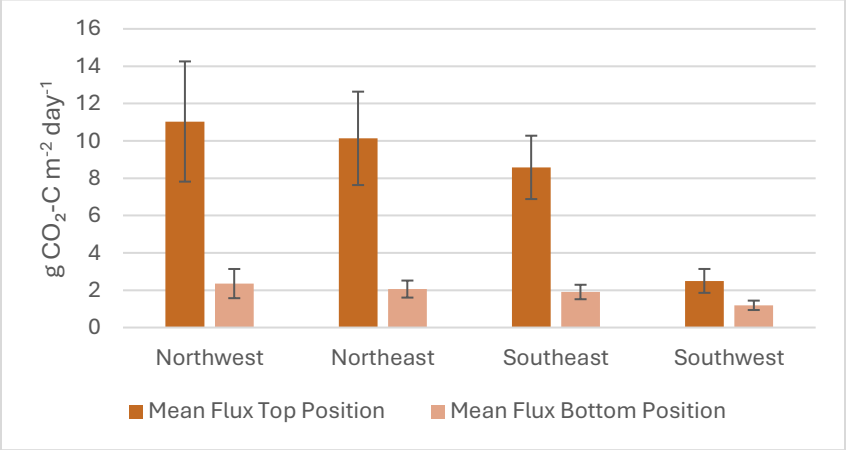

Figure 4.15: Mean CO_2 stockpile flux by aspect for the top and bottom positions with standard error bars.

For methane emissions by aspect (Figure 4.16), the data followed a non-normal distribution (Shapiro-Wilk, $p<0.01$) and the variance between categories was not homogenous ($p<0.005$). A Kruskal Wallice test determined significant differences for median CH_4 fluxes between aspects ($p<0.005$). A subsequent Pairwise Mann-Whitney test specified that the Northwest facing measurements had significantly higher CH_4 emissions (Median=1.84 mg CH_4-C m^{-2} day^{-1}) than those facing Northeast ($p<0.05$), Southeast ($p<0.05$), and Southwest ($p<0.0005$) (Medians=0.867, 0.68, & 0.28 mg CH_4-C m^{-2} day^{-1} respectively).

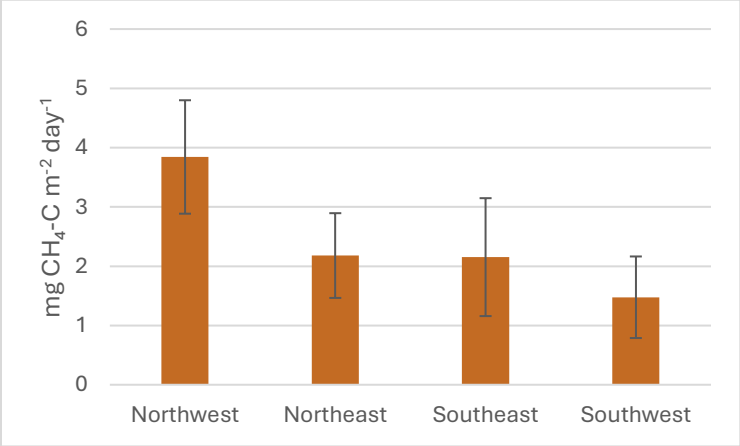

Figure 4.16: Mean CH_4 flux by aspect with standard error bars. Note that three large values were not plotted: 72.61 & 185.98 mg CH_4-C m^{-2} day-1 facing Southeast, and 81.46 mg CH_4-C m^{-2} day^{-1} facing Northeast.

4.3.1.4 Industry Designated Peat Grade

To assess for differences based on industry designated peat grades, CO_2 and CH_4 fluxes were grouped according to their grade, and one-way analysis of variance (ANOVA) was conducted (for each GHG separately). The results indicated no significant differences between peat grades for CO_2 (at the top and bottom positions) or CH_4 fluxes.

4.3.2 Approach 2: Fluxes Clustered by Pile

I originally used a Linear Mixed Effects to account for random effect (differences between piles) and fixed effects (differences based on position, seasonality, aspect, and industry grade) on the uncovered stockpile log-transformed flux data. However, the initial model had a singular fit, suggesting that the random effect (differences between piles) was too complex for the data to support. Consequently, the random effect was removed, resulting

in a Standard Linear Regression model, which had a better AIC than the initial Mixed Effects model (Table 4.4).

Table 4.4: Estimated co-efficient, standard error, lower CL, and upper CL for Standard Linear Regression Model exploring the relationship between log-transformed CO_2 flux (dependent variable) and several environmental factors. Values have been back transformed from log scale.

Variable	Co-efficient	Standard Error	Lower CL	Upper CL
Bottom	1.413	1.174	1.029	1.941
Top	4.280	1.171	3.130	5.859
East	3.557	1.241	2.319	5.458
North	3.193	1.241	2.081	4.894
South	2.779	1.237	1.822	4.233
West	1.160	1.242	0.755	1.782
August	2.313	1.196	1.623	3.287
July	4.477	1.430	2.206	9.116
November	0.924	1.186	0.659	1.297
September	3.824	1.301	2.270	6.424
Grade 2	1.684	1.204	1.164	2.435
Grade 3	3.152	1.266	1.974	5.003
Grade 5	2.807	1.209	1.927	4.096

The model explained 39.0% of the variance in the log-transformed CO_2 flux data and after adjusting for the number of predictors this reduced to of 34.8%. A substantial portion of the variability was not explained by the included predictor values, likely because moisture and temperature, having strong influence on decomposition, were not considered in the model, because we could not measure them at the center of the pile where most of the decomposition and GHG production takes place.

The emmeans function was employed to perform post-hoc comparisons between the levels of categorical variables. The emmeans function calculates the estimated marginal means (also known as least-squares means) representing the mean response (log-transformed CO_2 flux) adjusted for the other factors in the model. These adjusted means provide a clearer understanding of the effect of each factor level after accounting for the influence of other variables in the model. The use of emmeans with pairwise comparisons allowed for a detailed examination of the differences between specific levels within a factor, such as comparing the CO_2 flux between different positions, aspects,

grades, or months. I used the Bonferroni correction (adjust="bonferroni" argument) to adjust for multiple comparisons to control the family-wise error rate, and reduce the likelihood of false positives.

The top position fluxes were significantly greater than bottom position fluxes ($p<0.0001$), fluxes on the West face were significantly less than those on the North, East, and South faces ($p<0.05$), and fluxes taken in November were significantly less than those taken in July, August, and September ($p<0.005$). There were no significant differences between grades.

These results echo those from Approach 1, further supporting the hypothesis that fluxes from the same pile were spatially independent (i.e., those taken from the same pile were not more similar than those taken from other piles) and validates both the use and results of Approach 1.

4.3.3 Temperature and Moisture Profiles

For each flux measurement, a temperature profile (at 0, 20, 40, 60, 80, & 100 cm depths) and moisture profile (at 0, 20, 40, 60, and 80 cm) were taken perpendicular to the surface of the stockpile (adjacent to the surface flux position). These profiles were treated as independent variables and were evaluated for influences from: the top and bottom pile positions, seasonality, aspect, and grade.

4.3.3.1 Positional Differences

An unbalanced two factor ANOVA using regression was used to evaluate the effects of depth, position, and the interaction between them on temperature (Figure 4.17). The results of this analysis showed significant differences in temperature for all three factors ($p<0.005$). Tukey HSD tests revealed that the top position had significant differences between depths ($p<0.05$), where measurements taken at 0, 20, and 40 cm were similar, but significantly different from those recorded at 60, 80, and 100 cm.

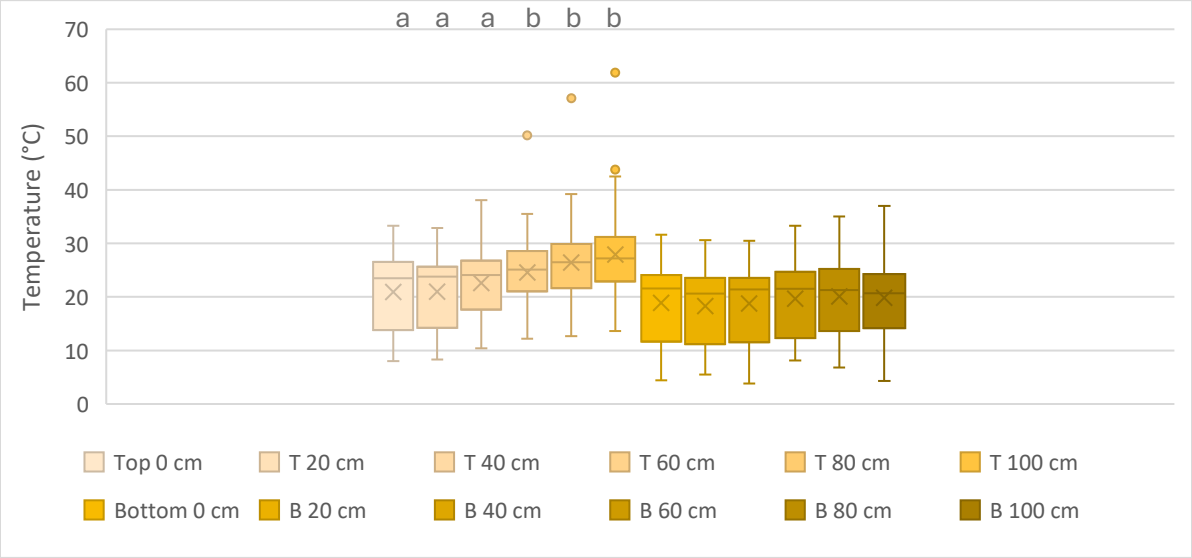

Figure 4.17: Distribution of temperature (°C) measurements taken on uncovered stockpiles by depth and position. Groups sharing the same letter are not significantly different.

The same analysis was repeated to evaluate the effects of depth, position, and the interaction between them on moisture (Figure 4.18). As before, the results showed significant differences in moisture for all three factors ($p<0.001$). Tukey's HSD then revealed that only the bottom position had significant differences between shallower and deeper VWC ($p< 0.05$).

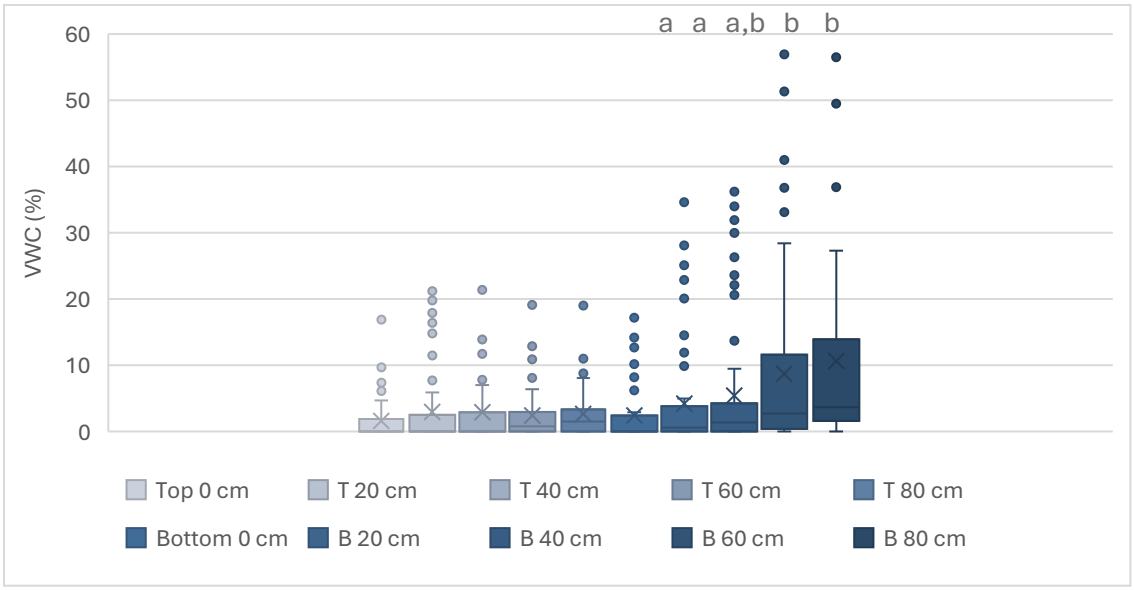

Figure 4.18: Distribution of moisture (VWC) measurements taken on uncovered stockpiles by depth and position. Groups sharing the same letter are not significantly different.

4.3.3.2 Seasonality, Aspect, and Grade

For all subsequent analyses, the top and bottom temperature profiles were considered separately. Depth was included for both positions, using separate unbalanced two factor ANOVAs using regression to evaluate differences in temperature and moisture profile based on seasonality, aspect, and grade. Follow up Tukey's HSD were then used to identify specific differences.

Significant temperature differences between depths persisted for only the top position in all subsequent tests ($p<0.0001$). In contrast, significant moisture differences between depths persisted for only the bottom position ($p<0.005$).

For temperature seasonality at both the top and bottom positions (Figure 4.19), temperature profiles in November were colder than those in July, August, and September ($p<0.0001$). At the bottom position only, temperatures in July also differed from the other months ($p<0.0001$).

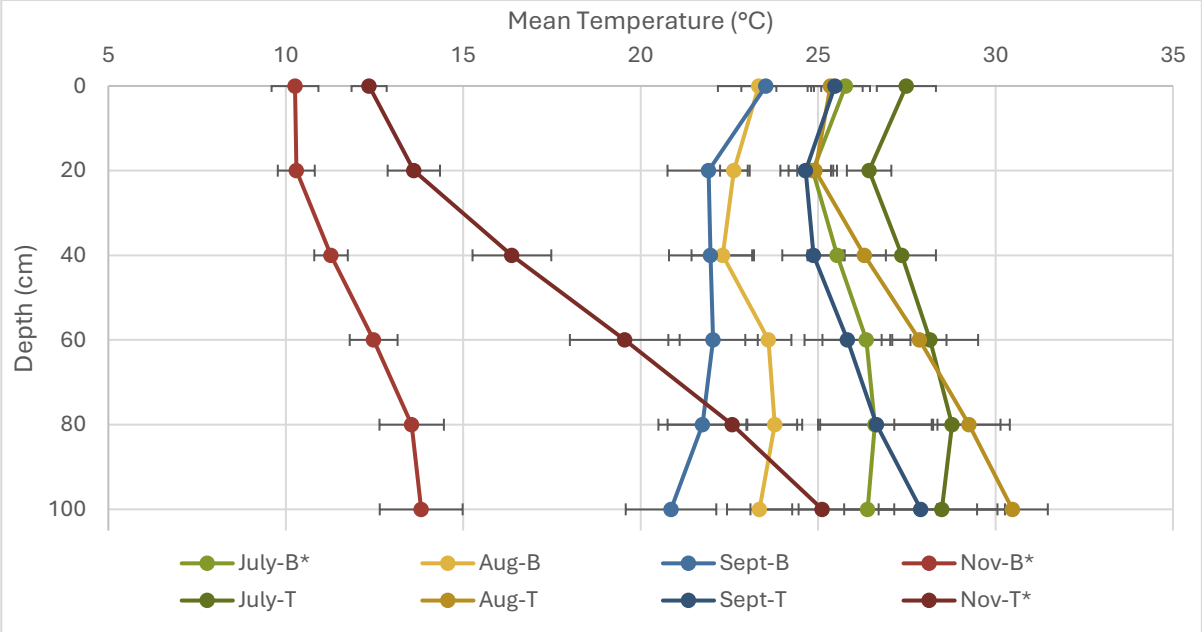

Figure 4.19: Mean monthly temperature profile for top (T) and bottom (B) positions of uncovered stockpiles, with standard error bars. *Indicates that temperatures for that month were significantly different from those of other months at the same position.

For moisture seasonality at both the top and bottom positions (Figure 4.20), November was significantly moister than all other months ($p<0.05$). At the top position, July and September were also significantly different $p<0.05$).

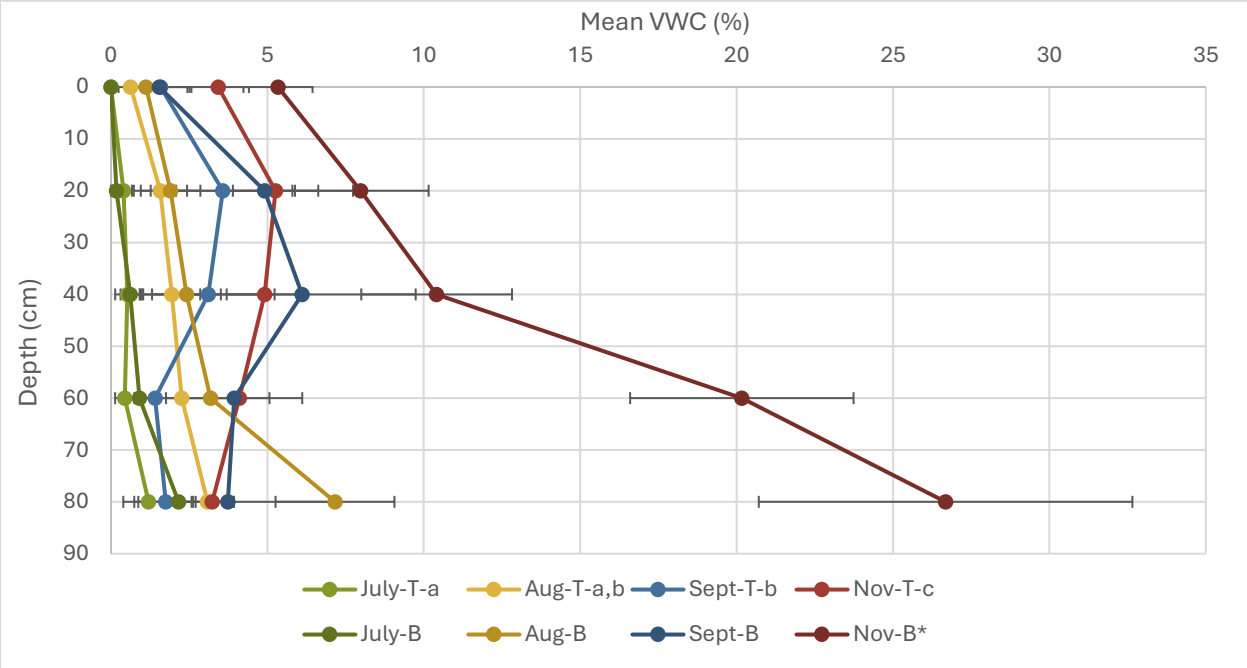

Figure 4.20: Mean monthly moisture profile for top (T) and bottom (B) positions of uncovered stockpiles, with standard error bars. For the top position, groups sharing the same letter are not significantly different. For the bottom position, *indicates that moisture for that month was significantly different from the others.

There were no differences in temperature profiles due to aspect or industry designated grade at both positions. For moisture profiles, there were significant differences in moisture profiles between aspects at the top position only ($p<0.0005$). Grade 5 was also found to be moister than Grades 2 and 3 at both the top and bottom positions ($p<0.05$).

4.4 Covered Stockpile Fluxes

For covered stockpiles, CO_2 and CH_4 fluxes were measured over the tarp, a covered hole, and an open hole, (Medians= 0.56, 5.88, 423.75 g CO_2-C m^{-2} day^{-1} & 0.2, 6.5, 600.8 mg CH_4-C m^{-2} day^{-1}, respectively) finding significant differences between measurements for both gas types (Kruskal Wallice $p<0.0001$) (Figure 4.21). A subsequent Pairwise Mann-Whitney test confirmed that all categories were significantly different from each other ($p<0.0001$). While the tarp was found to not be entirely impermeable to GHGs, significantly higher

emissions from holes covered with tape and open holes in the tarp suggest that GHGs are accumulating beneath the tarp due to obstructed diffusion.

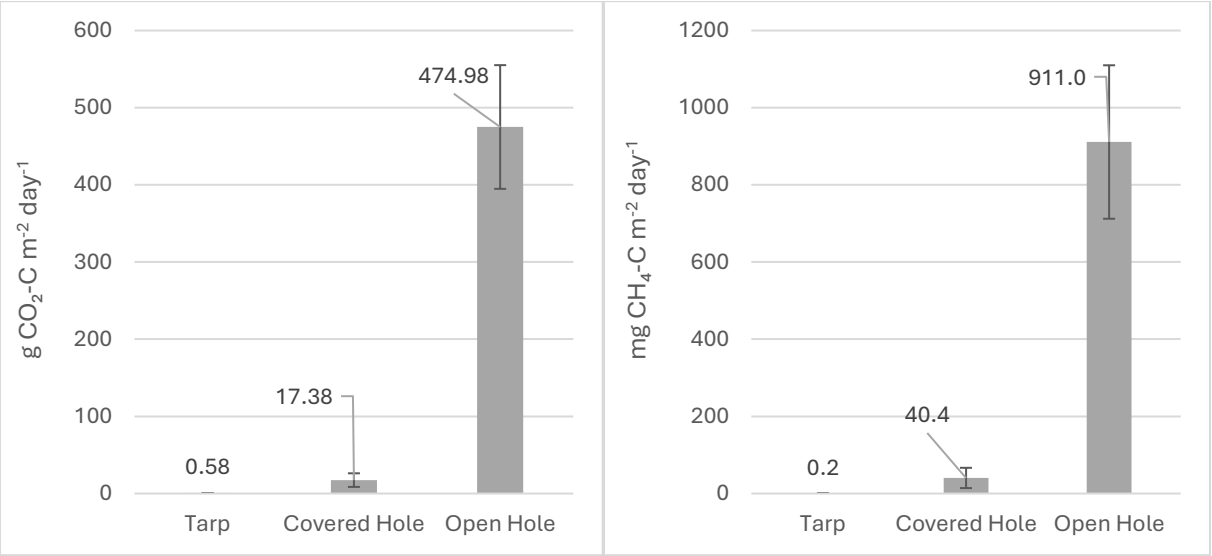

Figure 4.21: Mean CO_2 (left) and CH_4 (right) fluxes on covered stockpiles over the tarp, over a covered hole, and over an open hole, with standard error bars.

4.5 Stockpile CO_2 and CH_4 Storage

In this section, I first present an overview of GHG storage results for uncovered and covered stockpiles. Next, I analyze CO_2 storage in uncovered stockpiles, focusing on change in storage over time, temperature, and moisture. Following this, I provide a detailed analysis of CO_2 storage in covered stockpiles. Lastly, I compare the diffusion of CO_2 molecules based on stockpile management.

4.5.1 Overview Comparison of Stockpile Storage

Stockpile management impacted GHG storage (Figure 4.22). The largest concentration recorded for uncovered stockpiles was 34.02 g CO_2-C m^{-3} at the 300 cm depth V-top position (this was the only measurement at 300 cm in the study). Apart from this exception, the minimum storage concentration for covered stockpiles (32.35 g CO_2-C m^{-3}) exceeded the maximum concentration for uncovered stockpiles (28.18 g CO_2-C m^{-3}), resulting in no overlap between the distributions of the two management strategies.

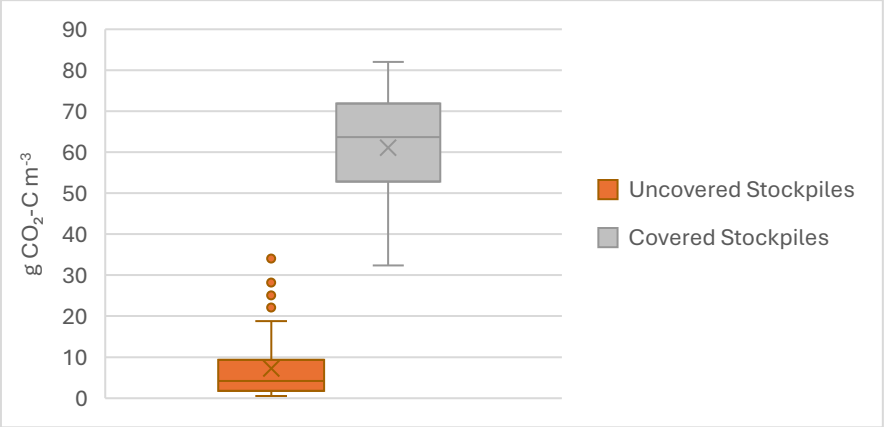

Figure 4.22: Distributions of CO_2-C concentrations (combined across all pile positions and depths) for covered and uncovered stockpiles (n=55 uncovered, n=98 covered).

Summary statistics for CO_2 and CH_4 storage concentrations (including depths from 25-200 cm) in covered and uncovered stockpiles (Table 4.5) reveal that covered stockpiles had an average concentration 9.1 times higher than uncovered piles, with a median concentration 16.3 times higher. Thus, covered stockpiles stored significantly more CO_2 than uncovered ones. However, both types of stockpiles had much larger concentrations than that of ambient air at 0.225 g CO_2-C m^{-3} (calculated from 421 ppm CO_2 using standard atmospheric conditions; NOAA 2022).

Table 4.5: Summary statistics for covered and uncovered stockpile GHG storage, across all piles and positions for the 25, 50, 75, 100, 150 and 200 cm depths (one measurement from an uncovered stockpile at the 300 cm depth is omitted).

GHG	Stockpile	Min Conc.	Max Conc.	Average	Median	Std. Error
g CO_2-C m^{-3}	**Uncovered**	0.50	28.18	6.73	3.90	0.91
	Covered	32.35	82.04	61.08	63.71	1.29
mg CH_4-C m^{-3}	**Uncovered**	0.3	14.3	2.9	2.2	0.3
	Covered	8.4	2077.7	580.3	460.7	56.0

All CH_4 concentrations were also greater than that of ambient air at 0.1 mg CH_4-C m^3 (calculated from 1911 ppb CO_2 using standard atmospheric conditions; NOAA 2022). Uncovered stockpiles had low CH_4-C storage, with a maximum of 14.3 mg CH_4-C m^{-3} detected. In contrast, covered stockpiles had CH_4-C concentrations ranging from 8.4 to 2077 mg CH_4-C m^{-3}, with an average of 580.3 mg CH_4-C m^{-3} across all pile depths and positions. Notably, the highest CH_4 concentrations (~ 2 g CH_4-C m^{-3}) were detected in Pile 10, which was the only stockpile placed on gravel instead of directly on the field. This

demonstrates that stockpiles themselves produce methane, in addition to any methane produced by the underlying field that either diffuses through (for uncovered) or accumulates within (for covered) stockpiles.

Given the minimal methane storage in the stockpiles, the following analyses focus on CO_2 storage. Temperature and moisture measurements at various depths were generally comparable for covered and uncovered stockpiles. Overall, covered stockpiles were slightly warmer, while uncovered stockpiles were slightly moister, as will be presented in subsequent sections.

4.5.2 Uncovered Stockpiles

4.5.2.1 CO_2 Storage

Two uncovered stockpiles (Pile 86-industry designated Grade 2, and Pile 253-industry designated Grade 5) were sampled to estimate GHG storage concentrations. Stored CO_2 concentrations were measured from gas samples taken at various positions and depths within the piles (see Methods §3.3.2 for details). CO_2-C concentrations generally increased with depth at all positions (Figure 4.23).

Pile 253 was sampled twice, at 39 and 81 days after its formation. Between the dates of sampling, CO_2 storage concentration generally increased, and new equipment allowed deeper sampling (200 and 300 cm in depth) on the second date, where higher concentrations were detected. The exact formation date of Pile 86 is unknown, but field observations suggest that the sampling date was somewhere between 14-45 days after the pile was formed.

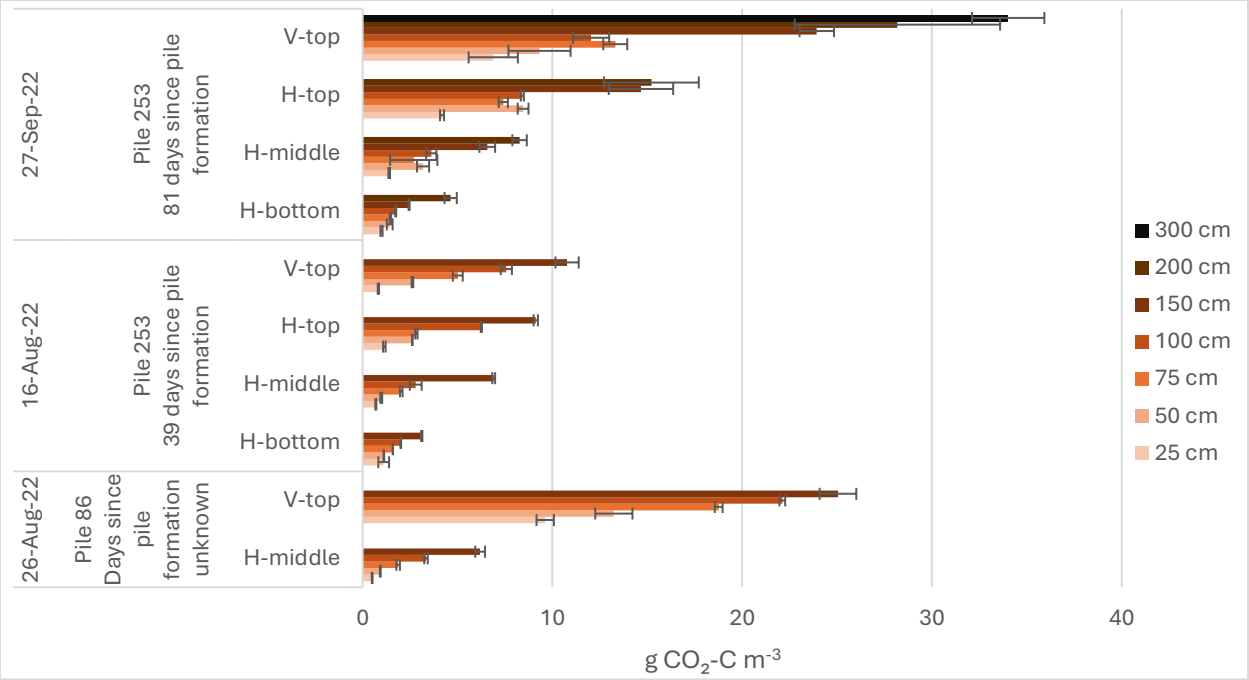

Figure 4.23: Uncovered stockpile CO_2-C storage concentrations at various depths and positions for Pile 86 (sampled once) and Pile 253 (sampled twice), with standard error bars.

4.5.2.2 Change in Storage Over Time

To assess the change in storage with time ($\Delta S/\Delta t$), CO_2 storage concentrations for Pile 253 were compared, considering only the depths sampled on both dates (25-150 cm; Figure 4.24). Average CO_2 concentrations across these depths increased by 88% from August 16th to September 27th, rising from 3.6 to 6.7 g CO_2-C m^{-3}. The average change in storage across all depths was 0.09 g CO_2-C m^{-3} day^{-1} from the pile's formation to the first sampling date ($\Delta S/t_1$) and 0.08 g CO_2-C m^{-3} day^{-1} between the first and second sampling dates ($\Delta S/t_2$). This indicates a small accumulation of CO_2 within the uncovered stockpile over time, with the majority of the CO_2 produced being emitted to the atmosphere from its surface.

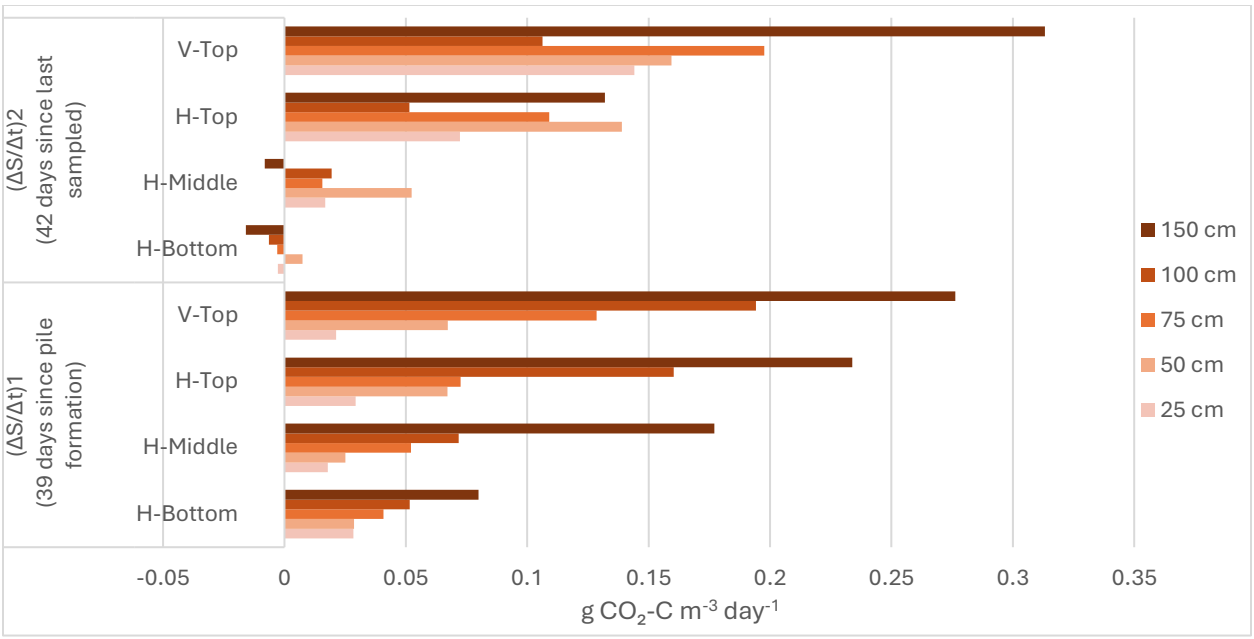

Figure 4.24: Change in storage (g CO_2-C m^{-3} day^{-1}) at various positions and depths for Pile 253 (uncovered), between its formation and first round of sampling ($\Delta S/\Delta t_1$), and between the first and second rounds of sampling ($\Delta S/\Delta t_2$).

4.5.2.3 Temperature and Moisture

The change in temperature and moisture measurements for Pile 253 were evaluated between August (1st sampling date) and September (2nd date) (Figure 4.25). Temperatures in September decreased at all horizontal positions, while the Vertical-top position showed increased stratification with depth. All changes were within 10°C, and therefore not biogeochemically significant, as reflected by the relatively steady change in storage over time. Volumetric moisture content (VWC) ranged from 0% to 10% at all positions and depths on both dates, except at the Vertical-top position, where VWC increased to 22-33% in September (Figure 4.26).

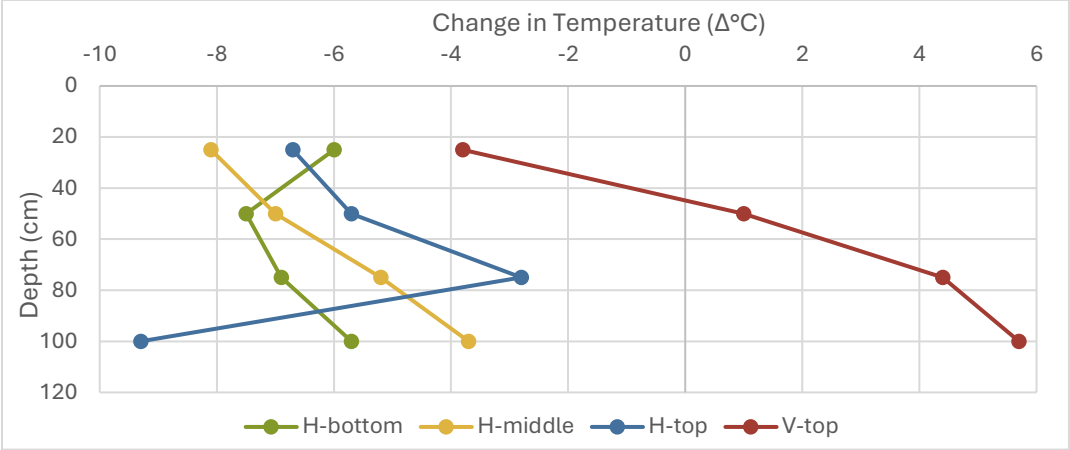

Figure 4.25 Change in Pile 253 temperatures (Δ°C) at depth from 16 August to 27 September 2022 (corresponding with GHG storage samples).

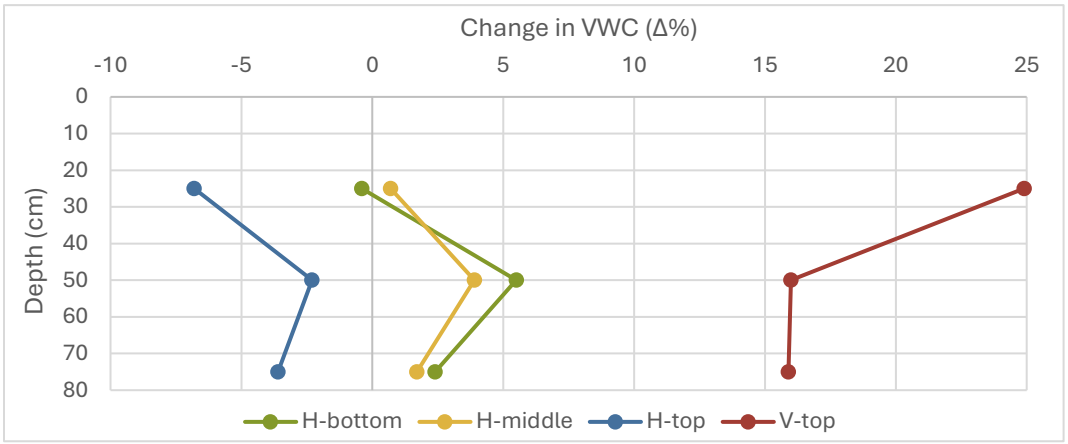

Figure 4.26: Change in Pile 253 moisture (ΔWVC%) at depth from 16 August to 27 September 2022 (corresponding with GHG storage samples).

4.5.3 Covered Stockpiles

4.5.3.1 CO_2 Storage

Three covered stockpiles (Pile 2–industry designated Grade "humide", Pile 10–Grade 3, and Pile 14–Grade 5) were sampled to estimate stored GHG concentrations. Samples were taken at two positions (Horizontal-middle and Vertical-top) and various depths within the piles on three separate dates, approximately one month apart (see Table 3.2 in Methods §3.3.2).

Unlike the trend observed in uncovered stockpiles, concentrations did not consistently increase with depth (e.g., Figure 4.27).

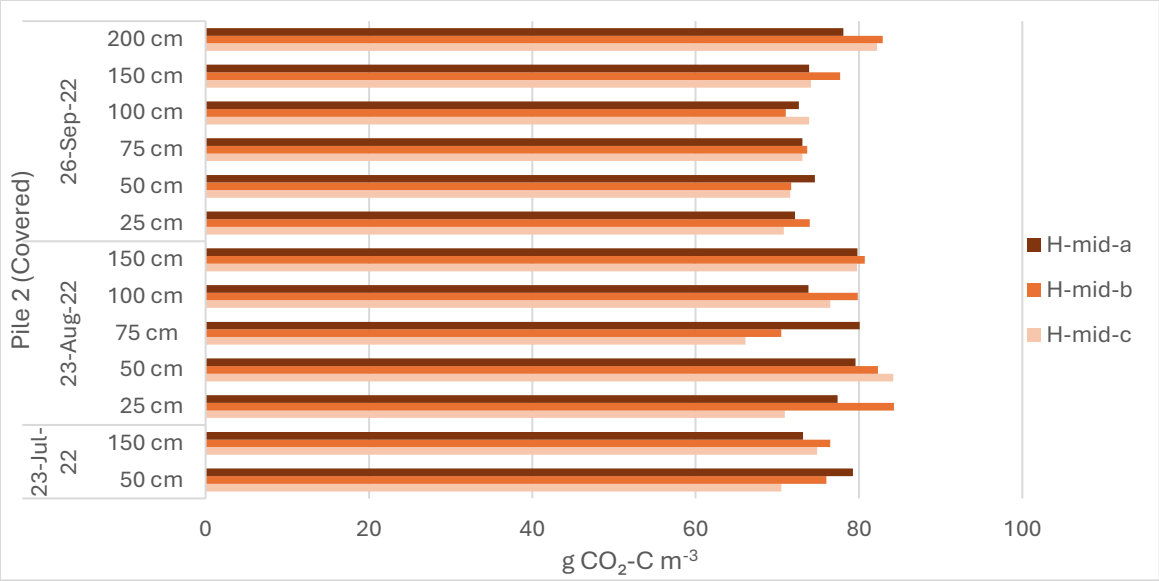

Figure 4.27: Comparison of triplicate samples for Pile 2 CO_2-C concentrations from the Horizontal-middle position, at available depths on three sampling dates. This figure exemplifies that there was no relationship between concentration and depth for covered stockpiles.

On each of the sampling dates, I conducted two-factor ANOVAs to determine differences in CO_2 concentrations by position and depth for each pile (a total of nine ANOVAs) (Table 4.6). For all nine tests, concentrations did not differ significantly between depths, but for seven of the nine tests, concentrations significantly differed between the H-middle and V-top positions ($p<0.05$). Subsequently, all depths were averaged for a given pile position on each of the sampling dates (e.g., concentrations from all depths for Pile 2's V-top position taken on 23-July were averaged).

Table 4.6: Summary of results for nine two-factor ANOVAs (by date and pile ID) determining significant differences in measured CO_2 concentrations by depth and position.

Sampling Date	***Pile 2***	***Pile 10***	***Pile 14***
23-July-22	Concentrations similar at all depths and positions.	Concentrations similar between depths, but significantly different between the H-middle and V-top positions $p<0.05$.	Concentrations similar between depths, but significantly different between the H-middle and V-top positions $p<0.05$.
23-Aug-22	Concentrations similar between depths, but significantly different between the H-middle	Concentrations similar between depths, but significantly different between the H-middle	Concentrations similar at all depths and positions.

	and V-top positions p<0.05.	and V-top positions p<0.05.	
26-Sept-22	Concentrations similar between depths, but significantly different between the H-middle and V-top positions p<0.05.	Concentrations similar between depths, but significantly different between the H-middle and V-top positions p<0.05.	Concentrations similar between depths, but significantly different between the H-middle and V-top positions p<0.05.

Pile positions for each of the sampling dates were compared (Figure 4.28). Most CO_2-C concentrations were between 50 and 80 g CO_2-C m^{-3}. For Piles 10 and 14, stored CO_2 increased from July to August, followed by a slight decrease from August to September for both H-middle and V-top, with alternating positions showing greater concentrations. For Pile 2, concentrations remained steady over time at approximately 65 g CO_2-C m^{-3} for V-top and 75 g CO_2-C m^{-3} for H-middle.

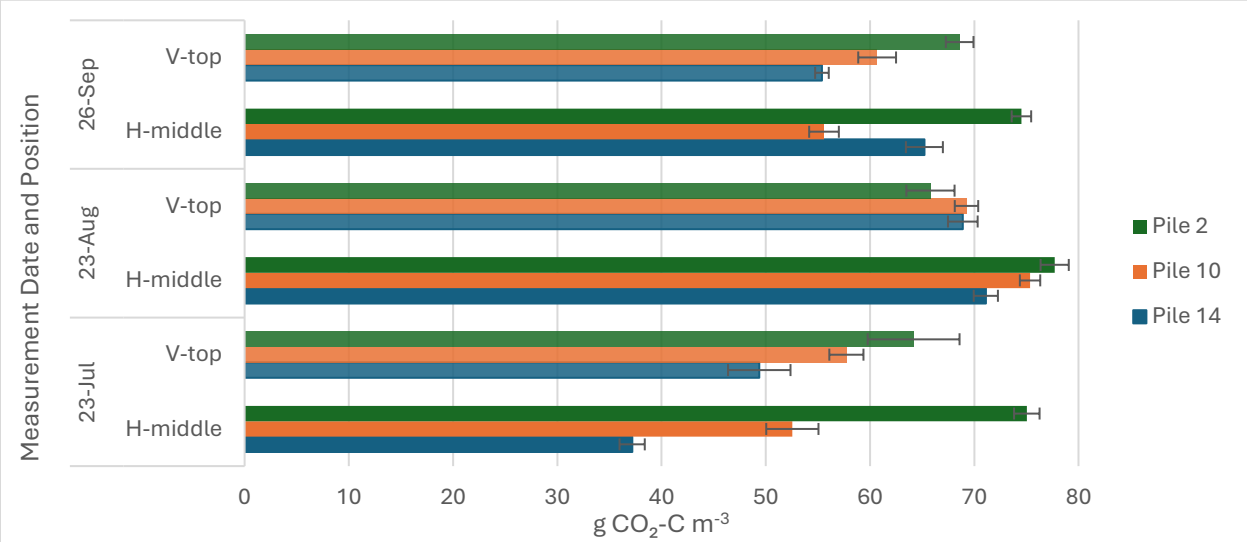

Figure 4.28: Comparison of average CO_2-C concentrations by date and position for 3 covered stockpiles with standard error bars.

4.5.3.2 Changes in Storage Over Time

I plotted the average CO_2-C concentration for each position by the number of days since the stockpile was covered (Figure 4.29). Since gas samples were taken from the three piles on the same days, external environmental variables were controlled for.

The percent increase in average CO_2-C from July to August ranged from 3% (Pile 2, V-top, from 18 to 49 days) to 91% (Pile 14, H-middle, from 4 to 35 days). In contrast, from August to September, CO_2-C decreased by -4% at Pile 2 (H-middle, from 49 to 84 days) and

-26% at Pile 10 (H-middle, from 43 to 78 days); only Pile 2 V-top experienced an increase of 4%. This finding demonstrates that CO_2 did not continue to accumulate underneath the tarp over time. It also suggests that concentrations increased rapidly once the stockpiles were covered, reaching a quasi steady-state after ~2 weeks of formation/covering. The highest storage concentrations from all three piles were recorded in August, 35 to 49 days after they had been covered.

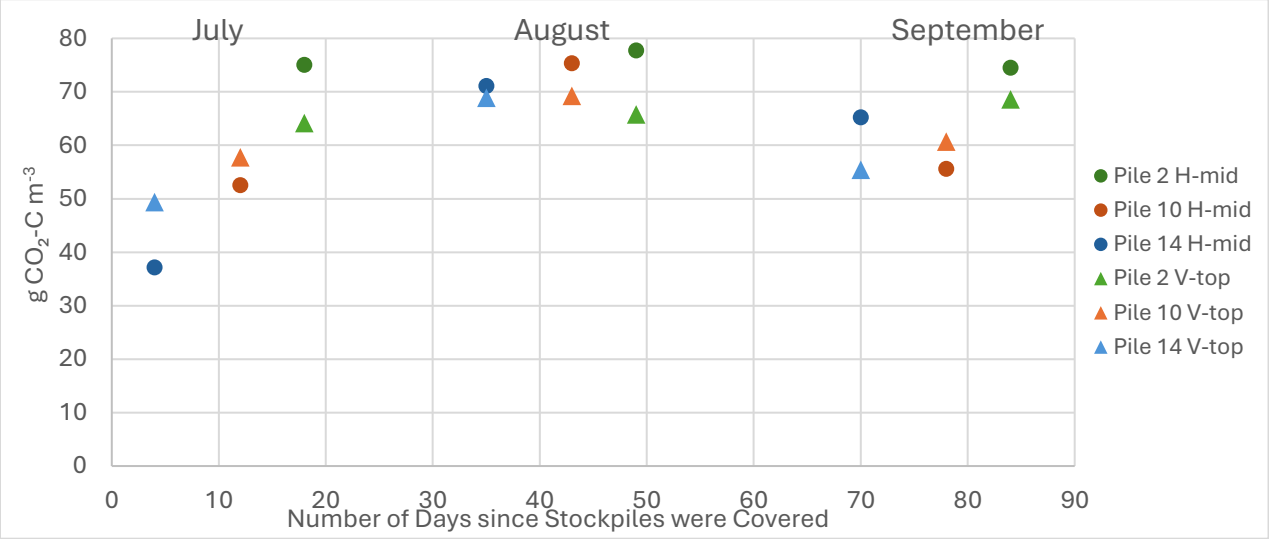

Figure 4.29: Average CO_2-C concentrations for samples taken from the H-middle (H-mid) and V-top positions on three covered stockpiles by the number of days the piles were left covered in the field.

To examine changes in stored CO_2 over time (Figure 4.30), I calculated the change in storage for each of the piles (see Methods §3.3.4). The largest change in storage occurred between the covering of the stockpiles and the first round of sampling. Pile 14, sampled just 4 days after being covered, had the largest initial change in storage per day at 9.3 (H-mid) and 12.3 (V-top) g CO_2-C m^{-3}, more than double that of Piles 2 and 10. $\Delta S/\Delta t_1$ for both positions on Piles 2 and 10 were between 3.6 to 4.8 g CO_2-C m^{-3} day^{-1}, having been covered for 12 and 18 days, respectively. $\Delta S/\Delta t_2$ ranged from 0.11 to 1.11 g CO_2-C m^{-3} day^{-1} and $\Delta S/\Delta t_3$ ranged from -0.56 to 0.11 g CO_2-C m^{-3} day^{-1}, for all piles and positions. The large decrease from $\Delta S/\Delta t_1$ to $\Delta S/\Delta t_3$ further supports the idea that stockpiles quickly accumulate CO_2 when they are first covered, but accumulation rates then slow over time.

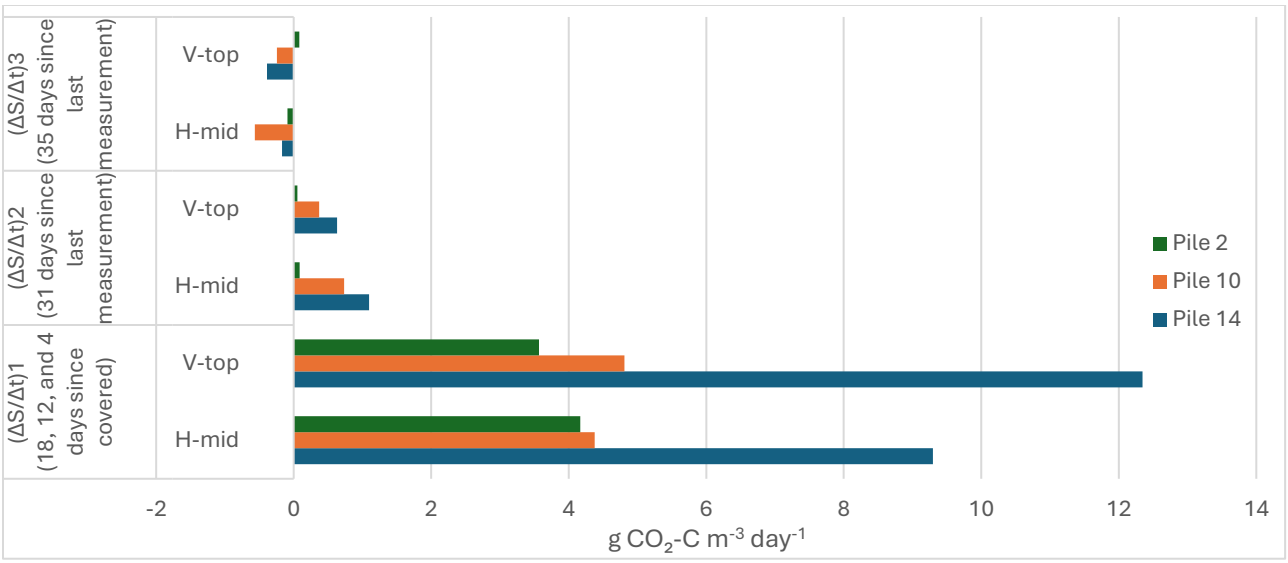

Figure 4.30: Change in storage over time (g CO_2-C per m^3 per day) between three sampling dates for three covered stockpiles at two sampling positions (H-mid and V-top).

4.5.3.3 Temperature and Moisture

Change in covered stockpile storage may have been influenced by temperature (Figure 4.31). At first glance, the slight decrease in storage between the August and September sampling dates appears to be driven by cooler temperatures. However, the reduction in temperature was smaller at greater depths, especially for the V-top positions, indicating that internal temperatures maintained their warmth compared to shallower depths within the pile. Based on these patterns, depths beyond our probe length were likely warmer than our measurements.

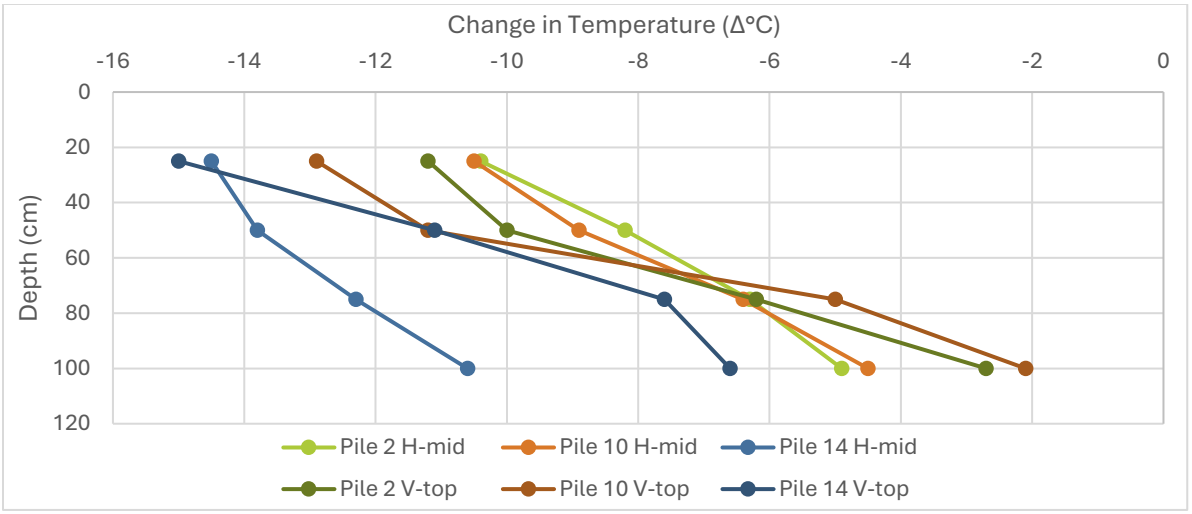

Figure 4.31: Change in temperatures (Δ°C) for Piles 2, 10, & 14, from 23 August to 27 September 2022 (corresponding with GHG storage samples).

As stockpiles remain in the field, they become more susceptible to leakage. Tarps may become ripped from storms, and repeated temperature probing (by the companies) can create leaks from the taped holes that are sealed after measurements. Therefore, the observed decrease in $\Delta S/\Delta t_3$ may more likely be attributed to increased leakage from the tarp over time rather than changes in temperature.

Moisture measurements revealed that the stockpiles were relatively dry (less than 6% VWC), with moisture levels fluctuating by less than 3% between measurement dates (Figure 4.32).

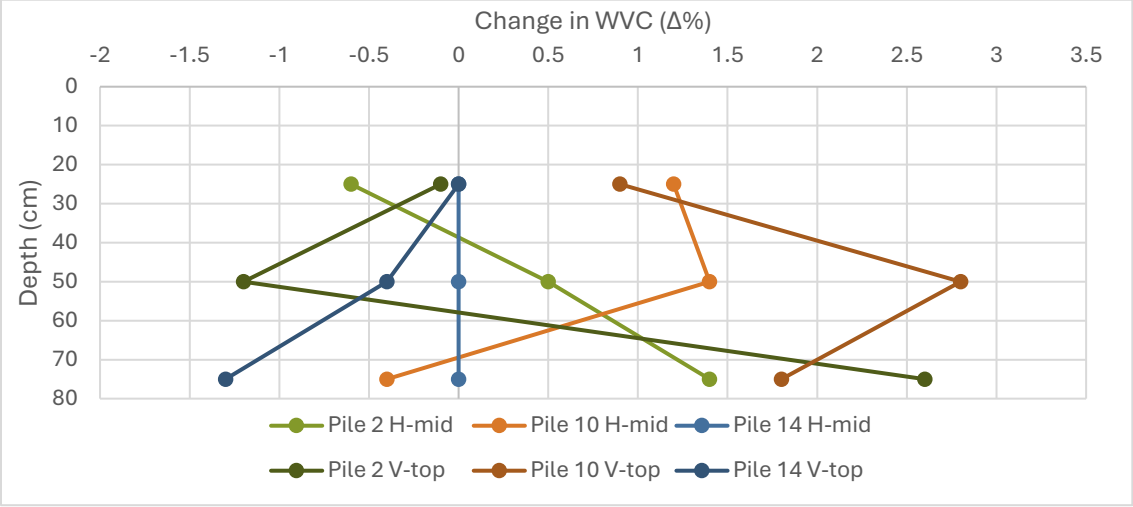

Figure 4.32: Change in moisture (ΔVWC%) for Piles 2, 10, & 14, from 23 August to 27 September 2022 (corresponding with GHG storage samples).

4.5.4 Diffusion Comparisons in Covered and Uncovered Piles

I compared CO_2 concentrations at depth for all four sampling positions for a covered and uncovered stockpiles that were in the field for 84 and 81 days, respectively (Figure 4.33). Both piles were industry designated Grade 5 from their respective companies. Only measurements at the 300 cm depth for the Vertical-top position on the 340 cm tall, uncovered stockpile were within range of the measurements recorded at any depth for the 520 cm tall, covered stockpile. The results highlight distinct differences in CO_2 concentration patterns between uncovered and covered stockpiles.

The covered stockpile referenced in Figure 4.33 had several holes in its tarp on the August 3rd sampling date, due to the presence of continuous measurement probes.

Therefore, it is unsurprising that it falls within the lower range of concentrations observed across the three covered stockpiles previously discussed in Section 4.2. This could also explain the greater variation between depths for this pile, whereas no significant differences were found between depths for covered Piles 2, 10, and 14.

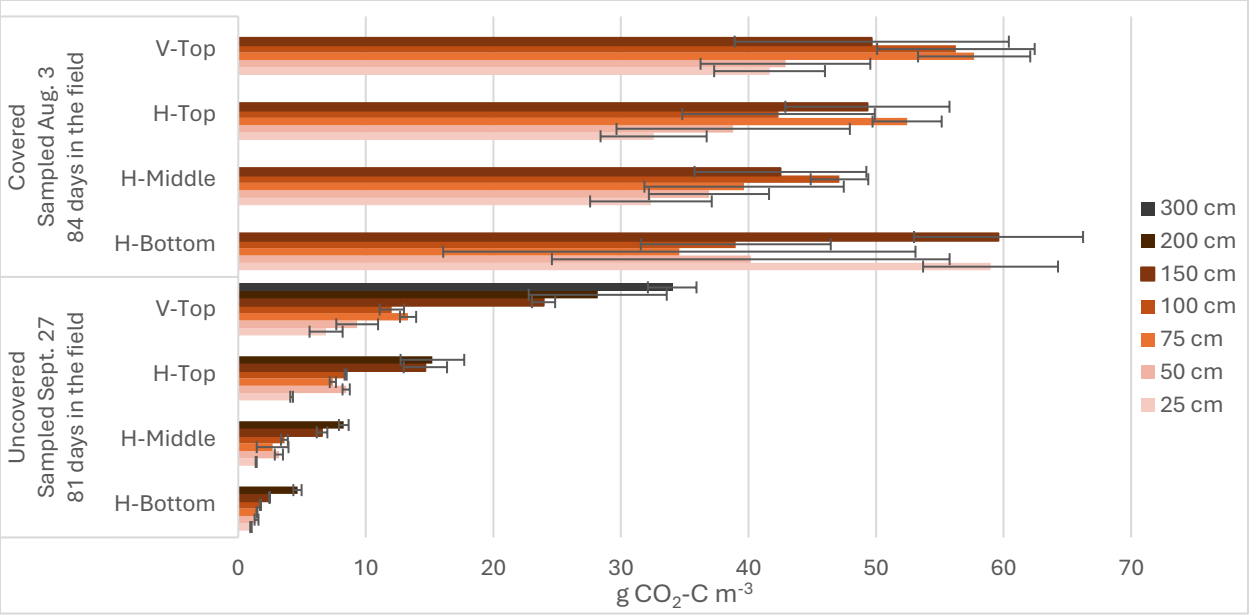

Figure 4.33: Comparison of CO_2-C from samples taken at various depth for four positions on a covered (McGill Pile) and uncovered (Pile 253) stockpile, having been in the field for a similar amount of time.

For uncovered stockpiles, CO_2 concentrations generally increased with depth and were higher at elevated horizontal positions on the pile; the H-bottom position had the least amount of stored CO_2 per m^3, while the H-top had the most. This confirms that most CO_2 produced diffuses upward to the surface of uncovered piles, where it is emitted into the atmosphere. V-top concentrations (moving from the top of a pile downwards through the center column) also increased with depth, indicating an inverse relationship with height and greater storage at lower depths, unlike the horizontal positions. This pattern reflects the triangular shape of stockpiles, where production is likely greatest near the base center (where the peat is most insulated), creating a stronger diffusion gradient between the center of the stockpile and the atmosphere above (visualized in Figure 4.34).

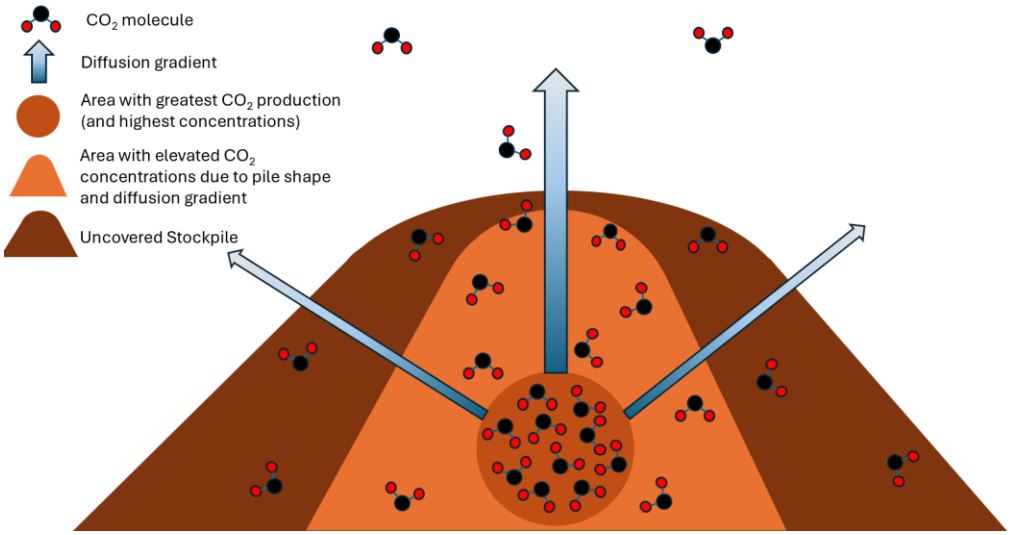

Figure 4.34: Conceptual diagram illustrating possible patterns of diffusion in uncovered stockpiles based on data from this study.

In contrast, covered stockpiles showed no apparent relationship between depth and CO_2 concentrations. The CO_2 levels at the H-bottom position of covered stockpiles were similar to, or greater than, those at the H-middle and H-top positions. This indicates that the tarp creates a barrier to diffusion from the pile to the atmosphere, leading to a more even distribution of gas molecules throughout the pore spaces of the peat within the pile (visualized in Figure 4.34b). Differences observed between positions are likely caused by the formation of temporary pockets of aggregated CO_2 molecules, which may shift as the stockpile's internal conditions change over time.

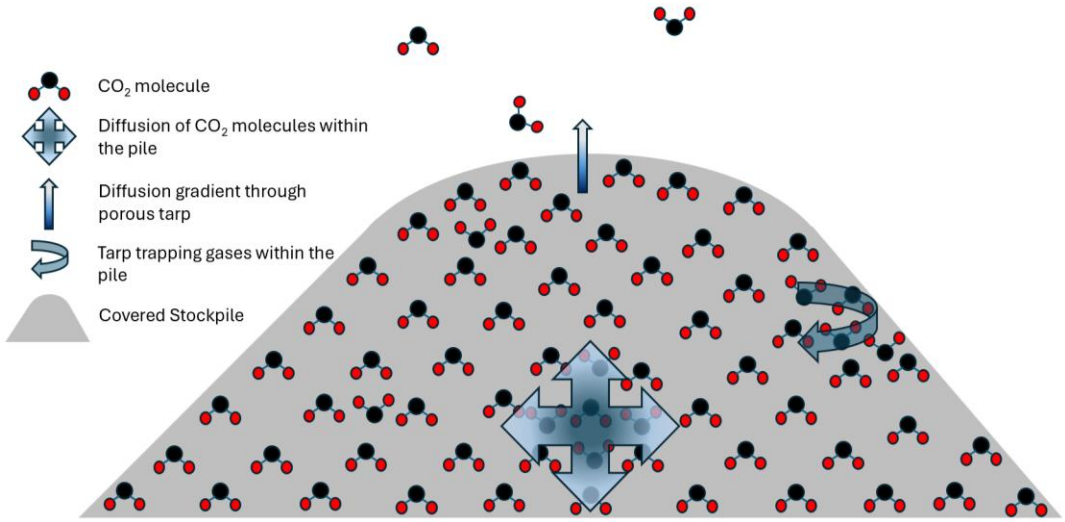

Figure 4.35: Conceptual diagram illustrating possible patterns of diffusion in covered stockpiles based on data from this study.

4.6 Contribution of Stockpiles to Overall Site CO_2 Emissions

In this section, I present differences in stockpile geometry between the study sites and the fluctuation in total number of stockpiles at Site B over time. Next, I examine the contribution of stockpiles to extraction site CO_2 emissions relative to the fields, considering bulk density and porosity to estimate the instantaneous loss of stored CO_2 when piles are removed. Lastly, I simulate the lifespan of Piles 2, 10, and 14 as covered and uncovered, to assess differences in cumulative emissions between the two management strategies.

4.6.1 Stockpile Geometry

The average surface and base areas of stockpiles measured at Company A, where most stockpiles were uncovered, were smaller than those at Company B, where most were covered (Figure 4.35). Satellite imagery and field observations showed that the few covered stockpiles at Site A were similar in size to the uncovered piles at that location. At Site B, the few uncovered stockpiles were also similar in size to the covered piles, although they were typically left uncovered for no more than three days. The difference in stockpile size between the two companies reflects management practices beyond the choice to cover.

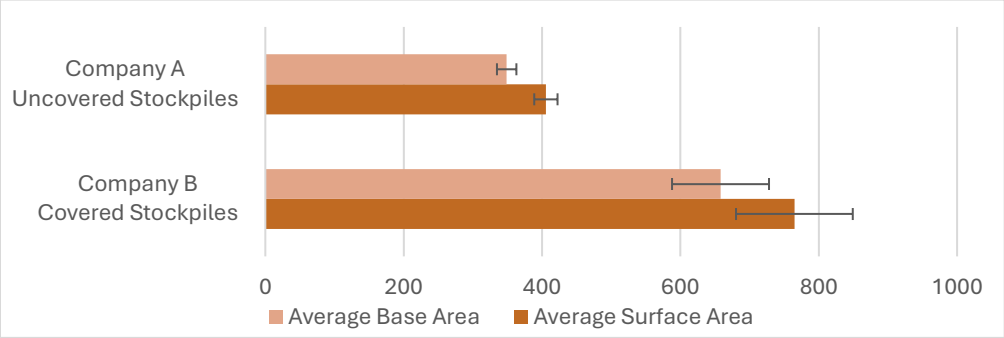

Figure 4.36: Average surface area and base area of covered and uncovered stockpiles measured at Companies A and B, with standard error bars.

4.6.2 Stockpile Accounting

The total number of individual stockpiles (including covered, uncovered, half covered, full sized, and half sized) was calculated at Site B on days with clear satellite imagery from May-December of 2022 (Figure 4.36). The figure includes the average total number of stockpiles for the month and the date used as a proxy for each month in subsequent analyses, except for October when fluxes were not measured.

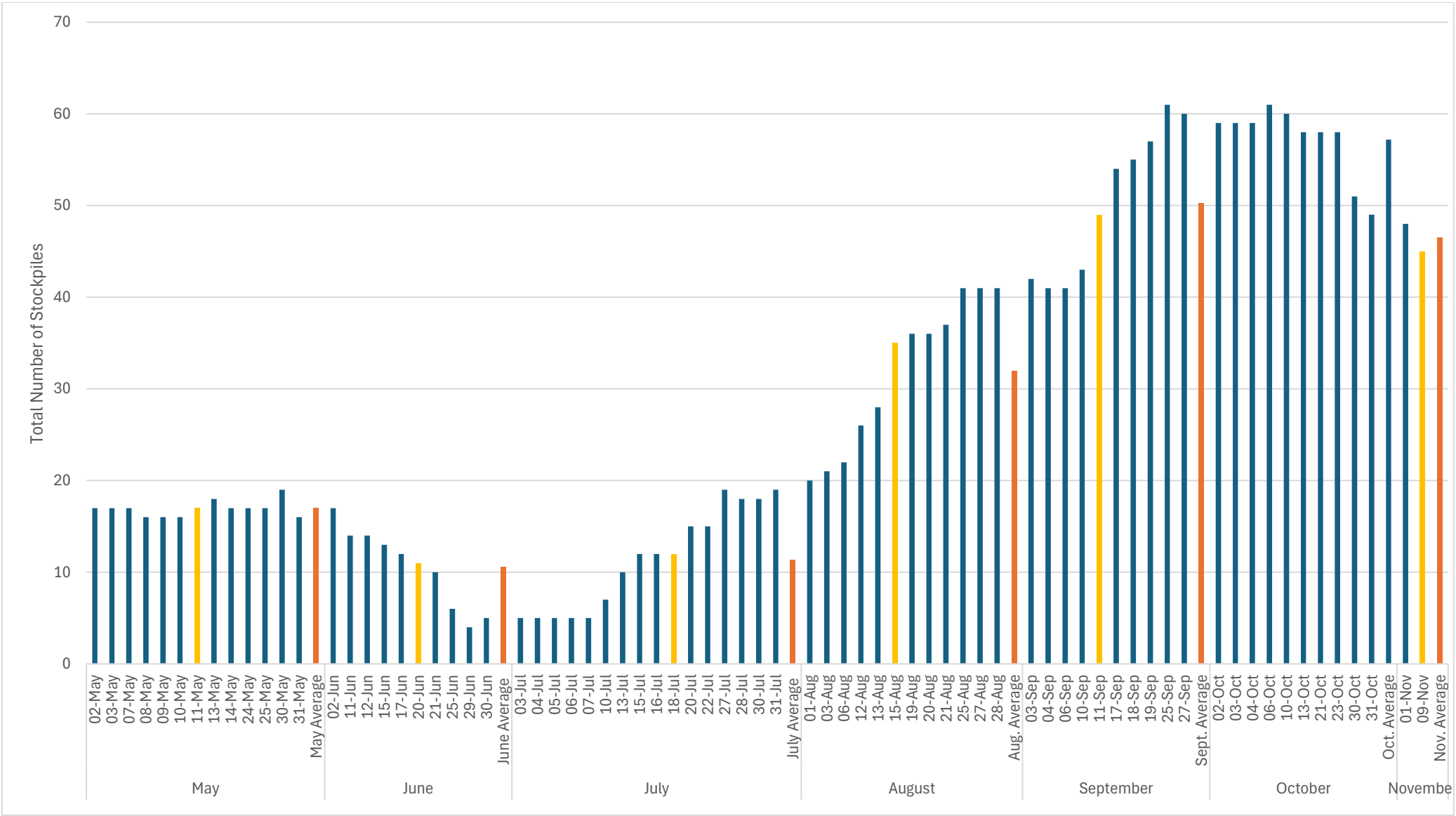

Figure 4.37: The total number of individual stockpiles observed at Company B from May-November. In orange: monthly average, and in yellow, proxy date used to estimate monthly emissions.

4.6.3 Estimated Contribution of Stockpiles

4.6.3.1 Bulk Density

Samples taken to assess stockpile density at depth (see Methods §3.4.3.2) showed that all but one of the measured dry bulk densities ranged from 144 to 205 kg m^{-3}, with both an average and median of 177 kg m^{-3}. A two-way ANOVA tested differences in bulk densities between depths (every 50 cm from the center outward) and axes (vertical, horizontal, and angled) from two separate stockpiles (totalling six axis categories), finding no significant differences.

Given that the piles were of different grades and that decomposition affects density, I conducted a t-test assuming equal variance between all dry bulk density measurements from the two piles (combining depths and axes) (Figure 4.37). The Grade 5 stockpile had significantly higher densities than the Grade 3 pile ($p<0.0001$).

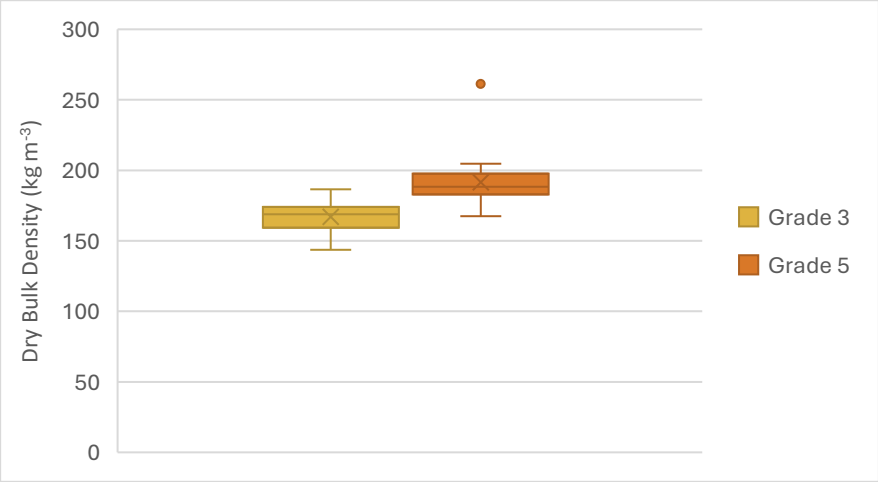

Figure 4.38: Dry bulk density measurements at depth compared between 2 uncovered stockpiles of different grades.

Since the sample densities were within the range (110-200 kg m^{-3}) quantified for the top 10 cm of surface peat for the fields at Site A, I assumed 82% porosity in accordance with Lai's (2022) findings for subsequent calculations (see Methods §3.4.3-6b).

4.6.3.2 Instantaneous Emissions Upon Stockpile Removal

The amount of CO_2 stored within the pore spaces of covered Piles 2, 10, and 14 was assumed to be instantaneously emitted upon the removal of the stockpile from the field (by uncovering the pile and bulldozing the peat to be transported for further processing). The

estimated values (Table 4.7) suggest that removing an average full-sized covered stockpile from Site B, after being in the field for more than 14 days, results in an instantaneous emission of approximately 52.5 kg CO_2-C (±8.0 kg CO_2-C).

Table 4.7: Estimate of average, minimum, and maximum instantaneous CO2 emissions from Piles 2, 10, and 14 upon the removal of the stockpiles.

Pile ID	**Stockpile Volume** (m^3)	**Average CO_2 Instantaneous E** (kg CO_2-C)	**Minimum CO_2 Instantaneous E** (kg CO_2-C)	**Maximum CO_2 Instantaneous E** (kg CO_2-C)
Pile 2	1021	52.6	45.9	59.2
Pile 10	1198	56.5	46.8	67.4
Pile 14	995	48.3	40.5	52.8
Average	1071	52.5	44.4	59.8

4.6.3.3 Proportional Contribution to Site CO_2 Emissions

To understand the contribution of stockpiles in overall emissions from extraction sites, I quantified the proportion of the study area occupied by fields and stockpiles, along with the percentages of total CO_2 emissions attributed to each, for every month of data collection at each site (Table 4.8).

For instantaneous emission calculations, I assumed 52.5 kg CO_2-C for every full-sized covered pile removed that month and 26.2 kg CO_2-C for each half-sized covered pile removed. For uncovered stockpiles removed (relevant for Site A only), the assumed instantaneous emissions were 3.1 kg CO_2-C per pile in July and August, 3.0 kg CO_2-C in September, and 2.8 kg CO_2-C in November. These estimates were derived by calculating the average volume of uncovered stockpiles at Site A (506 m^3), considering 82% porosity to determine the average pore space volume. Moisture content was factored into the pore space volume using the average VWC plus 9% (to account for probe error, see Results §4.1) for each month. The CO_2 storage was then calculated by subtracting the pore volume occupied by moisture and multiplying the remaining pore space by the average CO_2 storage concentration (6.73 g CO_2-C m^{-3}) measured across all uncovered stockpiles, positions, and depths (see Table 4.5).

Table 4.8: Percentage of field area (A) and pile area relative to the total study area, as well as the percentage of CO_2 emissions (E) from fields and stockpiles relative to overall emissions, including the instantaneous emissions from the stockpiles removed each month. The monthly contribution of stockpiles is the sum of the "% Pile E" and "% Instant. Pile E" columns.

Site	Month	% Field A	% Pile A	% Field E	% Pile E	% Instant. Pile E	% Pile A covered or uncovered
Site B Mostly Covered Stockpiles	***May***	99.42	0.58	98.92	0.64	0.43	92.09 covered
	Jun.	99.53	0.47	97.98	0.58	1.44	81.72 covered
	Jul.	99.51	0.49	99.00	0.62	0.38	91.72 covered
	Average	99.49	0.51	98.63	0.61	0.75	88.51 covered
Site A Mostly Uncovered Stockpiles	***Jul.***	99.54	0.46	97.98	1.94	0.08	100.00 uncovered
	Aug.	99.58	0.42	98.71	1.25	0.04	87.50 uncovered
	Sept.	99.52	0.48	97.88	1.98	0.14	80.00 uncovered
	Nov.	99.18	0.82	98.51	1.47	0.02	65.85 uncovered
	Average	99.46	0.55	98.27	1.66	0.07	83.34 uncovered

For Sites A and B, stockpiles represented less than 1% of the study area and accounted for approximately 1-2% of overall site emissions when including both surface fluxes and instantaneous emissions from pile removal (Figure 4.38).

4.6.4 Simulated Differences between Covered and Uncovered Pile Emissions

To further assess differences in emissions between stockpile management techniques, I simulated the lifespan (daily fluxes) and removal (instantaneous emissions) of Piles 2, 10, and 14, as both covered and uncovered. The results of this simulation suggest that the cumulative emissions would have been 20 to 40 kg CO_2-C greater had the stockpiles been left uncovered (Table 4.9). This likely represents CO_2 that was either leaked from the stockpiles, or not produced due to their coverings.

Table 4.9: Summary of simulated stockpile lifespan and removal as covered and uncovered, and the difference between them.

Pile ID	**Surface Area** (m^2)	**All E covered** (kg CO_2-C)	**All E uncovered** (kg CO_2-C)	**Difference** (g CO_2-C) All E covered – All E uncovered
Pile 2	627	73,860	112,310	-38,450
Pile 10	746	84,270	118,680	-34,400
Pile 14	678	67,790	89,470	-21,690

I estimated how much of this difference may have been from leakage during temperature probing. I assumed that a probe was inserted into the covered stockpiles to monitor their internal temperature twice per week throughout their lifespan, and at three different locations on the pile, causing 3 m^2 of the pile surface area to flux at the average open hole rate for 1 hour (19.79 g CO_2-C m^{-2} $hour^{-1} \cdot 3\ m^2 \cdot 1$ hour $\cdot$ # of probed days).

The results indicate that approximately 850 g CO_2-C would have leaked from Pile 2 during temperature probing over its lifespan, 746 g CO_2-C from Pile 10, and 611 g CO_2-C from Pile 14. This accounts for only 2.2 to 2.8% of the difference in cumulative stockpile emissions found in the table above.

Chapter 5: Discussion

The objective of my thesis research was to examine how peat management practices affected CO_2 and CH_4 emissions in actively extracted peatlands. Specifically, my research questions were: **(1)** Do the operations involved in peat extraction impact field GHG emission rates? and **(2)** How do management practices surrounding the storage of peat in stockpiles impact emissions?

I hypothesized that emissions from the fields would be impacted by field operations, resulting in differences in emissions between the phases of extraction (i.e., harrowed, drying, conditioned, and vacuum-harvested) and that the CO_2 emissions from stockpiles would be greater than those observed for the fields. I also hypothesized that carbon dynamics would differ between covered and uncovered stockpiles, and that stockpiles would be an important consideration for GHG accounting in managed peatlands.

My findings show that extraction phases themselves had little effect on field emissions, which were not overly different from average field emissions measured in previous studies. However, I found that disturbances from heavy machinery passing over the fields causes a temporary increase in CH_4 emissions, which dissipates over time. I also confirmed that uncovered stockpiles emit two to four times more CO_2 than extracted fields on a unit-area basis, and that while covering stockpiles reduces pile emissions by a factor of ten, the mass of CO_2 and CH_4 stored in covered stockpiles is more than ten times greater than their storage in uncovered piles. Finally, synthesizing all my work, I concluded that stockpiles, which represent less than 1% of the extraction area at both sites included in this study, contribute between 1-2% of total extracted site CO_2 emissions.

5.1 Field Operations

5.1.1 CO_2 Emissions Across Extraction Phases

There were no differences in CO_2 fluxes across the different phases of peat extraction, with an average emission rate of 0.91 (± 0.03) g CO_2-C m^{-2} day^{-1}. These results closely align with those reported by Clark et al. (2023), who found average CO_2 emissions of 0.90 (± 0.06) g

CO_2-C m^{-2} day^{-1} across various fields and sectors in the same geographic location. While my measurements were taken at Company B, Clark et al. (2023) conducted their study at Company A. Given that both sites were historically part of the same large, treed ombrotrophic bog ecosystem complex (Risi et al., 1953), the consistency in emission rates suggests a broader regional pattern. The measurements in both this study and Clark et al. (2023) were taken across numerous fields and sectors, supporting the idea that despite fluxes having high spatio-temporal variability, sampling from multiple locations within a landscape can reduce uncertainties in estimating average emissions at the landscape level (Wangari et al. 2022). Clark et al. (2023) achieved these results with a much larger sample size of 2161 chamber flux measurements, whereas my study captured similar average emissions with only 169 chamber flux measurements (7.8% of Clark et al. 2023's sample size) over similar-sized site areas (1.8 and 1.7 km^2, respectively). In comparison, Hunter et al. (2024) reported slightly higher CO_2 emission rates of 1.22 g CO_2-C m^{-2} day^{-1} for peatlands in Western Canada. Despite slight regional differences, the results from this study, Hunter et al. (2024), and Clark et al. (2023) all fall within the ranges of CO_2 emissions reported for other extracted boreal peat fields in the literature (see Supplementary Data 1 in He & Roulet 2023).

5.1.2 Disturbance-Driven Variability in Methane Emissions

Similar to other studies in the literature, methane emissions exhibited far greater variability than CO_2 emissions across the different phases of extraction, with the degree of variance differing significantly between phases. Because of this, I compared the medians of the four phases, rather than the means (see Methods §3.2.4). Methane emissions were significantly reduced during the drying phase of extraction, with median emissions of 9.3 mg CH_4-C m^{-2} day^{-1} (SD 19.8), which aligns with the average methane emissions reported by Clark et al. (2023) at 9.2 (± 4.0) mg CH_4-C m^{-2} day^{-1}, as well as other studies in the literature (e.g., Hunter et al. 2024; Manning et al. 2019; Sundh et al. 2000). In contrast, median emissions for the harrowed (45.0 mg CH_4-C m^{-2} day^{-1}, SD 697.2), conditioned (39.0, SD 110.5) and vacuum-harvested (28.0, SD 68.9) phases were similar to each other, but significantly

greater than drying, exceeding some of the values reported in the literature by an order of magnitude (see Table 2.3). However, methane emissions for all four phases were still far less than most documented natural peatland fluxes[2] (see Table 1 in Abdalla et al. 2016) which emit large amounts of methane despite their function as net carbon sinks (Huang et al. 2021; Strack et al. 2008; Byrne et al. 2004).

Knowing that flux rates are sensitive to variations in environmental conditions (Alm et al. 2007a; Kettunen 2003), I initially hypothesized that differences in field emissions between extraction phases would be the consequence of extraction processes modifying the environmental conditions of the fields, as summarized in Figure 5.1. Although there were statistically significant differences in conditions between phases, notably in moisture and surface temperature, these variations were not biogeochemically important.

The observed temperature differences were within 2-3°C from each other. Using Q_{10} values reported in the literature (e.g. Liu et al. 2024), these small differences in temperature would not be expected to produce large differences in respiration. Temperature profiles (from 10-100 cm in depth) between phases were also similar, indicating that temperatures at depth remain unaffected by disturbances at the surface. Similarly, surface moisture levels were below the optimal range (less than 64%) and varied by less than 5% across extraction phases. At depth, moisture content was within optimal levels for all phases, ranging from 70-80% VWC. Therefore, changes to field conditions due to extraction processes were not the cause of increased methane emissions in the harrowed, conditioned, and vacuum-harvested phases.

[2] To compare the daily fluxes reported in this study with annual fluxes from the literature, emissions during winter months, when the ground is frozen (~150 days/year), can be considered negligible.

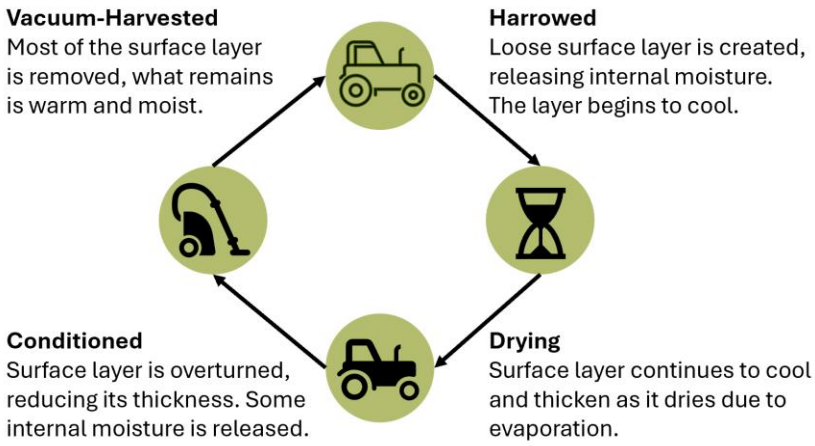

Figure 5.1: Qualitative summary of the impact of processes on surface layer conditions.

After harrowing, fields are typically left undisturbed for a period ranging from six hours to several days depending on daily weather conditions. Once the surface layer has sufficiently dried, the fields are conditioned and typically left in this state for approximately three hours unless there are delays due to weather or operations. Lastly, the fields are vacuum-harvested and do not typically remain in this phase for more than a few hours because operation supervisors prioritize initiating the harrowing phase as quickly as possible to restart the extraction cycle. As a result of this operations timeline, field flux measurements in the harrowed, conditioned, and vacuum-harvested phases were taken much closer to the last passing of heavy machinery over the field when compared to the drying phase.

As the first study to differentiate between extraction phases, it is likely that other studies measuring fluxes from actively extracted peat fields were done primarily during the drying phase, when the fields are left undisturbed for the longest period, making them more easily accessible. As a result, elevated emissions observed in other phases may have been caused by disturbance from heavy machinery, rather than modifications to field conditions specific to each phase. The observed decrease in methane emissions with time since disturbance supports this alternative hypothesis. Mechanical disturbance from machinery likely releases gas pockets trapped in the waterlogged soil below the surface, temporarily increasing methane emissions through ebullition. This well-documented

phenomenon (e.g., Tokida et al. 2007; Baird et al. 2004) could partially explain the sporadic instances of very high methane emissions recorded in this study, such as those observed within 0-2 hours post-disturbance (1.1, 3.0, and 3.9 g CH_4-C m^{-2} day^{-1}).

5.1.3 Implications for GHG Accounting

Clark et al. (2023) reported average field CO_2 emissions of 0.90 (± 0.06) g CO_2-C m^{-2} day^{-1} and CH_4 emissions of 9.2 (± 4.0) mg CH_4-C m^{-2} day^{-1}. In contrast, this study showed that average methane emissions could increase by a factor of 25 between 0 and 3.5-hours post-disturbance, later stabilizing at an 88–96% reduced emission rate sometime between 10 and 22 hours. Even at these higher emissions rates, methane is still a much smaller contributor than CO_2 to overall extraction site emissions. If machinery were to pass over the fields every three hours, the additional methane would increase the average carbon mass of total emissions by 25%. However, this does not account for the radiative properties of methane, having a 100-year global warming potential (GWP) of 27–30 and a 20-year GWP of 81–83. This is because methane has a higher radiative efficiency (absorbs more energy) than CO_2, but lasts in the atmosphere for considerably less time (EPA 2024). This indicates that emissions could be underestimated if using the baseline values in the literature from undisturbed fields. However, since machinery traffic is highly dependent on weather, extraction is unlikely to occur at regular time intervals between processes, and actual field fluxes are likely to vary considerably throughout the day.

Further research is needed to refine GHG accounting by creating a continuous 24-hour time series of field methane fluxes, to determine the persistence time of post-disturbance flux rates. Additionally, models should account for how methane fluxes may vary based on the intensity and frequency of extraction activities.

5.2 Covered vs. Uncovered Stockpiles

Average CO_2 emissions from stockpiles of either management type were at least two times larger than those from the fields, except for fluxes taken over the sealed tarp of covered stockpiles, which was found to hinder gaseous diffusion (Figure 5.2). Average methane

fluxes from uncovered stockpiles and over-sealed tarps were smaller than those from the fields. Whereas average methane fluxes from holes in the tarp covered with tape were within the range of field emissions, while those from open holes in the tarp were more than triple field emissions. Nevertheless, methane emissions from stockpiles are negligible for daily emissions accounting (<0.01 g CH_4-C m^{-2} day^{-1}).

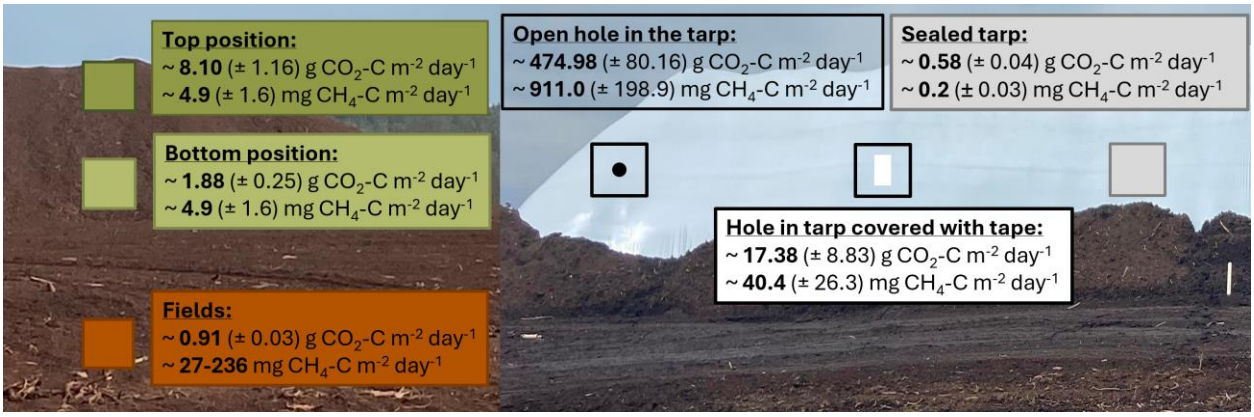

Figure 5.2: Overview of average covered and uncovered stockpile CO_2 and CH_4 fluxes compared to emissions from the fields, with standard error in brackets.

I expected that stockpiles would emit more CO_2 than the fields because the peat in stockpiles has been moved from the water saturated soil to an aerobic environment, increasing heterotrophic respiration and consequently, CO_2 emissions. Stockpiles are typically placed along access roads on top of the extracted fields, which doubles or triples the height of decomposing mass compared to the fields alone. This is reflected by four times higher CO_2 emissions observed from the top of uncovered stockpiles relative to the bottom.

Two different approaches were used to confirm that uncovered stockpile fluxes were impacted by both position and seasonality, but not by industry grade. Approach 1 allowed me to analyze fluxes from the top and bottom positions independently, which was advantageous for considering localized conditions that may affect emissions. I provided a more accurate representation of stockpile GHG emissions on a per m^2 basis by calculating weighted emissions means by month (Table 5.1). There were significantly reduced CO_2 emissions from the southwest face of uncovered stockpiles at the top position, which

coincided with the predominant direction of winds and gusts (see Figure 3.3). This suggests that the southwest face may be more ventilated than the others, and that aspect does not need to be considered in GHG accounting.

Table 5.1: Weighted mean of uncovered stockpiles fluxes by month, assuming 25% of stockpile surface area emitting at top position rates, and 75% emitting at bottom rates.

Month	Top	Bottom	Weighted Mean	Standard Error
July	5.62	2.56	3.33	0.84
August	7.67	2.15	3.53	0.4
September	8.46	2.35	3.88	0.59
November	5.75	0.76	2.01	0.41

These averages are an order of magnitude smaller than the only other study to directly measure CO_2 emissions from uncovered peat stockpiles at a rate of 19.66 g CO_2-C m^{-2} day^{-1} (Ahlholm & Silvola 1990), as well as most other simulated values in the literature (see Table 2.4). Ahlholm & Silvola observed non-significant differences in CO_2 emissions based on seasonality, a finding consistent with the results of this study. However, their seasonal emission trends correlated with air temperatures while ours did not. The relationship between emissions and seasonality is likely more reflective of the longevity of stockpiles in the field, rather than the influence of atmospheric conditions. There were very few stockpiles in July due to relatively high levels of precipitation prohibiting extraction operations. The number of stockpiles continually increased over the month of August (see Figure 4.36), which was much drier. Because of this, the stockpiles measured in September were likely to have been in the field for longer, allowing the internal temperatures of the insulated peat within the piles to increase over time, in turn driving higher CO_2 emissions. This is consistent with the industry's knowledge of heat generation at the inner core of stockpiles, as the low conductivity of dry peat hinders heat dissipation through the layers of the pile. This creates an insulating effect that accelerates decomposition at greater depths (Cleary et al. 2005), which necessitates the regular probing of stockpiles to monitor internal temperatures and avoid spontaneous combustion. We also documented evidence of this, as temperatures increased with depth for both kinds of piles, especially in later months.

The main reason for covering stockpiles is to reflect solar radiation back to the atmosphere to slow their warming. However, more temperatures above 25°C were recorded within the profiles of covered stockpiles at various depths and positions, than within uncovered ones. This indicates that environmental factors such as wind and air circulation may play a bigger role in regulating uncovered stockpile temperatures than anticipated. Moisture dynamics also differed, with covered stockpiles having relatively low moisture content, ranging from 0 to 5.6%, while the moisture levels in uncovered stockpiles went up to 32%. This reflects the impermeability of tarps preventing precipitation from infiltrating covered stockpiles from their surface. However, this may not be the case at greater depths within the stockpile that we could not capture by our probes. Overall, the lower moisture content and slightly higher temperatures in covered stockpiles suggest that the tarp acts not only as a physical barrier to gas diffusion but also alters the microenvironment within the pile, impacting GHG dynamics.

Unexpectedly, I found that the “impermeable” reflective tarp of covered stockpiles was somewhat permeable to gases, allowing for some diffusion through its pore spaces at significantly reduced, but relatively steady rates. Considering that most covered stockpiles surface area is made up of sealed tarp, uncovered stockpiles have significantly higher fluxes than covered ones. However, measurements taken over holes in the tarp that were covered with tape revealed significantly higher emissions with considerable variability, indicating facilitated release of accumulated GHGs into the atmosphere through leakage. Further measurements over open holes showed that exposing covered stockpiles to the atmosphere creates a rapid outflow of accumulated CO_2 and CH_4, resulting in a considerable burst of instantaneous GHG emissions, especially of CO_2. However, these open hole flux measurements do not accurately represent true daily emissions. The elevated fluxes stem from a small hole within the measured surface area, rather than reflecting a square meter of open surface. Additionally, these high rates of gas release are likely transient, driven by the newly established diffusion gradient between the atmosphere and the accumulated GHGs beneath the tarp.

Stockpiles stored much higher GHG concentrations than ambient air (see Results §4.5.1), with covered stockpiles storing greater concentrations of GHGs (61.08 g CO_2-C m^{-3}; 580.3 mg CH_4-C m^{-3} averaged across all depths and positions) compared to uncovered stockpiles (6.73 g CO_2-C m^{-3}; 2.9 mg CH_4-C m^{-3}). The large amount of methane accumulated in covered stockpiles suggests that the extent of microbial activity and the resulting emissions may be moderated by reduced aeration within covered piles. The lack of oxygen—from accumulated GHGs and lack of ventilation—may limit aerobic decomposition, leading to a potential shift toward anaerobic processes that produce methane as a byproduct.

Overall, these findings indicate that while covering stockpiles reduces immediate surface emissions, it causes large amounts of GHGs to accumulate within, which are likely instantaneously emitted to the atmosphere when the tarp is removed. Therefore, covered stockpiles likely emit similar amounts of GHGs as uncovered ones, when both cumulative emissions from their surface and instantaneous emissions from their storage release are considered.

5.2.1 Temperature and Moisture Response in Uncovered Stockpiles

In addition to gas flux measurements, I assessed how position, aspect, grade, and seasonality influenced the temperature and moisture profiles of uncovered stockpiles. The temperature and moisture profiles in this section refers only to the ancillary measurements taken with uncovered stockpile fluxes presented in Results §4.3.3.

Temperatures at the bottom remained uniform across depths, whereas at the top, deeper layers (60-100 cm) were significantly warmer than the surface layers (0-40 cm). Seasonality further emphasized these differences, with the most stratified temperature profiles observed in November. While surface temperatures at the top position averaged 12.4°C, temperatures at 100 cm depth reached 25.1°C. Even the bottom position exhibited a slight increase of about 3°C between the surface and the 100 cm depth in November. Conversely, moisture profiles exhibited an opposite trend. Moisture levels at the top of stockpiles were uniform across depths, while at the bottom, moisture content significantly

increased with depth. Moisture was highest in November, with surface VWC at the bottom position around 5%, rising to 27% at 100 cm. This increase may have been from the percolation of increased precipitation, as well as increased moisture from vapour flux in the absence of evaporation. However, the moisture regime of stockpiles remains complex and uncertain.

The concurrent increases in temperature and moisture at depth during November—the coldest and wettest month of the study—are biogeochemically significant. Based on the average Q_{10} for peat respiration in bogs quantified by Liu et al. (2024), temperature differences greater than 10°C would lead to tripled decomposition rates at the center of the pile compared to the shallower depths. Additionally, the increased moisture creates more favorable conditions for microbial activity, driving decomposition (Waddington et al. 2009; Kechavarzi et al. 2010). Although these conditions promote decomposition, the overall volume of the stockpile exposed to these more optimal conditions was smaller in November than in other months, resulting in a reduction in CO_2 emissions by approximately 1.5 g CO_2-C m^{-2} day^{-1} during this period.

Temperature profiles did not exhibit significant variation based on aspect or grade; however, moisture profiles showed notable differences. Specifically, Grade 5 peat, categorized as the lowest quality, was significantly wetter than Grades 2 and 3. This observation is likely attributed to the higher degree of humification in lower-quality peat, which enhances its water retention capacity and provides some support for the validity of industry-designated quality levels.

Interestingly, the northwest face of stockpiles was significantly wetter than other faces, apart from the southwest. This is consistent with higher CH_4 emissions observed from the northwest face, as methane production requires anaerobic conditions that are facilitated by higher moisture content. It is likely that both the northwest and southwest faces receive more precipitation due to dominant wind patterns, but the southwest face dries faster due to wind exposure and solar radiation, limiting methane production. Although these findings provide interesting biogeochemical insights, the methane

emissions on the northwest face were only approximately 2 mg CH_4-C m^{-2} day^{-1} greater than the other faces, and need not be considered in overall stockpile GHG accounting.

5.2.2 Impact of Stockpile Uncovering and Removal on CO_2 Emissions

The duration and number of stockpiles on site are important consideration for accurate stockpile GHG accounting. In this study, the number of stockpiles fluctuated throughout the extraction season, ranging from 4 to 61 on any given day. In May, most stockpiles were remnants from the winter. Their numbers steadily decreased throughout June due to heavy rainfall, remained low through early July, and began rising again by mid-July. Stockpiles peaked in September and stayed at a consistent level throughout October as the extraction season slowed down, then decreased slightly in November as new stockpiles were no longer added.

For stockpiles left in the field for over two weeks, the instantaneous release of CO_2 upon removal at Company B was estimated at 52.5 ± 8 kg CO_2-C. This delayed but large instantaneous emission should be factored into stockpile management, emphasizing the need for companies to track the longevity of stockpiles in the field. Simulation results suggested that cumulative emissions could have been 20 to 40 kg CO_2-C greater if stockpiles had been left uncovered. Tarps tend to degrade over time and are prone to leakage through regular temperature probing. However, under the assumptions used for these calculations, I estimate that only 2-3% of the difference in cumulative CO_2 is likely due to probing. This suggests that a larger portion of CO_2 is either leaking through the edges of the tarp (held down by moist peat at the base of stockpiles) or escaping through some other form of undetected leakage. Alternatively, less CO_2 may be produced over time when stockpiles are covered due to reduced oxygen availability. This phenomenon warrants further exploration, and more research is needed to determine whether tarps consistently reduce cumulative emissions when stockpiles remain in the field for extended periods (over two weeks), or if substantial emissions are unaccounted for in this study (i.e., through leakage, or due to geometric differences between the stockpiles at Sites A and B).

Contrarily, shorter-lived covered stockpiles are likely to exhibit higher cumulative emissions compared to uncovered stockpiles. For instance, measurements from a covered stockpile that had been in the field for only four days (Pile 14) indicated elevated CO_2 accumulation rates (between 8 to 12 g CO_2-C m^{-3} day^{-1}). Had this pile been uncovered and removed after four days, its cumulative emissions would have been 2 to 3 times greater than if it had remained uncovered.

These findings highlight the need to consider stockpile longevity and management practices, as the timing of removal and covering may influence overall emission dynamics. Additionally, 100% of stockpiles GHG storage was assumed to be lost when stockpiles were uncovered and removed from the fields. However, more research is needed to confirm the proportion of stored CO_2 lost upon stockpile removal.

5.3 Total Stockpile Area to Total Emissions Ratio

Stockpiles represented less than 1% of the total area of the study sites (0.01 ± 0.005 km^2 of stockpile base area within a total area of 1.7 to 1.8 km^2). Despite their small footprint, stockpiles accounted for approximately 1-2% of overall site CO_2 emissions, including both surface fluxes and instantaneous emissions from stockpile removal. Although the underestimation of site-wide CO_2 GHG emissions is relatively small if stockpiles are ignored, they contribute disproportionately to GHG emissions.

Both the proportion of area occupied by stockpiles and their contribution to total site emissions were smaller in this study than in other estimates found in the literature. For example, Alm et al. (2007b) estimated that stockpiles occupied 5-10% of the harvested area, contributing approximately 41-60% of overall emissions. Similarly, Statistics Finland (2024) reported that stockpiles occupied 2% of the harvested area, contributing 40-46% of CO_2 emissions. Nykänen et al. (1996) did not specify stockpile area but estimated that stockpiles contributed approximately 16% of total site emissions.

My study derived these numbers from direct measurements of stockpile emissions, paired with satellite imagery to monitor changes in stockpile numbers over the extraction

period at two different study sites. I calculated the proportion of stockpile area and their contribution to emissions using monthly data, ensuring a consistent approach. These findings (stockpile areas constituting less than 1% and contributing 1-2% of CO_2 emissions) remained consistent across sites owned by different companies and throughout the study period. This more comprehensive methodology suggests that earlier estimates, primarily stemming from Ahlholm & Silvola's (1990) study (see Table 2.4), may have overestimated stockpile emissions.

5.4 Limitations and Directions for Future Research

While this study is the first to compare emissions and storage between covered and uncovered stockpiles, our measurements faced several limitations. Notably, we could not measure fluxes or storage during and after tarp removal, due to safety concerns posed by the heavy machinery involved in removing stockpiles from the field. While there is evidence that storage is released to the atmosphere from holes in the tarp emitting at high rates and uncovered stockpiles accumulating very little storage, more research is needed to confirm the proportion of stored GHGs in covered stockpiles that is released to the atmosphere, which may have been overestimated in this study that assumed it to be 100%. However, our probes were also insufficiently long to reach the center depths of stockpiles, where microbial activity and GHG production is likely most abundant.

In addition, some findings suggested that stockpile geometry can influence emissions. I used differing management strategies at two companies' sites to directly compare between covered and uncovered stockpiles, but stockpiles at Site A were generally smaller than those at Site B. Consequently, the simulated cumulative emissions for covered piles, had they been left uncovered, may have been underestimated due to the assumption that flux dynamics measured on smaller stockpiles, would be applicable to larger ones (Results §4.5.4).

Questions remain about the potential creation of anaerobic conditions within covered stockpiles, the impact of stockpile size on emissions, the differences in GHG

production rates between covered and uncovered stockpiles, GHG leakage from the edges of tarps, and the proportion of stored GHGs lost to the atmosphere when piles are removed from the field. To refine our understanding of these management strategies, future research should simulate covered and uncovered stockpiles of similar dimensions in a controlled environment. The piles should be formed simultaneously using similar types of peat, and frequent monitoring of fluxes and storage should last approximately three months to capture the average stockpile lifespan. Using smaller stockpiles than those found in the field could enhance the feasibility of the experiment, allowing for a focused investigation into remaining knowledge gaps in comparing stockpile management strategies.

To simulate the removal of stockpiles, fluxes from the surface of piles could be taken as the tarp is removed from the covered pile. Then, sipper measurements at depth from before and after the removal of the tarp should be compared. Some peat could then be physically removed, while continuing to measure GHG storage at depth and surface fluxes. Temperature and moisture probes could also be placed throughout the central column of the piles for continuous monitoring, to determine if one type of stockpile heats up more quickly at depth than the other across layers. Litter bags could also be placed at the center of both piles to investigate differences in decomposition rates between them. The findings from this controlled study could then be applied to observations from transient stockpiles in the field.

This study also demonstrated increased field methane emissions resulting from extraction processes such as harrowing, conditioning, and vacuum harvesting. However, our initial aim was to determine differences between specific field phases rather than the time elapsed since the last operation. Future studies would benefit from an experimental design that creates a 24-hour time series of field methane emissions post-disturbance for various processes throughout the entire extraction season. Based on our findings, methane emissions appeared to stabilize between 10 and 22 hours after disturbance, but it would be valuable to have a more accurate estimate of the time needed for increased emissions to dissipate.

Chapter 6: Conclusion

My study highlights the significant impacts of peat extraction management practices on greenhouse gas emissions and peat conditions across both extracted fields and stockpiles. In particular, my research provides novel insights into how specific field operations and stockpile management strategies influence carbon fluxes, and temperature and moisture profiles, with important implications for GHG accounting and peatland management.

In terms of field operations, carbon dioxide emissions remained steady across all phases of peat extraction. The average emission rate of 0.91 g CO_2-C m^{-2} day^{-1} (± 0.03) in this study closely aligns with existing research, further supporting a broader regional pattern of CO_2 fluxes from extracted peatlands. However, methane emissions exhibited greater variability, especially during the phases with the most recent mechanical disturbance. Methane fluxes were found to be highest from immediately after machinery passed over the fields, at an average rate of 235.9 mg CH_4-C m^{-2} day^{-1}, later stabilizing at an 88 to 96% reduced emission rate. These findings emphasize the importance of accounting for both the intensity and timing of mechanical disturbance in methane emission estimates, to avoid underestimating site GHG fluxes.

Additionally, environmental conditions across extraction phases showed that operations are modifying the surface peat layer as expected, but that changes to temperature and moisture are biogeochemically insignificant, and not reflected at depth. As a result, the differences in methane emissions between phases appear to be driven by machinery disturbance causing the release of methane stored in peat pore spaces, rather than by changes in biogeochemical conditions within the peat itself.

Stockpile emissions present another underexplored dimension of GHG emissions from peat extraction. Both covered and uncovered stockpiles contribute to more carbon loss than the fields, primarily in the form of CO_2 due to a shift towards aerobic decomposition, with key differences in surface fluxes and GHG storage between management methods. Notably, uncovered stockpiles emit most of the CO_2 produced to

the atmosphere, while covered stockpiles store the majority underneath the tarp, which is likely instantaneously emitted to the atmosphere when the tarp is removed. The accumulation of CO_2 underneath the tarp may create anaerobic conditions over time, leading to the production of methane within covered stockpiles. However, more research is needed to understand these mechanisms. In particular, the amount of stored GHGs that are emitted when the tarp is removed, and whether there is leakage around the tarp's perimeter. Since methane fluxes and accumulation for stockpiles were relatively small compared to CO_2, and reduced compared to natural peatlands, overall emissions accounting in this study focused on CO_2.

Stockpiles occupied less than 1% of the overall extraction site area, but had a disproportionate impact on emissions relative to their area, responsible for 1 to 2% of total site CO_2 emissions. The contribution of stockpiles to overall CO_2 emissions varies based on the size of the extraction site and the number of stockpiles present, necessitating the consideration of stockpiles in GHG assessments. However, for the sites in this study, the underestimation of site GHG emissions from ignoring stockpiles would be relatively small, as the fields make up most of the area. These findings are smaller than other estimates for the proportional area of stockpiles and emissions, but are based on rigorous data collection and analysis.

In summary, my research offers a comprehensive understanding of how peat extraction operations and stockpile management practices influence GHG fluxes and peat conditions. It is the first study to quantify the impacts of peat extraction operations on field GHG fluxes, to quantify and compare GHG fluxes and storage for both covered and uncovered stockpiles, and to estimate the contribution of stockpiles to overall site emissions based on these direct measurements. These insights will help to improve GHG accounting methodologies and management strategies, to mitigate the environmental impacts of peat extraction.

Chapter 7: References

Abdalla, M., Hastings, A., Truu, J., Espenberg, M., Mander, Ü., & Smith, P. (2016). Emissions of methane from northern peatlands: A review of management impacts and implications for future management options. *Ecology and Evolution*, *6*(19), 7080–7102. https://doi.org/10.1002/ece3.2469

Ahlholm, U., & Silvola, J. (1990). *CO2 release from peat-harvested peatlands and stockpiles* [Conference Proceedings]. International Conference on Peat Production and Use, Jyväskylä, Finland.

Alm, J., Shurpali, N. J., Tuittila, E.-S., Laurila, T., Maljanen, M., Saarnio, S., & Minkkinen, K. (2007a). Methods for determining emission factors for the use of peat and peatlands-Flux measurements and modelling. *Boreal environmental research, 12*, 85-100. https://www.borenv.net/BER/archive/pdfs/ber12/ber12-085.pdf

Alm, J., Shurpali, N. J., Minkkinen, K., Aro, L., Hytonen, J., Laurila, T., Lohila, A., Maljanen, M., Martikainen, P. J., & Makiranta, P. (2007b). Emission factors and their uncertainty for the exchange of CO2, CH4 and N2O in Finnish managed peatlands. *Boreal Environment Research, 12*(2), 191–210. https://jukuri.luke.fi/bitstream/handle/10024/513695/AlmJ.pdf?sequence=1&isAllowed=y

Andersen, R., Francez, A.-J., & Rochefort, L. (2006). The physicochemical and microbiological status of a restored bog in Québec: identification of relevant criteria to monitor success. *Soil Biology & Biochemistry, 38*, 1375-1387. https://www.gret-perg.ulaval.ca/fileadmin/Fichiers/centre_recherche/Andersen_etal_2006_02.pdf

Andersen, R., Chapman, S. J., & Artz, R. R. E. (2013). Microbial communities in natural and disturbed peatlands: A review. *Soil Biology and Biochemistry, 57*, 979–994. https://doi.org/10.1016/j.soilbio.2012.10.003

Artz, R. R. E., Anderson, I. C., Chapman, S. J., Hagn, A., Schloter, M., Potts, J. M., & Campbell, C. D. (2007). Changes in Fungal Community Composition in Response to Vegetational Succession During the Natural Regeneration of Cutover Peatlands.

Microbial Ecology, *54*(3), 508–522. https://doi.org/10.1007/s00248-007-9220-7

Baird, A. J., Beckwith, C. W., Waldron, S., & Waddington, J. M. (2004). Ebullition of methane-containing gas bubbles from near-surface Sphagnum peat. *Geophysical Research Letters*, *31*(21). https://doi.org/10.1029/2004GL021157

Baldocchi, D. D. (2003). Assessing the eddy covariance technique for evaluating carbon dioxide exchange rates of ecosystems: past, present and future. *Global Change Biology, 9*(4), 479–492. https://doi.org/10.1046/j.1365-2486.2003.00629.x

Basiliko, N., Henry, K., Gupta, V., Moore, T., Driscoll, B., & Dunfield, P. (2013). Controls on bacterial and archaeal community structure and greenhouse gas production in natural, mined, and restored Canadian peatlands. *Frontiers in Microbiology*, *4*. https://www.frontiersin.org/article/10.3389/fmicb.2013.00215

Blok, C., Baumgarten, A., Baas, R., Wever, G., & Lohr, D. (2019). Chapter 11:Analytical Methods Used With Soilless Substrates. In M. Raviv, J. H. Lieth, & A. Bar-Tal (Eds.), *Soilless Culture* (Second Edition) (pp. 509–564). Elsevier. https://doi.org/10.1016/B978-0-444-63696-6.00011-6

Blok, C., Eveleens, B. & van Winkel, A. (2021). Growing media for food and quality of life in the period 2020-2050. *Acta Hortic. 1305*, 341-356. https://doi.org/10.17660/ActaHortic.2021.1305.46

Byrnes, K.A., Chojnicki, B. Christensen, T. R., Drosler, M. Frolking, S. Lindroth, A., Mailhammer, J., Malmer, N., Selin, P., Turunen, J., Valentini, R., & Zetterberg, L. (2004). *EU Peatlands: Current Carbon Stocks and Trace Gas Fluxes.* Geosphere-Biosphere Centre, Univ. of Lund, Sweden. https://scholars.unh.edu/cgi/viewcontent.cgi?article=1489&context=earthsci_facpub

Campbell Scientific. (2020). *Product Manual: HS2 and HS2P (HydroSence II)*. https://s.campbellsci.com/documents/us/manuals/hs2.pdf

Campos Mota, L., Van Meeteren, U., & Blok, C. (2007). Comparison of the physical properties of vermicompost from paper mill sludge and green compost as substitutes for peat-based potting media. *Acta Horticulturae, 819*, 143–150. https://doi.org/10.17660/ActaHortic.2007.819.17

Carbone, M. S., Seyednasrollah, B., Rademacher, T. T., Basler, D., Le Moine, J. M., Beals, S., Beasley, J., Greene, A., Kelroy, J., & Richardson, A. D. (2019). Flux Puppy – An open-source software application and portable system design for low-cost manual measurements of CO2 and H2O fluxes. *Agricultural and Forest Meteorology*, *274*, 1–6. https://doi.org/10.1016/j.agrformet.2019.04.012

Clark, L., Strachan, I. B., Strack, M., Roulet, N. T., Knorr, K.-H., & Teickner, H. (2023). Duration of extraction determines CO_2 and CH_4 emissions from an actively extracted peatland in eastern Quebec, Canada. *Biogeosciences*, *20*(3), 737–751. https://doi.org/10.5194/bg-20-737-2023

Clymo, R.S., Turunen, J., & Tolonen, K. (1998). Carbon accumulation in peatland. *Oikos, 81*(2), 368-388.

Charman, D. J. (2009). Peat and Peatlands. In G. E. Likens (Ed.), *Encyclopedia of Inland Waters* (pp. 541–548). Academic Press. https://doi.org/10.1016/B978-012370626-3.00061-2

Choi, S., Xu, L., & Kim, H.-J. (2019). Influence of physical properties of peat-based potting mixes substituted with parboiled rice hulls on plant growth under two irrigation regimes. *Horticulture, Environment, and Biotechnology*, *60*(5), 679–689. https://doi.org/10.1007/s13580-019-00179-9

Croft, M., Rochefort, L., & Beauchamp, C.J. (2001). Vacuum-extraction of peatlands disturbs bacterial population and microbial biomass carbon. *Applied Soil Ecology,* 18, 1e12. https://citeseerx.ist.psu.edu/document?repid=rep1&type=pdf&doi=b5e81fa04c169eda70bb7286945032f1bf21e502

CSPMA. (2017). *2017 Statistics about Peatland Areas Managed for Horticultural Peat Harvesting in Canada*. Peat and Peatlands. https://tourbehorticole.com/wp-content/uploads/2020/01/Summary_2016_2017_Indutry_Statistic_AREAS_WEB.pdf

CSPMA. (2022). *Peat Moss Harvesting*. Canadian Peat Moss. Retrieved July 30, 2024, from https://peatmoss.com/peat-moss-harvesting/

CSPMA. (2022b). Peat. Canadian Peat Moss. https://peatmoss.com/peat/

Cleary, J., Roulet, N. T., & Moore, T. R. (2005). Greenhouse gas emissions from Canadian peat extraction, 1990–2000: a life-cycle analysis. AMBIO: *A Journal of the Human Environment, 34*(6), 456-461. https://doi.org/10.1579/0044-7447-34.6.456

Environment and Climate Change Canada. (2024a). *Canadian Climate Normals 1981 – 2010 Station Data: St Arsene* [Data set]. Government of Canada: Environment and natural resources. *https://climate.weather.gc.ca/climate_normals/results_1981_2010_e.html*

Environment and Climate Change Canada. (2024b). *Daily Data 2022: Riviere-du-Loup Quebec 2022* [Data set]. Government of Canada: Environment and natural resources. https://climat.meteo.gc.ca/climate_data/daily_data_e.html

ESRI. (2023). *ArcGIS Pro (3.1.0.)*. ESRI.

Fascella, G. (2015). Growing Substrates Alternative to Peat for Ornamental Plants. In Md., Asaduzzaman (Ed.), *Soilless Culture – Use of Substrates for the Production of Quality Horticulture Crops* (pp. 47–68). IntechOpen. https://doi.org/10.5772/59596

Gorham, E. (1995). The Biogeochemistry of Northern Peatlands and Its Possible Responses to Global Warming. In G. M. Woodwell & F. T. Mackenzie (Eds.), *Biotic Feedbacks in the Global Climatic System: Will the Warming Feed the Warming?* (p. 169-187). Oxford University Press. https://doi.org/10.1093/oso/9780195086409.003.0011

Gnatowski, T., Szatyłowicz, J., Pawluśkiewicz, B., Oleszczuk, R., Janicka, M., Papierowska, E., & Szejba, D. (2018). Field Calibration of TDR to Assess the Soil Moisture of Drained Peatland Surface Layers. *Water*, *10*(12), Article 12. https://doi.org/10.3390/w10121842

Goldstein, A., Turner, W. R., Spawn, S. A., Anderson-Teixeira, K. J., Cook-Patton, S., Fargione, J., Gibbs, H. K., Griscom, B., Hewson, J. H., Howard, J. F., Ledezma, J. C., Page, S., Koh, L. P., Rockström, J., Sanderman, J., & Hole, D. G. (2020). Protecting irrecoverable carbon in Earth's ecosystems. *Nature Climate Change*, *10*(4), 287–295. https://doi.org/10.1038/s41558-020-0738-8

Harris, L. I., Richardson, K., Bona, K. A., Davidson, S. J., Finkelstein, S. A., Garneau, M., McLaughlin, J., Nwaishi, F., Olefeldt, D., Packalen, M., Roulet, N. T., Southee, F. M.,

Strack, M., Webster, K. L., Wilkinson, S. L., & Ray, J. C. (2021). The essential carbon service provided by northern peatlands. *Frontiers in Ecology and the Environment*, *20*(4), https://doi.org/10.1002/fee.2437

He, H., Clark, L., Lai, O. Y., Kendall, R., Strachan, I., & Roulet, N. T. (2023). Simulating Soil Atmosphere Exchanges and CO2 Fluxes for an Ongoing Peat Extraction Site. *Ecosystems, 26*(6), 1335–1348. https://doi.org/10.1007/s10021-023-00836-2

He, H., & Roulet, N. T. (2023). Improved estimates of carbon dioxide emissions from drained peatlands support a reduction in emission factor. *Communications Earth & Environment*, *4*(1), 1–6. https://doi.org/10.1038/s43247-023-01091-y

Hirschler, O., & Osterburg, B. (2021). Peat market in Europe: evolution and climate relevance. *Acta Hortic. 1305*, 357-364. DOI: 10.17660/ActaHortic.2021.1305.47

Hirschler, O., & Osterburg, B. (2022). Peat extraction, trade and use in Europe: a material flow analysis. *Mires and Peat, 28*. DOI: 10.19189/MaP.2021.SNPG.StA.2315

Hooijer, A., Page, S., Jauhiainen, J., Lee, W. A., Lu, X. X., Idris, A., & Anshari, G. (2011). Subsidence and carbon loss in drained tropical peatlands: Reducing uncertainty and implications for CO 2 emission reduction options. *Biogeosciences Discussions*, *8*(5). https://doi.org/10.5194/bg-9-1053-2012

Huang, Y., Ciais, P., Luo, Y., Zhu, D., Wang, Y., Qiu, C., Goll, D. S., Guenet, B., Makowski, D., De Graaf, I., Leifeld, J., Kwon, M. J., Hu, J., & Qu, L. (2021). Tradeoff of CO2 and CH4 emissions from global peatlands under water-table drawdown. *Nature Climate Change*, *11*(7), 618–622. https://doi.org/10.1038/s41558-021-01059-w

Hunter, M. L., Frei, R. J., Strachan, I. B., & Strack, M. (2024). Environmental and Management Drivers of Carbon Dioxide and Methane Emissions From Actively-Extracted Peatlands in Alberta, Canada. *Journal of Geophysical Research: Biogeosciences, 129*(3), e2023JG007738. https://doi.org/10.1029/2023JG007738

IPCC. (2006). *2006 IPCC guidelines for national greenhouse gas inventories: Volume 4: Agriculture, forestry, and other land use*. Prepared by the National Greenhouse Gas Inventories Programme (H. S. Eggleston, L. Buendia, K. Miwa, T. Ngara, & K. Tanabe, Eds.). IGES.

https://www.ipccnggip.iges.or.jp/public/2006gl/pdf/4_Volume4/V4_07_Ch7_Wetlands.pdf

IPCC. (2014). 2013 supplement to the 2006 IPCC guidelines for national greenhouse gas inventories: Wetlands (T. Hiraishi, T. Krug, K. Tanabe, N. Srivastava, J. Baasansuren, M. Fukuda, & T. G. Troxler, Eds.). IPCC. https://www.ipccnggip.iges.or.jp/public/wetlands

IPS. (2021). *Peatlands international: Just Transition and Hybrid Substrates*. https://peatlands.org/document/peatlands-international-1-2021/

IUCN. (2021, November). *Issues in Brief: Peatlands and climate change*. IUCN. https://www.iucn.org/resources/issues-briefs/peatlands-and-climate-change

IUCN UK Committee Peatland Programme. (2019). *Peat Bog Ecosystems: Key Definitions*. https://www.iucn-uk-peatlandprogramme.org/sites/default/files/2019-05/1%20Definitions%20final%20-%205th%20November%202014.pdf

Jones, S. B., & Or, D. (2003). Modeled effects on permittivity measurements of water content in high surface area porous media. *Physica B: Condensed Matter*, *338*(1), 284–290. https://doi.org/10.1016/j.physb.2003.08.008

Joosten, H., & Couwenberg, J. (2008). *Assessment on Peatlands, Biodiversity and Climate change. Main Report.* Global Environment Centre & Wetlands International. https://www.researchgate.net/publication/284054686_Peatlands_and_carbon

Kechavarzi, C., Dawson, Q., Bartlett, M., & Leeds-Harrison, P. B. (2010). The role of soil moisture, temperature and nutrient amendment on CO2 efflux from agricultural peat soil microcosms. *Geoderma*, *154*(3), 203–210. https://doi.org/10.1016/j.geoderma.2009.02.018

Kettunen, A. (2003). Connecting methane fluxes to vegetation cover and water table fluctuations at microsite level: A modeling study: Connecting CH_4 Fluxes to Site Specific Factors. *Global Biogeochemical Cycles*, *17*(2). https://doi.org/10.1029/2002GB001958

Kitir, N., Yildirim, E., Şahin, Ü., Turan, M., Ekinci, M., Ors, S., Kul, R., Ünlü, H., & Ünlü, H. (2018). Peat Use in Horticulture. In T. Bülent & T. Metin (Eds.), *Peat*. IntechOpen. https://doi.org/10.5772/intechopen.79171

Klingenfuß, C., Roßkopf, N., Walter, J., Heller, C., & Zeitz, J. (2014). Soil organic matter to soil organic carbon ratios of peatland soil substrates. *Geoderma*, *235–236*, 410–417. https://doi.org/10.1016/j.geoderma.2014.07.010

Koehler, A.-K., Sottocornola, M., & Kiely, G. (2011). How strong is the current carbon sequestration of an Atlantic blanket bog? Global Change Biology, 17(1), 309–319. https://doi.org/10.1111/j.1365-2486.2010.02180.x

Lai, O. Y. (2022). *Peat Moisture and Thermal Regimes for Peatlands Undergoing Active Extraction* [Master's thesis], McGill University. eScholarship@McGill. https://escholarship.mcgill.ca/concern/theses/d791sn38s

Lamarre, A., Garneau, M., & Asnong, H. (2012). Holocene paleohydrological reconstruction and carbon accumulation of a permafrost peatland using testate amoeba and macrofossil analyses, Kuujjuarapik, subarctic Québec, Canada. *Review of Palaeobotany and Palynology*, *186*, 131–141. https://doi.org/10.1016/j.revpalbo.2012.04.009

Lapveteläinen, T., Regina, K., & Perälä, P. (2007). Peat-based emissions in Finland's national greenhouse gas inventory. *Boreal Environmental Research, 12 (225-236)*. https://jukuri.luke.fi/bitstream/handle/10024/464276/Lapvetelainen.pdf?sequence=1&isAllowed=y

Liu, H., Rezanezhad, F., Zhao, Y., He, H., Van Cappellen, P., & Lennartz, B. (2024). The apparent temperature sensitivity (Q10) of peat soil respiration: A synthesis study. *Geoderma*, *443*, 116844. https://doi.org/10.1016/j.geoderma.2024.116844

Loisel, J., Gallego-Sala, A. V., Amesbury, M. J., Charman, D. J., Roland, T. P., Korhola, A., Valiranta, M., Juutinen, S., Minkkinen, K., Piilo, S., Magnan, G., Garneau, M., Anshari, G., Beilman, D. W., Benavides, J. C., Blewett, J., Naafs, B. D. A., Camill, P., Chawchai, S., … Wu, J. (2021). Expert assessment of future vulnerability of the global peatland carbon sink. *Nature Climate Change*, *11*(1), 70–77. https://doi.org/10.1038/s41558-020-00944-0

Manning, F. C., Kho, L. K., Hill, T. C., Cornulier, T., & Teh, Y. A. (2019). Carbon Emissions From Oil Palm Plantations on Peat Soil. *Frontiers in Forests and Global Change*, *2*. https://doi.org/10.3389/ffgc.2019.00037

McNeil, P., & Waddington, J. M. (2003). Moisture controls on Sphagnum growth and CO2 exchange on a cutover bog. *Journal of Applied Ecology, 40*(2), 354–367. https://doi-org.proxy3.library.mcgill.ca/10.1046/j.1365-2664.2003.00790.x

Mundim, K. C., Baraldi, S., Machado, H. G., & Vieira, F. M. C. (2020). Temperature coefficient (Q10) and its applications in biological systems: Beyond the Arrhenius theory. *Ecological Modelling*, *431*, 109127. https://doi.org/10.1016/j.ecolmodel.2020.109127

Nilsson, M., Sagerfors, J., Buffam, I., Laudon, H., Eriksson, T., Grelle, A., Klemedtsson, L., Weslien, P., & Lindroth, A. (2008). Contemporary carbon accumulation in a boreal oligotrophic minerogenic mire—A significant sink after accounting for all C-fluxes. *Global Change Biology, 14*(10), 2317–2332. https://doi.org/10.1111/j.1365-2486.2008.01654.x

Nugent, K. A., Strachan, I. B., Roulet, N. T., Strack, M., Frolking, S., & Helbig, M. (2019). Prompt active restoration of peatlands substantially reduces climate impact. *Environmental Research Letters*, *14*(12), 124030. https://doi.org/10.1088/1748-9326/ab56e6

Nykaenen, H., Martikainen, P. J., Silvola, J., & Alm, J. (1996). Fluxes of greenhouse gases CH_4, CO_2 and N_2O on some peat mining areas in Finland. In R. Laiho, J. Laine, & H. Vasander (Eds.), *Northern Peatlands in Global Climactic Change*. Academy of Finland. https://www.osti.gov/etdeweb/servlets/purl/458164

Oertel, C., Matschullat, J., Zurba, K., Zimmermann, F., & Erasmi, S. (2016). Greenhouse gas emissions from soils—A review. *Geochemistry*, *76*(3), 327–352. https://doi.org/10.1016/j.chemer.2016.04.002

Olefeldt, D., Roulet, N. T., Bergeron, O., Crill, P., Backstrand, K., & Christensen, T. (2012). Net carbon accumulation of a high-latitude permafrost palsa mire similar to permafrost-free peatlands. *Geophysical Research Letters, 39*, L03501.

https://doi.org/10.1029/2011GL050355

Page, S., Morrison, R., Malins, C., Hooijer, A., & Rieley, J. (2011). *Review of Peat Surface Greenhouse Gas Emissions from Oil Palm Plantations in Southeast Asia*. International Council on Clean Transportation White Paper 15, 1-78. https://theicct.org/wp-content/uploads/2021/06/ICCT_Peat-Emissions_Sept2011.pdf

Pelletier, L., Garneau, M., & Moore, T. R. (2011). Variation in CO2 exchange over three summers at microform scale in a boreal bog, Eastmain region, Québec, Canada. Journal of Geophysical Research: Biogeosciences, 116(G3). https://doi.org/10.1029/2011JG001657

Penman, J., Gytarsky, M., Hiraishi, T., Krug, T., Kruger, D., Pipatti, R., Buendia, L., Miwa, K., Ngara, T., Tanabe, K., & Wagner, F. (Eds.) (2018). *Good Practice Guidance for Land Use, Land-Use Change and Forestry*. Hayama, Japan: Institute for Global Environmental Strategies (IGES) for the IPCC. https://www.ipcc.ch/site/assets/uploads/2018/03/GPG_LULUCF_FULLEN.pdf

Peters, J., & von Unger, M. (2017). *Peatlands in the EU Regulatory Environment*. Federal Agency for Nature Conservation. https://doi.org/10.19217/skr454

Peters, J., Hirschelmann, S., Krüger, S., Hedden-Dunkhorst, B., Salathé, T., & Kopansky, D. (2019). *Policy Brief: Peatland Strategies in Europe Why and how to develop national strategies for peatlands.* German Agency for Nature Conservation (BfN), Michael Succow Foundation and the Ramsar Convention Secretariat. https://www.bfn.de/sites/default/files/2021-06/policy-brief-peatland-strategies-bfn.pdf

Planet Labs PBC. (2018). *Planet Application Program Interface: In Space for Life on Earth*. Planet. https://api.planet.com

Prasad, M. (2021). *Review of the use of Pear Moss in Horticulture*. https://assets.gov.ie/213283/b110a6f6-bebf-4496-9c76-92f3cf0faf35.pdf

Qiu, C., Zhu, D., Ciais, P., Guenet, B., & Peng, S. (2020). The role of northern peatlands in the global carbon cycle for the 21st century. *Global Ecology and Biogeography*, *29*(5), 956–973. https://doi.org/10.1111/geb.13081

R Core Team. (2024). *R: A Language and Environment for Statistical Computing*. R Foundation for Statistical Computing, Vienna, Austria. https://www.R-project.org

Rankin, T., Strachan, I., & Strack, M. (2018). Carbon dioxide and methane exchange at a post-extraction, unrestored peatland. *Ecological Engineering, 122*(241-251). doi: https://doi.org/10.1016/j.ecoleng.2018.06.021

Rinaldi, P. S., Akromah, Z. N., Ramadhan, H., Husna, S., Syamsudin, D. L., Panggabean, P. B., Murdianti, R. A., Fatahillah, M. H., Perala, I., Rizqia, E. K., Yahya, S. A., Novitasari, A., & Wibowo, C. (2019). Physical and chemical analysis of land in forest peat swamp in resort Pondok soar, Tanjung Puting National Park, Central Kalimantan. *Iop Conference Series: Earth and Environmental Science, 394*(1). https://doi.org/10.1088/1755-1315/394/1/012037

Risi, J., Brunette, C.E., Spence, D., & Girard, H. (1953). *A Chemical Study of the Peats of Quebec.* Province of Quebec, Canada, Department of Mines, Laboratories Branch P.R. https://gq.mines.gouv.qc.ca/documents/examine/RP282(A)/RP282(A).pdf

Robert, P-É. (1965). *Les tourbières du Bas-Saint-Laurent* (Annexe Technique 17). Mont-Joli, Québec: B.A.E.Q. Retrieved https://numerique.banq.qc.ca/patrimoine/details/52327/2988939

Rosset, T., Binet, S., Rigal, F., & Gandois, L. (2022). Peatland Dissolved Organic Carbon Export to Surface Waters: Global Significance and Effects of Anthropogenic Disturbance. *Geophysical Research Letters*, *49*(5). https://doi.org/10.1029/2021GL096616

Roulet, N. T., Lafleur, P. M., Richard, P. J. H., Moore, T. R., Humphreys, E. R., & Bubier, J. (2007). Contemporary carbon balance and late Holocene carbon accumulation in a northern peatland. *Global Change Biology, 13*(2), 397–411. https://doi.org/10.1111/j.1365-2486.2006.01292.x

Rydin, H., & Jeglum, J. K. (2013). *The Biology of Peatlands* (2nd edition). Oxford University Press. https://www.researchgate.net/publication/284054686_Peatlands_and_carbon

Statistics Finland. (2006). *Greenhouse Gas Emissions in Finland 1990-2004: National Inventory Document under the UNFCCC*. https://stat.fi/tk/yr/2_fin_2006_nir_20061215.pdf

Statistics Finland. (2024). *Greenhouse Gas Emissions in Finland 1990-2022: National Inventory Report to the UNFCCC*. https://stat.fi/media/uploads/tup/khkinv/fi_nid_eu_2022_2024-03-15_v2.pdf

Strack, M., Waddington, J.M., Turetsky, M., Roulet, N.T., & Byrne, K.A. (2008). Northern Peatlands, greenhouse gas exchange and climate change. In M. Strack. Editor (Eds.), *Peatlands and climate change, IPS, International Peat Society* (pp. 44-69). International Peat Society, Vapaudenkatu 12, 40100 Jyväskylä, Finland. https://www.researchgate.net/publication/285329850_Northern_peatlands_greenhouse_gas_exchange_and_climate_change

Sundh, I., Nilsson, M., Mikkelä, C., Granberg, G., & Svensson, B. H. (2000). Fluxes of Methane and Carbon Dioxide on eat-mining Areas in Sweden. *AMBIO: a Journal of the Human Environment, 29*(8), 499-503. https://doi.org/10.1579/0044-7447-29.8.499

Tokida, T., Miyazaki, T., Mizoguchi, M., Nagata, O., Takakai, F., Kagemoto, A., & Hatano, R. (2007). Falling atmospheric pressure as a trigger for methane ebullition from peatland. *Global Biogeochemical Cycles, 21*(2). https://doi.org/10.1029/2006GB002790

Trettin, C. C., Laiho, R., Minkkinen, K., & Laine, J. (2006). Influence of climate change factors on carbon dynamics in northern forested peatlands. *Canadian Journal of Soil Science*, *86*(Special Issue), 269–280. https://doi.org/10.4141/S05-089

UN Comtrade (2022). *Trade data* [Data set]. Online at: https://comtradeplus.un.org/TradeFlow?Frequency=A&Flows=X&CommodityCodes=TOTAL&Partners=0&Reporters=all&period=2021&AggregateBy=none&BreakdownMode=plus. Accessed September 2024.

UNEP. (2022). *Global Peatlands Assessment – The State of the World's Peatlands: Evidence for action toward the conservation, restoration, and sustainable management of peatlands*. Main Report. Global Peatlands Initiative. United Nations Environment

Programme, Nairobi. https://globalpeatlands.org/sites/default/files/2022-12/peatland_assessment.pdf

UNFCCC. (2014). *United states climate action report 2014*. https://unfccc.int/files/national_reports/annex_i_natcom/submitted_natcom/application/pdf/2014_u.s._climate_action_report%5B1%5Drev.pdf

US EPA, O. (2024, August 8). *Understanding Global Warming Potentials* [Overviews and Factsheets]. Accessed on 18 October 2024: https://www.epa.gov/ghgemissions/understanding-global-warming-potentials

USGS. (2018). *Peat* [Data set]. U.S. Geological Survey, Mineral Commodity Summaries. Online at https://d9-wret.s3.us-west-2.amazonaws.com/assets/palladium/production/mineral-pubs/peat/mcs-2018-peat.pdf. Accessed September 2024.

USGS. (2020). *Peat* [Data set]. U.S. Geological Survey, Mineral Commodity Summaries. Online at https://pubs.usgs.gov/periodicals/mcs2020/mcs2020-peat.pdf. Accessed September 2024.

USGS. (2022). *Peat* [Data set]. U.S. Geological Survey, Mineral Commodity Summaries. Online at https://pubs.usgs.gov/periodicals/mcs2022/mcs2022-peat.pdf. Accessed September 2024.

USGS. (2024). *Peat* [Data set]. U.S. Geological Survey, Mineral Commodity Summaries. Online at https://pubs.usgs.gov/periodicals/mcs2024/mcs2024-peat.pdf. Accessed September 2024.

Waddington, J. M., Plach, J., Cagampan, J. P., Lucchese, M., & Strack, M. (2009). Reducing the carbon footprint of Canadian peat extraction and restoration. *Ambio*, *38*(4), 194–200. https://doi.org/10.1579/0044-7447-38.4.194

Wangari, E. G., Mwanake, R. M., Kraus, D., Werner, C., Gettel, G. M., Kiese, R., Breuer, L., Butterbach-Bahl, K., & Houska, T. (2022). Number of chamber measurement locations for accurate quantification of landscape-scale greenhouse gas fluxes: Importance of land use, seasonality, and greenhouse gas type. *Journal of Geophysical*

Research: Biogeosciences, 127, e2022JG006901. https://doi.org/10.1029/2022JG006901

Webster, K. L., Bhatti, J. S., Thompson, D. K., Nelson, S. A., Shaw, C. H., Bona, K. A., Hayne, S. L., & Kurz, W. A. (2018). Spatially-integrated estimates of net ecosystem exchange and methane fluxes from Canadian peatlands. *Carbon Balance and Management*, *13*(1), 16. https://doi.org/10.1186/s13021-018-0105-5

Wilson, D., Dixon, S. D., Artz, R. R. E., Smith, T. E. L., Evans, C. D., Owen, H. J. F., Archer, E., & Renou-Wilson, F. (2015). Derivation of greenhouse gas emission factors for peatlands managed for extraction in the Republic of Ireland and the United Kingdom. *Biogeosciences, 12*(18), 5291–5308. https://doi.org/10.5194/bg-12-5291-2015

Winsborough, C., & Basiliko, N. (2010). Fungal and bacterial activity in northern peatlands. *Geomicrobiology Journal*, *27*(4), 315–320. https://doi.org/10.1080/01490450903424432

Young, D. M., Baird, A. J., Charman, D. J., Evans, C. D., Gallego-Sala, A. V., Gill, P. J., Hughes, P. D. M., Morris, P. J., & Swindles, G. T. (2019). Misinterpreting carbon accumulation rates in records from near-surface peat. *Scientific Reports*, *9*(1), 17939. https://doi.org/10.1038/s41598-019-53879-8

Yu, Z., Loisel, J., Brosseau, D. P., Beilman, D. W., & Hunt, S. J. (2010). Global peatland dynamics since the Last Glacial Maximum. *Geophysical Research Letters, 37*(13), L13402. https://doi.org/10.1029/2010GL043584

Yu, Z. C. (2012). Northern peatland carbon stocks and dynamics: A review. *Biogeosciences*, *9*(10), 4071–4085. https://doi.org/10.5194/bg-9-4071-2012

Zaiontz, C. (2023). *Real Statistics Using Excel*. www.real-statistics.com

Appendix A: Simulated Total Stockpile Cumulative Emissions

To further assess differences in emissions between stockpile management techniques, I simulated the lifespan (daily fluxes) and removal (instantaneous emissions) of Piles 2, 10, and 14, as both covered and uncovered. I calculated the cumulative emissions for each pile and management scenario as follows:

Assumptions

I. The piles were removed on August 24th, 2022 (which was not the case).
II. Stored CO_2 was equivalent to the average concentrations (across all depths and positions) measured on August 23rd for each pile.
III. Moisture was equivalent to the average VWC plus 9% (to account for probe error) measured on August 23rd for each pile.
IV. 82% porosity (Lai 2022).
V. GHGs emitted from the surface below the piles were negligible, despite Piles 2 and 14 being situated on extracted fields, while Pile 10 was on gravel.
VI. Had these piles been left uncovered, their surface emissions would have been equivalent to those quantified for uncovered stockpiles in July and August at Site A, despite these being larger stockpiles.
VII. When stockpiles were un-tarped and removed, all stored CO_2 was instantaneously emitted to the atmosphere.
VIII. Methane emissions were relatively small, and therefore omitted.

Calculations

I used the following equations to estimate cumulative emissions had each of the stockpiles been covered ($All\ E_{covered}$) and uncovered ($All\ E_{uncovered}$)

$$All\ E_{covered} = Instant\ E_{covered} + [3\ m^2 \cdot E_{ch} + (SA - 3m^2) \cdot Etarp] \cdot days \qquad (A.1)$$

$$Total\ E_{july,aug} = (SA \cdot 0.25 \cdot Etop_{month}) + (SA \cdot 0.75 \cdot Ebottom_{month}) \qquad (A.2)$$

$$All\ E_{uncovered} = Instant\ E_{uncovered} + \left(Total\ E_{July} \cdot days_{July}\right) + \left(Total\ E_{Aug} \cdot days_{Aug}\right) \quad (A.3)$$

Relevant variable values are reported in Tables A.1 and A.2.

Table A.1: Variables used in simulated calculations.

Simulated tarp removal on 24-Aug-2022	**Pile 2**	**Pile 10**	**Pile 14**
Volume (m^3)	1021	1198	995
Surface Area (m^2)	627	746	678
Date Covered	05-Jul	11-Jul	19-Jul
Number of days in the field (field days)	50	44	36
Average VWC% measured on Aug. 23 (+9% correction)	11.52	11.28	9.28
Average g CO_2-C m^{-3} measured on Aug. 23	71.76	72.31	70.01
Pore space (m^3)	837.22	982.36	815.9
Moisture (m^3)	96.42	110.84	75.74
Covered CO_2 storage (g CO_2-C)	53159.13	63016.18	51816.42
Surface Flux E covered (g CO_2-C)	20703	21255.52	15971.04
All E covered (g CO_2-C)	73862.13	84271.70	67787.46
July flux days	26	20	12
August flux days	24	24	24
July Emissions (g CO_2-C m^{-2} day^{-1})	54204.15	49609	27052.2
August Emissions (g CO_2-C m^{-2} day^{-1})	53119.44	63201.12	57440.16
Uncovered CO_2 storage (g CO_2-C)	4985.59	5865.31	4981.26
All E uncovered (g CO_2-C)	112309.18	118675.43	89473.62
Difference All E uncovered-All E covered	38447.04	34403.73	21686.16

Table A.2: Flux rates used in simulated calculations.

	July	**August**
Uncovered Top Flux (g CO_2-C m^{-2} day^{-1})	5.62	7.67
Uncovered Bottom Flux (g CO_2-C m^{-2} day^{-1})	2.56	2.15
Etarp (flux over intact tarp) (g CO_2-C m^{-2} day^{-1})	0.58	0.58
Ech (flux over covered hole) (g CO_2-C m^{-2} day^{-1})	17.38	17.38